INVESTIGATING SOLID PARTICLE EROSION OF PIPELINE MATERIAL

A THESIS SUBMITTED IN PARTIAL FULFILMENT OF THE REQUIREMENTS FOR THE DEGREE OF MASTER OF SCIENCE BY RESEARCH AT THE UNIVERSITY OF HUDDERSFIELD

BY

Eduardo J Samuel Matthew
B.Eng. University of Huddersfield U.K 2015

Director of Studies: Dr. Taimoor Asim
Energy, Emissions and the Environment Research Group

School of Computing and Engineering
University of Huddersfield
UK
January 2017

I dedicate this volume of work to the memory of my late mother Dr. Doreen Matthew Hodge and my daughter Adanna J Richardson

ABSTRACT

In the oil and gas industry, the integrity of pipelines is paramount, owing to the consequences which arise from the failure of these assets. Reduced production, loss of assets, increased maintenance cost, fatalities and loss of product through spillage, coupled with the far reaching environmental effects, are all by-products of the failure of pipelines. One of the major contributing factors impacting the integrity of these assets is that of the localised degradation of the pipeline material due to solid particle impingement. As a result, it is crucial to understand and quantify the manner in which a material responds to a myriad of erosive conditions. The occurrence of erosion on a material surface is influenced by a considerable number of factors. Research has found that the impact of each contributing parameter varies based on the conditions. As such the field of erosion studies has been heavily reliant on establishing empirical relationships.

The work presented in this thesis is backed by an established experimental approach to solid particle erosion, replicating practical engineering problems found in oil conveying pipelines with entrained solid particles. The first aspect of the work conducted focuses on the evaluation of erosion through experimentation, using a slurry erosion test pot. For this study, olivine, which is a naturally occurring mineral has been used as the erodent, with mild carbon steel representing the target material. A qualitative assessment was conducted on the friability of olivine under the operating conditions, giving an insight into how the recirculating nature of the test pot affects the initial particle parameters, principally the size and angularity. Both qualitative and quantitative analysis have been carried out on the impact of flow velocity, time and three distinct size ranges of multi-sized particle slurries on the material loss of the target material. The relationship of velocity has been found to be consistent with that found in literature, while the effect of increasing the diameter of the multi-sized particles produces a different response from that found in literature for equi-sized particles. Time has been found to have no noticeable effect on the erosion rate under the conditions evaluated in this study. Moreover, a novel erosion rate prediction model has been developed based on the Zhang/Tulsa model, which now encompasses the influence of the weighted mass particle size for multi-sized slurries.

The second aspect of this study assesses the nature in which the surface texture of the material changes as the erosive conditions change. Using a non-contact surface measurement method, the change in the material surface roughness is assessed as a function of exposure time, impact angle, velocity and weighted mass particle size. This work presents the first in-depth assessment of the change in developed interfacial area ratio as a result of slurry erosion. A qualitative and quantitative investigation was carried out on the results obtained, from which the impact of each parameter evaluated has been presented, showing that each parameter has an impact on the change in developed interfacial area ratio. Additionally, a comparison is presented between the developed interfacial area ratio and the arithmetical mean height. This highlighted the influence of the measurement parameter on the results being processed.

DECLARATION

- The author of this thesis (including any appendices and/or schedules to this thesis) owns any copyright in it (the "Copyright") and he has given The University of Huddersfield the right to use such Copyright for any administrative, promotional, educational and/or teaching purposes.

- Copies of this thesis, either in full or in extracts, may be made only in accordance with the regulations of the University Library. Details of these regulations may be obtained from the Librarian. This page must form part of any such copies made.

- The ownership of any patents, designs, trademarks and any and all other intellectual property rights except for the Copyright (the "Intellectual Property Rights") and any reproductions of copyright works, for example graphs and tables ("Reproductions"), which may be described in this thesis, may not be owned by the author and may be owned by third parties. Such Intellectual Property Rights and Reproductions cannot and must not be made available for use without the prior written permission of the owner(s) of the relevant Intellectual Property Rights and/or Reproductions.

The University of Huddersfield

ACKNOWLEDGEMENTS

I am cognisant of the fact that this work would not have been possible, in its present state, without the direct and indirect contributions and support of many parties, I would be remiss not to specifically thank the following people: -

1. Chris Dawson - Metrology Engineer, CPT/EPSRC
2. Richard Bailey - Team Leader (Mechanical and Automotive), UoH
3. Steven Goldstein - Senior Technician (Mechanical and Automotive), UoH
4. Hayley Markham - Senior Technician, School of Applied Sciences, UoH
5. Ghada Aboufares - PhD Student: Energy, Emissions and the Environment Research Group
6. Martin Zahariev - MSc Researcher: Energy, Emissions and the Environment Research Group
7. Obie Ogheneochuko - PhD Student: Systems Engineering Research Group
8. Ayodele Onilude - PhD Student: Systems Engineering Research Group
9. Terence Zimvu - Mechanical Engineer

I would also like to thank my sisters Melissa and Joanne for their support, my father Eduardo for his words of encouragement and my partner Ayo Sanussi for her patience and contributions through this journey. Finally, I would like to acknowledge the work of my supervisor Dr Taimoor Asim and my co supervisor and leader of the Energy, Emissions and the Environment Research Group Prof. Rakesh Mishra, firstly, for providing me the opportunity to work within this strong research group and more directly for their guidance and professionalism, without which this work wouldn't be possible.

CONTENTS

LIST OF FIGURES

LIST OF TABLES

NOMENCLATURE, SYMBOLS AND SUBSCRIPTS

A, C, K	Empirical constants used in erosion models
BH, B	Brinell hardness of target material (N/mm^2)
C_w	Solid particle concentration (%)
CFD	Computational Fluid Dynamics
D, d	Particle diameter (m, mm or μm dependent on model)
d_{wn}	Weighted mass particle size for multi-sized particle slurry
E, ER	Erosion ratio, Erosion rate (differs depending on model)
EDAX	Energy Dispersive X-ray Analyser
F_s	Shape Factor
$F(\theta)$, $F(\alpha)$	Angle function
H_v	Target wall hardness (Vickers Scale)
LDV	Laser Doppler Velocimeter
m, n, p	Empirical exponents (specified as per model)
SEM	Scanning Electron Microscopy
U, V, v	Particle velocity/ Flow velocity (m/s)
UDF	User Defined Function
ρ	Density (kg/m^3)
α, β, θ	Impact angle (rad)
Target Material	EN3B/ AISI 1020/ 070M20
L-filter	Short Wavelength Pass Filter (waviness filter)
S-filter	Long Wavelength Pass Filter (noise filter)
Sa	Arithmetical Mean Height
S_{dr}	Developed Interfacial Area Ratio

Uni-sized, equi-sized, mono-sized used interchangeably

Chapter 1 INTRODUCTION

In the petrochemical industry, particularly in the exploration and extraction of crude oil, the nature of the reservoir fluid is almost always inherently multiphase. The composition of the flow is such that it may contain one or more of the following, sand/fines, gas or saline water. The integrity of oil pipelines and by extension the oil infrastructure is constantly at a risk of degradation due to both the harsh nature of the elements being transported, which can corrode the interior of the pipeline as well as the potential erosion of material, which can arise from the migration of solid particles and gas bubbles in the reservoir fluids. This chapter sets the scene for the research work being conducted, providing a general overview of the petrochemical industry, as it relates to the use of pipelines as a method of transportation, while also probing the elements of solid particle erosion investigation.

1.1 Oil and Gas Supply Chain

The petroleum industry as we know it today, finds its origins in the 1840's and 1850's, when the drilling of oil wells for commercial enterprise was established from the Black City of Baku (Azerbaijan) to the Oil Creek of north-western Pennsylvania in what is now the Oil Creek National Park [1].

The use and application of petroleum has been recorded as far back as the Jin Dynasty of 4th century China, and for centuries prior to this throughout Mesopotamia by the Babylonian empire for the purpose of road building. Its use in lubrication, heating, lighting and waterproofing of woven baskets were all recorded through the ancient world [2]. However, it wasn't until the period just following the industrial revolution which saw the development of distillation processes of fossil fuels for the production of lamp oil, and the use of steam engines for the purpose of drilling, that sparked the commercial industry we refer to as the petrochemical industry [3].

The commercialization of petroleum, relied on two symbiotic activities:

1. The extraction process – this is a multi-stage activity that involves:
    - Finding a suitable location where oil and gas deposits exist
    - The drilling of a well in order to tap into the oil and gas traps beneath the surface.
2. Refinement process – in its natural state crude oil is in and of itself not entirely useful, however, the distillation process allows for the crude to be separated into its various components which add the value to product.

Klass and Meinhardt describe one of the challenges faced in the North American and European context to be the distance between the areas of production and the urban centres where most of the resulting products of crude oil were used. As such, the transportation of this commodity became a central aspect of the industry [4]. In the early days of the industrial expansion of oil, it was captured and stored in barrels, and would be transported from the reservoir to the nearest railway line or waterway by horse drawn wagons. However, the increasing production of oil coupled with the poor and dilapidating infrastructure of the mud roads meant that this became untenable [5].

1.1.1 Pipelines Transport of Fluids

The use of pipelines for the transportation of fluids dates back centuries in the form of aqueducts used by the Romans and the Assyrian. The development of iron production by the end of the industrial revolution introduced the use of steel and cast iron for pipelines. By the 1850's, many cities employed the use of pipelines for water systems and gas distribution, paving the way to the use of pipelines for the transportation of oil [4].

Early pipeline systems were used to transport fluids in single phase, be it a liquid or gas, and as described by Miesner and Leffler, oilmen found the mixture of oil and gas a nuisance, and would resort to simply burning off the natural gas and pumping the oil [5]. The introduction of pipelines ushered in the obsolescence of the traditional barrels, horse drawn wagons and teamsters who would transport the barrels between the reservoir and the nearest rail head. This provided several advantages to the industry:

- It allowed for the continuous flow of oil, in contrast to the batch deliveries that were being made by barrels.

- For large volumes of oil, it represented a reduction in the operating cost despite demanding high capital investment
- With an increasing demand for crude oil and its derivatives, pipelines allowed for the expansion of the distribution network and wherever possible, provided a single method of conveyance directly to refineries.

The importance of oil pipelines is further cemented by the fact that it forms a principle aspect of the current oil supply chain in the form of long haul pipelines and short delivery lines, some of the notable lines can be seen in Figure 1-1 [6-8].

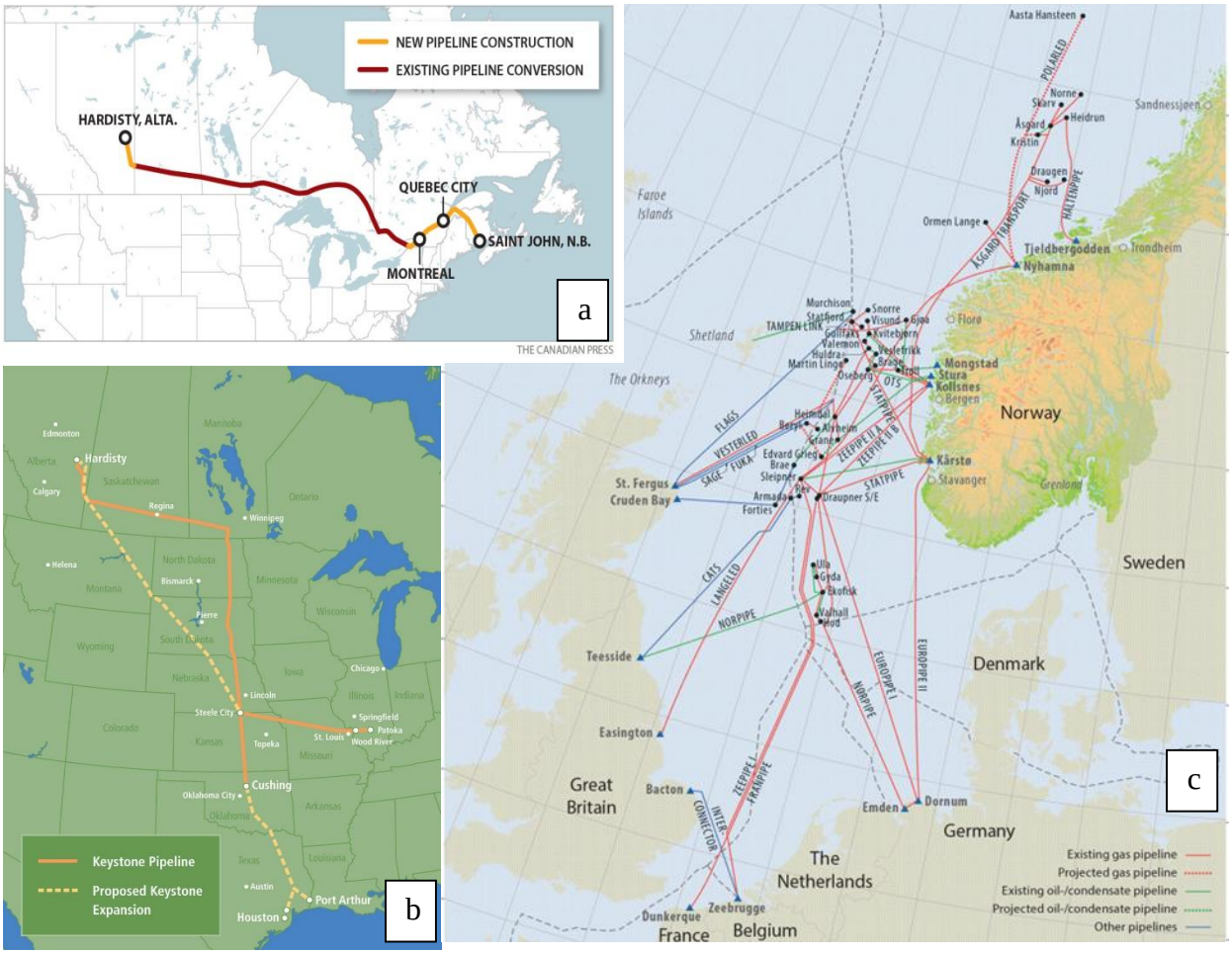

Figure 1-1 Maps displaying notable long haul oil and gas pipelines in North America and Europe (a) TransCanada Energy East Pipeline [6](b) Keystone pipeline [7] (c) Norwegian domestic and international pipelines [8]

1.2 Sand Production

Sand production is the introduction and entrainment of solid particulates into the fluid flow during oil extraction. It is caused when the strength of rock formations is exceeded by the pressures and forces exerted on them by the drilling and extraction operations. In order to prevent these particles from entering the bore, several methods are employed, one of which is standalone screens, these act as filters allowing the hydrocarbons to pass through while effectively sieving out the solid particles. Sand control describes all measures employed to minimize sand production [9].

When sand is produced, but fails to travel to the surface, it remains down-hole leading to a decline or stoppage in production. Down-hole build-up, is caused by flow velocities which are insufficient to transport the particles to the surface. Contrastingly, when the velocity is high enough, the sand fines travel up the bore, where the sand accumulates in surface equipment. This can be costly, as additional maintenance time has to be allotted, additionally the conveying of solid particles to the surface, could also lead to the erosion of both down-hole tubing and surface equipment [10].

1.3 Erosion

The oil industry has always grappled with the issue of solid particulates in the transport of fluids through pipelines. A great deal of work has been done in the industry to control the incursion of sand/fines into the flow, however despite best efforts, it has not proven entirely possible to completely eliminate sand production, consequently leading to the occurrence of solid particle erosion.

The term Solid Particle Erosion is used to describe the process by which small particulates breach the surface of a material, thus resulting in a loss of mass, as seen in Figure 1-2. Many studies have been conducted examining the parameters that govern the occurrence of metal erosion, both [11] and [12] provide comprehensive reviews of these parameters. The particle shape, size, density and hardness, the fluid velocity, temperature and flux, as well as the target wall properties, angle of impact and the velocity of particle at the point of impact are some of the factors affecting erosion rates.

Figure 1-2 Pipe bend with visible erosive wear due to solid particle impingement [17]

The process by which erosion occurs, and by extension the mechanisms of erosion have been the subject of many of the early studies. Finnie [13] outlines a model of erosion in which particles, when impacting the surface at low angles, cause micro-cutting. This continues until the material which has been cut away is dislodged from the surface of the target wall. Figure 1-3 displays an illustration of the proposed mechanism. In a follow-up study, Finnie [14] focused on developing the micro-cutting models further by analysing the behaviour of both ductile and brittle materials, when subjected to solid particle impacts.

Further works established that the mechanism described by Finnie was limited as it did not account for how erosion acts on a surface when the angle of impact of the particle is increased tending towards 90^{o}. In his 1963 study of erosion phenomena released in two parts, Bitter [15, 16] describes the principle mechanisms for erosion wear as being from the repeated impingement of particles resulting in both deformation and cutting of the target surface.

These understandings of the mechanisms of erosion have been developed and refined to facilitate the development of mathematical models for the prediction of erosion as will be discussed further in Chapter 2.

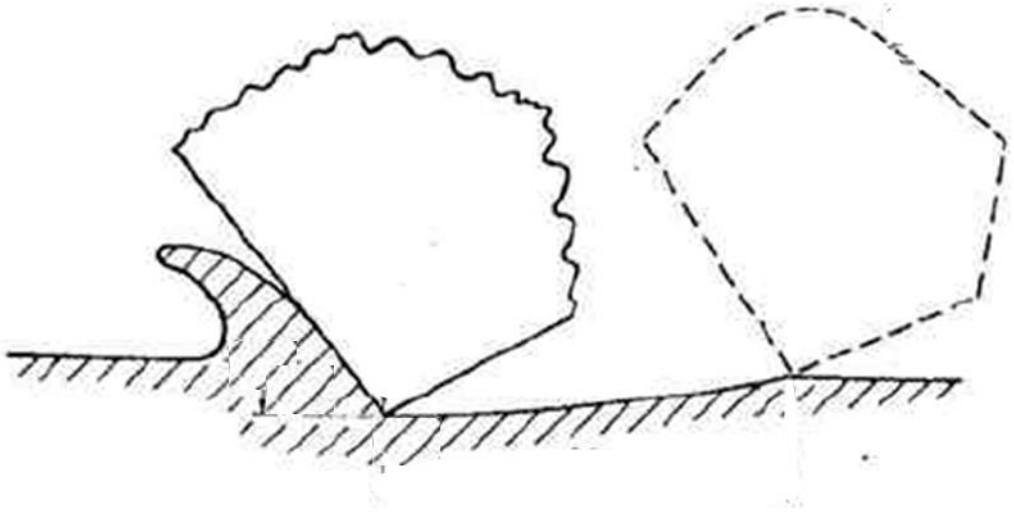

Figure 1-3 Micro-cutting of a target material by an abrasive solid particle [14]

1.3.1 Parameters in Solid Particle Erosion

The onset and propagation of erosion on a surface is influenced by a large number of factors, which fall broadly into three categories, fluid and flow properties, target wall material and particle properties. Understanding how these factors affect the erosion of a material are key in establishing the erosion rate under given conditions. The number of factors are so exhaustive that no one mathematical model has yet to account for all of the factors. Appendix I shows a table compiled by Mazdak et al [12], containing thirty-five physical characteristics utilized across twenty-three different erosion models. Though the list in Appendix I is extensive, it is not exhaustive. What can be deduced from the table however, is the lack of consideration given to flow variables in the models which have been developed.

1.3.2 Particle Size

Many studies have assessed the influence of the particle size on the mechanism of erosion, [11] and [18, 19, 20], are some of the works that focus on the effect of particle size. To a large extent, all agree on the concept of the erosion rate being proportional to a function of particle size. It has been found that erosion rate decreases as the particle size decreases, due to the particles susceptibility to being diverted around the target wall by the streamline of the flow, while larger particles are able to follow a more direct path to the target wall as illustrated in Figure 1-4 [21].

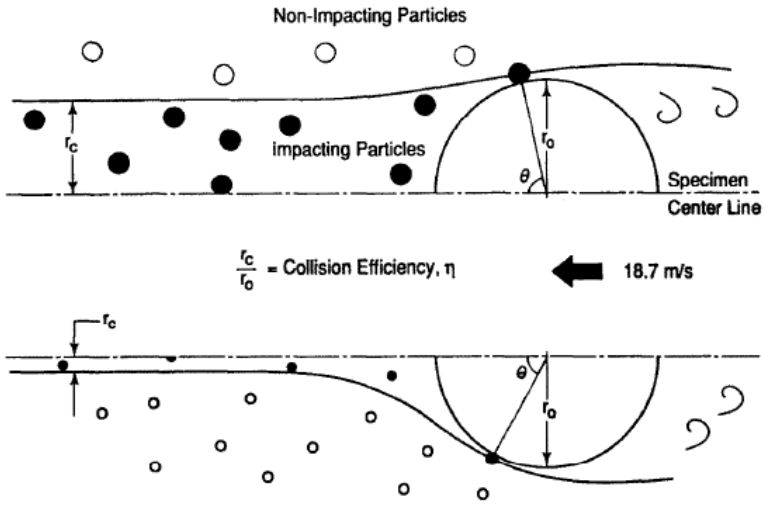

Figure 1-4 Effect of flow on particles based on the size of the particle [21]

Further work determined that erosion increases with the increase in particle size to a limiting size, from which the erosion rate then decreases as the particle size increases, graphically represented in Figure 1-5. This location of maximum erosion as a function of particle size has not been fully explored in literature, particularly for conditions of multi-sized particle diameters [22].

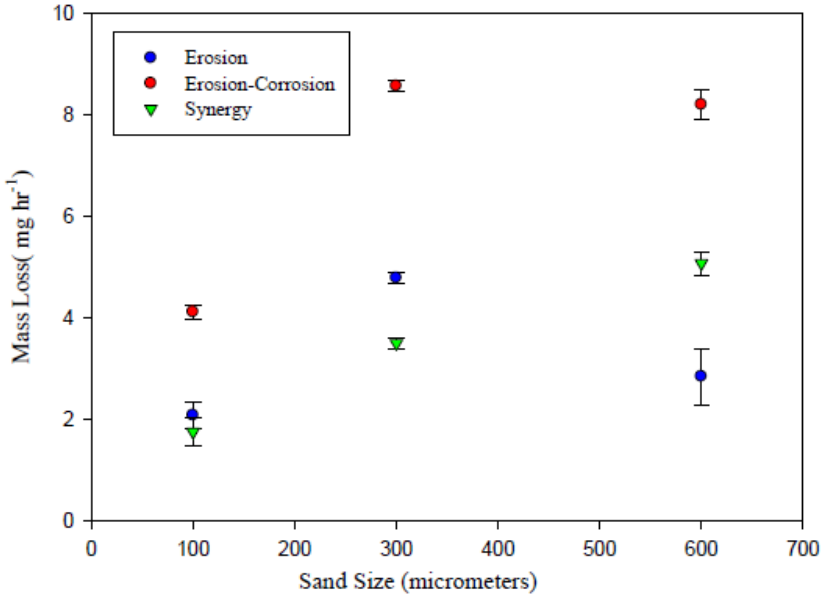

Figure 1-5 Variations in erosion and erosion-corrosion synergy with a varying particle size [22]

This phenomenon is not valid for all conditions, as such experimentation is required in order to predict the erosion rate curve as the particle diameter is altered, this is primarily due to the interdependence of the erosion variables. The behaviour of the erosion rate as a function of the particle diameter results in unconventional outcomes based on experimental conditions, as has been presented by Kleis and Kulu [11], through the curves displayed in Figure 1-6 and Figure 1-7, which cover a range of experimental setups. Figure 1-6 corroborates the findings of Rajaharam's study [22], and shows a general pattern in which the erosion curves all have the same profile, with the maximum wear rate (I_g), being measured between 0.2 mm and 0.4 mm, followed by a decline in the wear rate as the average diameter (d_m) increases further. What is detailed in the findings is the sharp decline in the erosion rate from the maximum when the velocities are increased (velocities 1-4 are 225, 166, 120 and 83 (ms^{-1}) respectively).

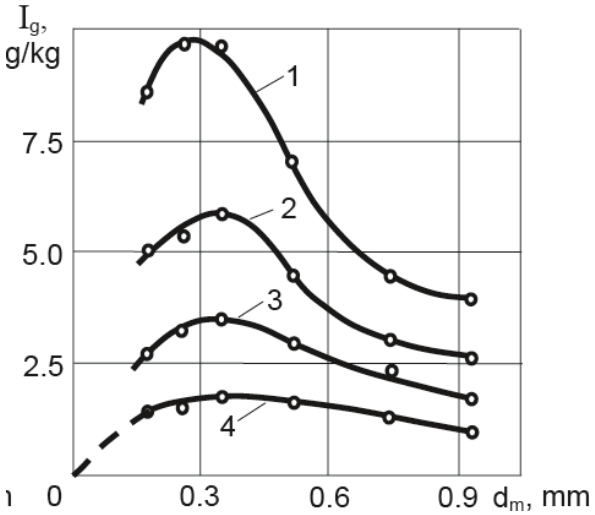

Figure 1-6 Wear rate versus particle size at 90° impact angle and four different particle velocities [12]

Kleis and Kulu [11] presented the results of two studies conducted using the same target material. The effect of changing the experimental setup results in varying responses in the erosion rate when plotted as a function of the average particle diameter. Figure 1-7(a) curve 1 uses sharp-edges cast iron pellets, 83 ms^{-1} at 30°, lines 2-4 all use spherical cast iron pellets, at 120 m s^{-1} 90°, 120 m s^{-1} 30° and 83 m s^{-1} 90° respectively. All present a fundamentally different pattern of wear rate. Figure 1-7(b) is a representation of the result of using a different testing method while maintaining the same target material, sand and velocity.

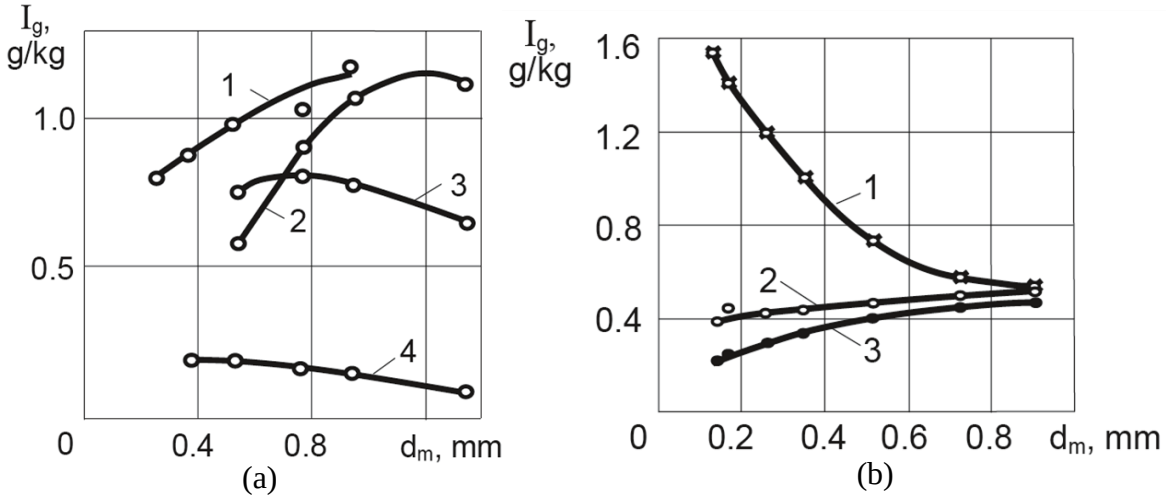

Figure 1-7 Wear rate as a function of diameter (a) 0.2% steel (130 HV) using 4 different erodents (b) sand, 0.2% C steel (130 HV) at 38° using three different erosion testing equipment [12]

1.3.3 Impact Angle and Shape

Early work done on the mechanism of erosion as referenced in Chapter 2 indicate that the process of erosion is highly dependent on the angle at which the particle impacts the surface of the wall. This gives rise to the two predominant mechanisms seen in the wear pattern of eroded material, namely direct impact which occurs at impact angles that tend towards normal, and abrasive wear which occurs at shallow impact angles.

In his book on tribology Hutchings describes the dependence which erosion by solid particles has on the angle of impact. The importance of the impact angle as a principle contributing factor in the erosion rate of metals can be deduced from Figure 1-8. The figure displays the typical behaviour of ductile materials by which the erosion rate increases to a maximum at angles between 20^o and 30^o, with the wear rate falling significantly at angles tending towards zero (0^o), and falling to less than half of the maximum erosion rate as the angle increases towards normal [23].

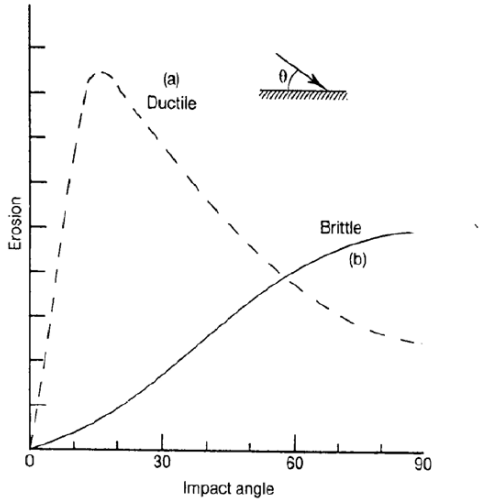

Figure 1-8 Variations in erosion rate as a function of impact angle for both ductile and brittle materials [23]

In experimental studies using particles in an aqueous environment, it is not entirely possible to govern the specific impact angle of the particles when interfacing with the target wall. This is a direct consequence of the flow field near the target wall, however, when employing the use of a test pot, this effect can be minimised through the use of flat bar as opposed to a cylindrical bar [24].

In practice a bulk slurry would contain irregularly shaped particles which may be clustered under all shape classifications. For any given impact angle, the degree and type of surface damage also differs as a result of the particle shape, and by consequence the manner in which the particle rotates about its own axis [25]. An angled particle rotating forward at impact results in a different quantity of material being displaced than is caused by a spherical (blunt) particle as seen in Figure 1-9.

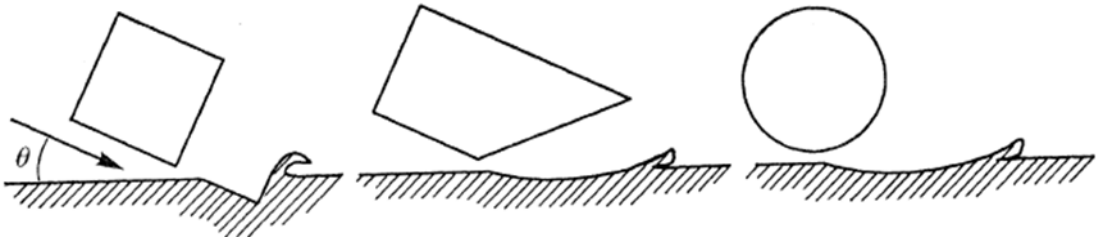

Figure 1-9 Mechanisms of erosion based on particle shape [25]

1.3.4 Particle and Fluid Velocity

The kinetic energy dissipation of solid particles as well as the erosion rate have been studied, and their relationship examined by Clark and Wong [26]. A proportionality was found between the particle velocity and the erosion rate. This relationship is described by equation (1-1) and graphically illustrated through Figure 1-10, which displays the volumetric wear rate against the particle velocity.

$$E = v^n \tag{1-1}$$

In equation (1-1), E represents the erosion rate, v is the particle velocity and n is a constant found empirically [14]. The value of n has been determined to be between 0.3 and 4.5 when assessing a wide assortment of research studies [12]. The exact behaviour of particles in an aqueous environment has not yet been fully understood. This was distinctly emphasised by Clark [19] through which the interdependence of the flow variables and their influence on the erosion rate, is highlighted as one of the major unknowns. It has been found that a change in the test speed of a bulk slurry has an effect on both the impact angle and the efficiency of the collisions, as a result, doubling the velocity does not always result in a doubling of the erosion rate.

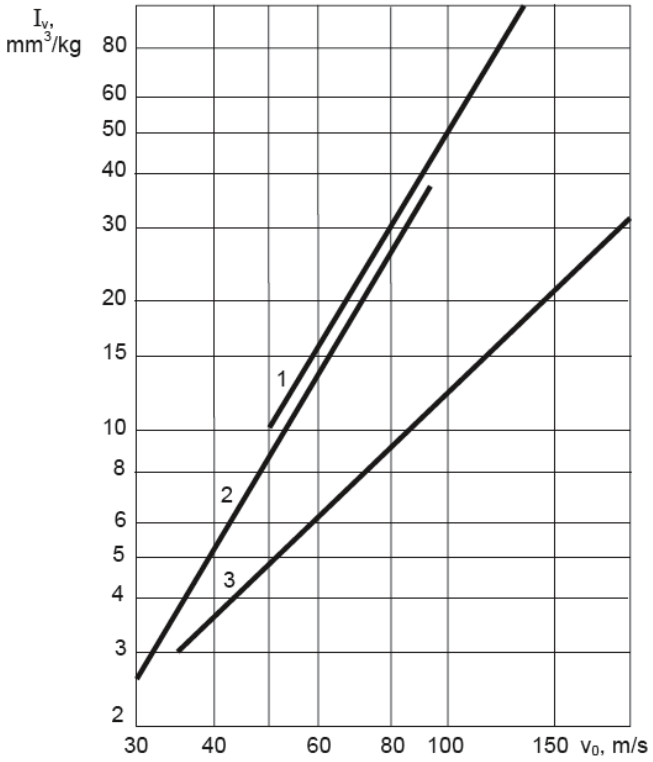

Figure 1-10 relationship between the particle velocity and the erosion rate under three test conditions [12]

The velocity of a solid particle in a fluid is assumed in many studies to be comparable to that of the fluid itself. However, the particle would be subject to drag force, particle-particle contact force and gravitational force, all of which would affect the particle velocity. Furthermore the velocity of the particle at the surface of the target wall is further affected by the squeeze film effect, which acts as a buffer layer on the material surface, potentially retarding the velocity, and thus the kinetic energy of the particle, as it penetrates this layer, prior to impacting the target wall [27].

1.3.5 Time Dependence

Of the key factors that contribute to solid particle erosion, most fall under two categories; they are either spatial in nature which includes the velocity and impact angle or they are material specific, including the hardness, particle size, particle shape, target wall ductility among a host of other factors. However, the temporal nature of this phenomenon also has a fundamental role to play in the rate at which the material degrades. Fry et al [28] states that the erosion rate increases with exposure time, however, this statement does not hold true for all conditions. A study by Rao and Buckley [29] provided a review of findings assessing the time dependent nature of erosion, and presented details of the distinct phases in the onset of erosion, as well as the three basic responses which are exhibited by materials.

The periods are classified as; the incubation period, this describes the stage where negligible mass loss occurs, the periods of acceleration and deceleration, and finally the attainment of a steady state as can be seen in the curves schematically shown in Figure 1-11(a). Steady state is at times described as maximum rate, however this can at times be less than the peak erosion rate as seen in Figure 1-11(b).

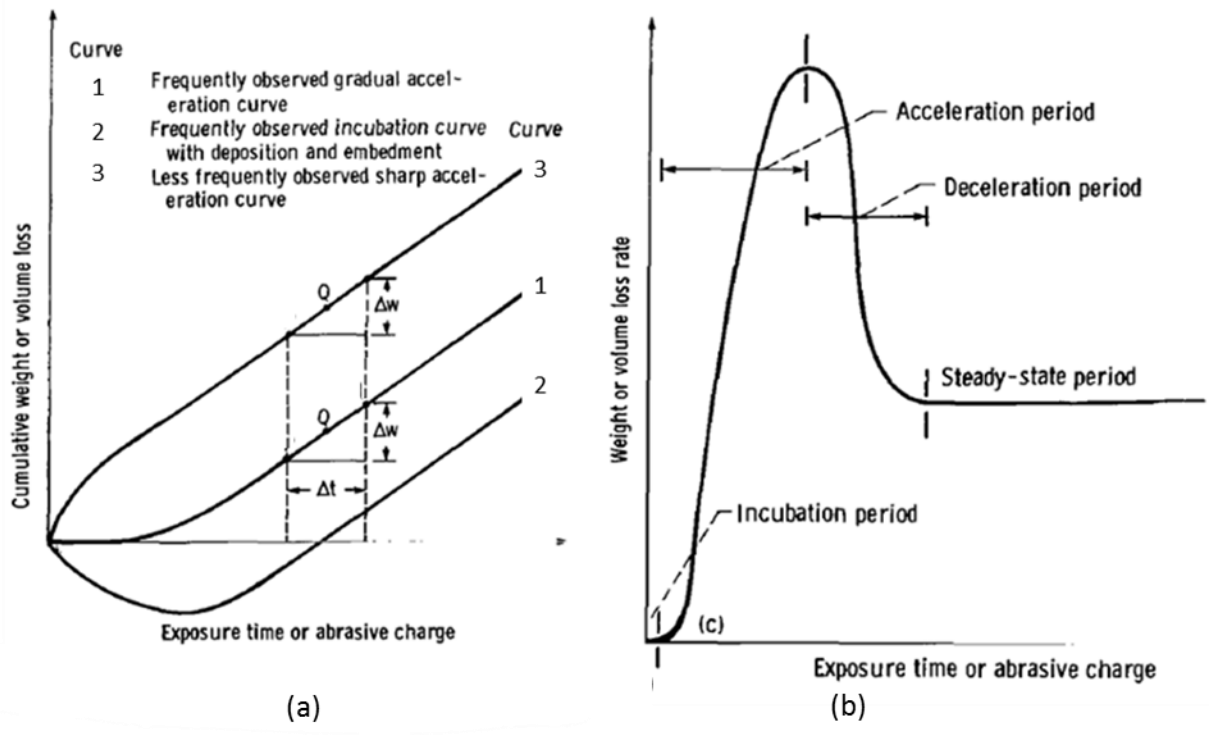

Figure 1-11 Variation in (a) Weight/volume loss as a function of time (b) erosion rate as a function of time [29]

A considerable number of literature describe both the exposure time and abrasive charge as interchangeable parameters as is seen in Figure 1-11. Tilly [30] states that steels have no discernible incubation period and as such arrive at a steady state condition from the onset. The studies reviewed in this work were largely conducted at relatively high velocities some in excess of 250 m s^{-1}. Young and Ruff [31] provided data that conflicts with the assertions of [30], and found the erosion rate of 304 steel to have a curve comparable to Figure 1-11(b) when plotted against the abrasive charge.

1.3.6 Particle Concentration

Solid particle concentration, also referred to as solid particle loading or flux, is a description of the quantity of particles in a given control volume, this can be described in terms of percentage weight or volume of the solid particles in the bulk fluid. The realm of this research will focus on dilute solutions that are classified as having mass loading of up to 10% by weight. Intuitively one may consider that as more particles are introduced to the system the erosion rate should increase, however this is not always the case as the relationship between concentrations is not a linear relationship. Turenne et al [32] outlines how the erosion efficiency (W/C), which is a ratio of mass loss to concentration of solid particle, changes as the concentration (C) changes. As the concentration increases, the erosion efficiency decreases to a steady state as seen in Figure 1-12. The study also offered that for a constant mass of erodent, the mass loss would be more for a concentration of 1% compared to that of 20%.

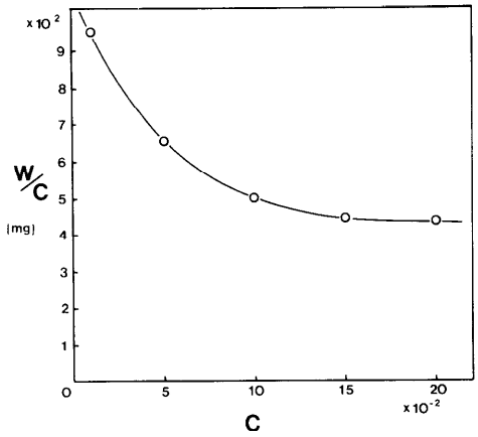

Figure 1-12 Erosion efficiency plotted against the solid particle mass concentration [32]

These findings are supported by a number of studies including that of Deng et al [33] that found the erosion rate at pipe bends to decrease with an increase in the particle flux as seen in Figure 1-13.

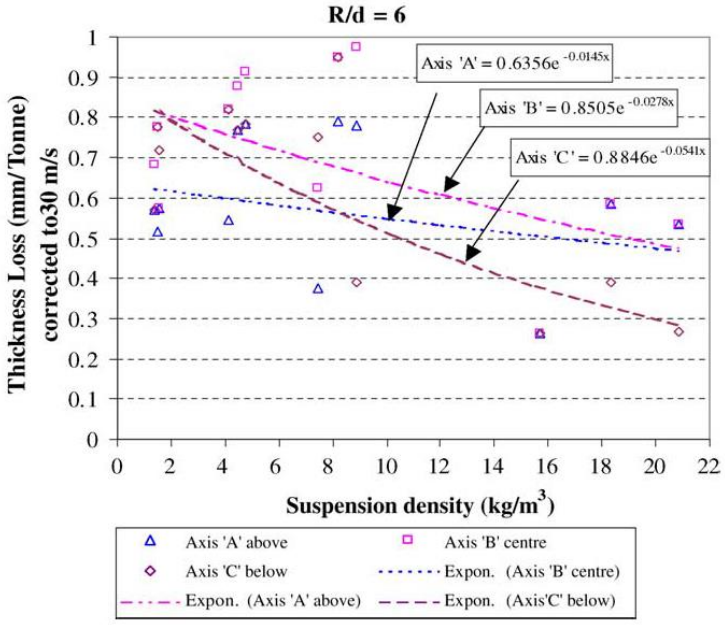

Figure 1-13 Thickness loss as a function of Solid particle concentration, for pipe bend radius of six (radius of bend over pipe diameter) [33]

1.3.7 Fluid Characteristics

The area of fluid characteristics, is one of the most underappreciated aspects of the factors contributing to solid particle erosion. Physical properties such as the fluid viscosity and density have a direct impact of the drag force acting on the particles, and hence the particle velocity. The temperature of fluid can have both a contributing effect through the softening of the surface of the target wall and protective effect through the formation of thicker oxide coatings at higher temperatures [34]. Furthermore, the flow characteristics, described by the flow regime, directly informs the particle motion. The motion of the fluid has to be considered from both a global and a local perspective. Parsi et al [12] states that the extent to which the flow impacts the erosion rate is influenced greatly by the geometry. Hence pipe bend and pipe tee experience a direct impact form of erosion, while in straight pipes erosion occurs as a result of low angle abrasive impingement, caused by turbulent fluctuations which divert particles towards the pipe wall.

Assessing the local parameters in solid particle erosion are further complicated as the flow conditions have an influence on both the local flux, and local particle motion, which could differ from the global order. As a consequence, the local impact angle, particle velocity and the effect of particle-particle interaction would be different than in the global flow [34].

Quantifying the effect of viscosity on the rate of solid particle erosion can provide crucial data towards understanding the gains that can be achieved when comparing factors like pumping power versus erosion in a pipeline system. Viscosity can be fundamentally described as a fluid's resistance to flow, as such it can be reasoned that an increase in the viscosity of a fluid would result in a decrease in the velocity of the particles [35]. Moreover, the squeeze film effect described in section 1.3.4 is further amplified [36].

Most studies being conducted have corroborating information regarding the decrease in erosion rate as the viscosity increases. However, a study carried out by Mansouri et al [37] demonstrates both increasing and decreasing erosion rates that vary depending on the impact angle of the particles, as can be seen in Figure 1-14.

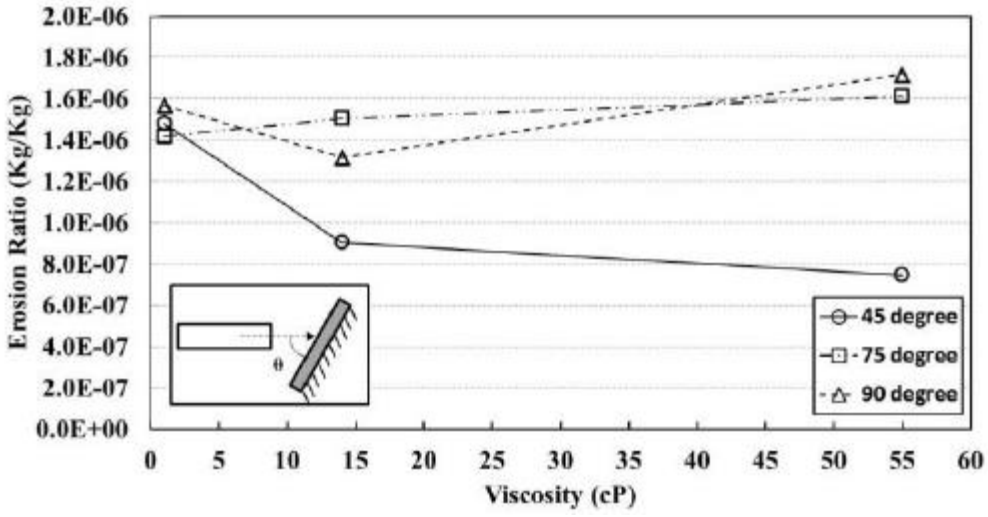

Figure 1-14 Erosion ratio as a function of viscosity at three different angles [37]

Due to limited studies into the effect of fluid temperature on the erosion rate, a consolidated concept has not yet been developed. A comprehensive study by Smeltzer, Gulden and Compton [38] found that the erosion rate decreased as a result of significant increases in temperature in a gaseous fluid. However, temperature was found to have a different effect which varied based on the target material, from this study, Sundararajan and Roy [39] describes three distinct categories of responses which a material exhibits in its erosion rate as a function of temperature, with a gas as the carrier fluid. Some metals follow a trend of decreasing erosion rate to a minimum, followed by an increase in the rate as the temperature increase. Another group of metals have a negligible response to an increase in temperature up to a critical value from which point the erosion rate increase and the final set display an increasing erosion rate as the temperature increase, with no critical value. Figure 1-15, provides a comparison plot of a wide range of materials and their respective curves.

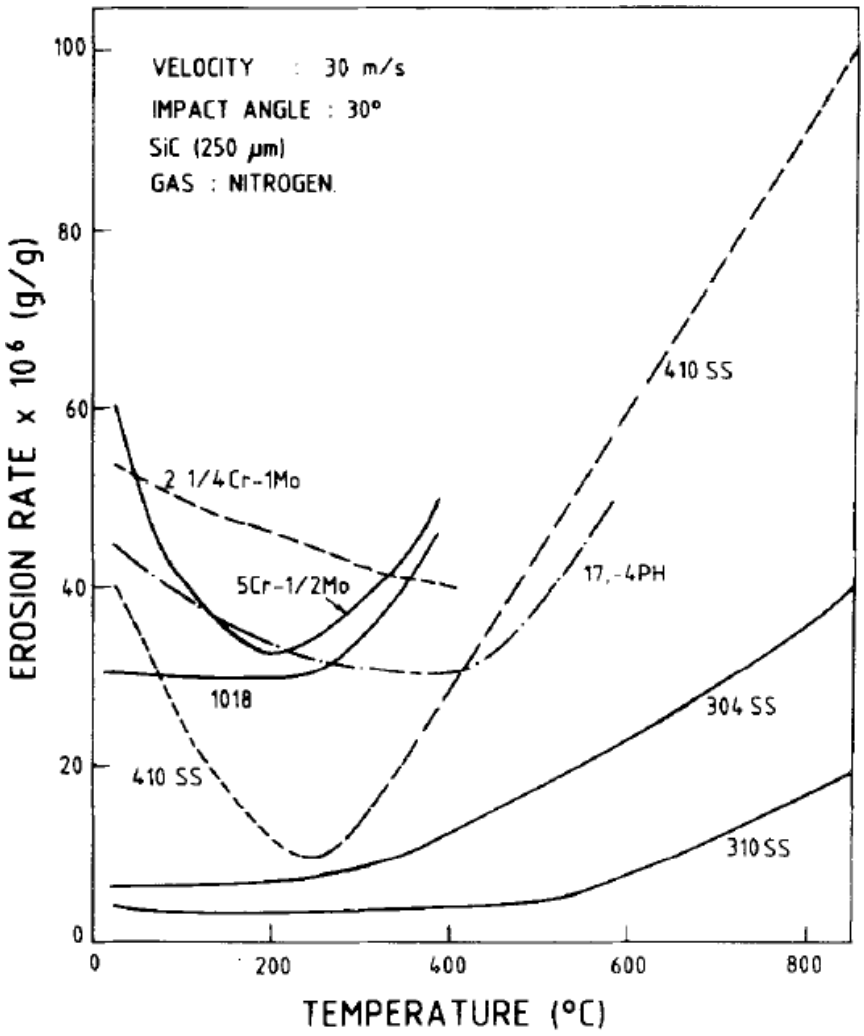

Figure 1-15 Variations in erosion rate against temperature for a range of different metals [39]

1.4 Methodologies of Erosion Research

This section provides a general overview of the techniques that have been employed in the examination of solid particle erosion; examining mature methodologies such as jet impingement experimentation, to newer approaches like the use of surface topography.

1.4.1 Experimental

The empirical nature of erosion studies, have resulted in a number of different rigs being designed in order to mimic a wide range of environmental conditions. The most common of these rigs will be discussed below.

In examining erosion of pipelines, investigators replicate a pipeline through the use of a scaled down pilot plant as shown in Figure 1-16. The use of a pipe flow loop allows for the geometric effects of pipe bend, tee and elbow to be evaluated while also allowing for the location of erosion wear due to particle stratification to be investigated. A pipe flow loop generally consists of a slurry tank and reservoir, flow control valves as well as horizontal and or vertical pipelines. Flow loops are not more widely used as they can be costly and require additional maintenance. Consideration also has to be given for the floor space which is required. This has been used in many studies including Mishra et al [40] and is used extensively by Alberta Innovates Technology Futures [41].

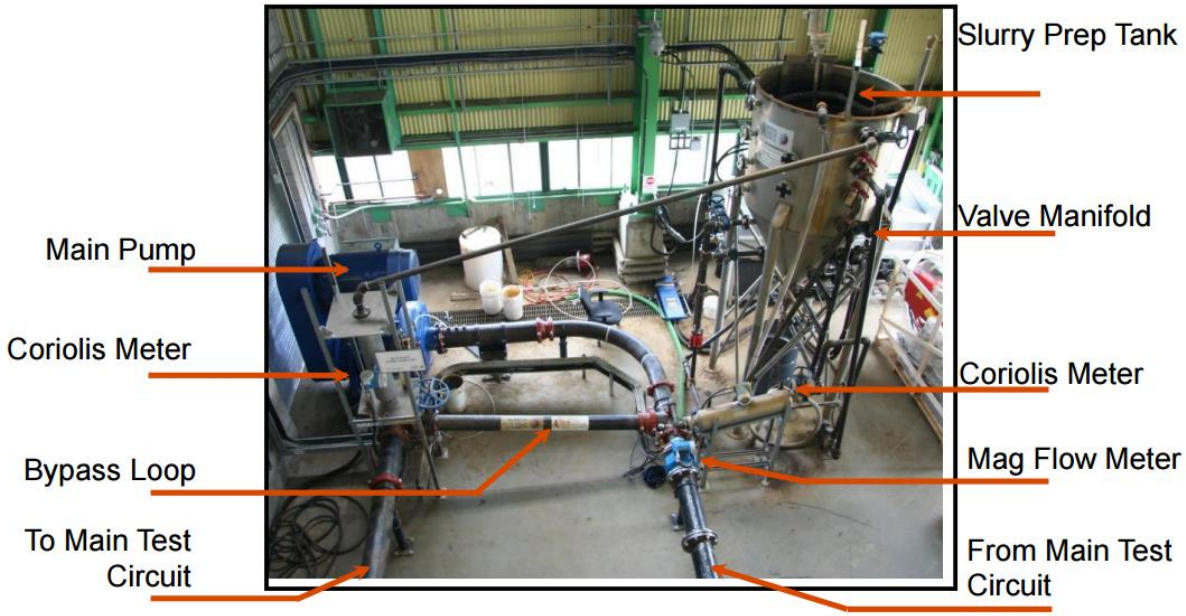

Figure 1-16 Flow loop [41]

Jet impingement rigs are another type of rig used in the study of solid particle erosion. In these rigs the solid particulates are introduced into a high velocity stream of air or water which then propels the particles towards target material. It provides several advantages, allowing both target material and erodent to be changed over relatively easily, while also giving the opportunity to conduct extremely high velocity tests. As jet impingement rigs do not recirculate particles, there is no adverse effect to the experimental erosion rate as a result of particle degradation. The schematic shown in Figure 1-17 is that of the jet impingement nozzle and the target material at angle α.

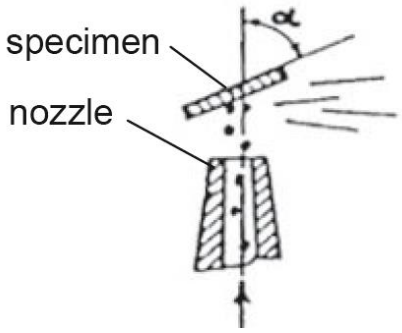

Figure 1-17 Schematic of the nozzle and target material of a jet impingement rig [12]

The slurry test pot is a simple and relatively cheap method of conducting solid particle erosion testing. Its basic configuration is a small tank, with a sample holder at the end of a shaft which is connected to a motor and variable speed drive which allows for the speed of rotation to be adjusted as necessary. Slurry test pots have been extensively used and have proven to provide good results under given conditions. Their operation is limited to relatively low speeds, when compared to jet impingement rigs and the recirculating nature of the mixture means that particle attrition is a major concern in experimentation. There have been several design modifications of the slurry pot tester made over the decades, however, basic principle remains the same. Slurry pot tester will be discussed extensively throughout Chapter 2 and Chapter 3.

1.4.2 Computational Modelling

The ability to use computational fluid dynamics in the prediction of erosion has been explored extensively in research. Chapter 2 of this work discusses many studies which have successfully used numerical analysis to predict erosion, many of which have been carried out alongside experimentation. One of the greatest limitations in erosion modelling is the nonexistence of a universal erosion model. Some of the widely accepted models used in literature have been briefly outlined below, with a general description of the parameters considered by the model compiled from [12], [42-46]. The general model, described by equation (1-2) is the general form of erosion prediction models proposed by a number of early researchers. In this model, V represents the particle velocity, f is a function of the impact angle and k and n are empirical constants.

$$ER = KV^{n}f(\theta) \tag{1-2}$$

Tulsa (E/CRC) angle dependent model represented by equation (1-3) is one of the most widely used models for determining the erosion rate of steels. In this model, Fs is the shape factor that defines the roundness/sharpness of the solid particles, C is a constant and BH is the Brinell hardness of the target material. Several models have been advanced from the E/CRC model with the value of n varying from one experimenter to another. The influence of the impact angle θ is determined by the angle function F(θ), which can take the form of equation (1-4), with the value of A being determined empirically or equation (1-5), which is the Mansouri angle function, which combines a modified Oka angle function with the Tulsa model.

$$ER = C(BH)^{-0.59}F_{s}v_{p}^{n}F(\theta) \tag{1-3}$$

$$F(\theta) = \sum_{i=0}^{5} A_{i}\,\alpha^{i} \;\text{ or }\; F(\theta) = \sum_{i=1}^{5} A_{i}\,\alpha^{i} \tag{1-4}$$

$$F(\theta) = A(\sin(\theta))^{n1}(1 + Hv^{n3}(1 - \sin(\theta)))^{2} \tag{1-5}$$

Another model developed is the Oka model which is a mechanistic model, shown in equation (1-6). This model considers the plastic deformation represented by the normal impact angle erosion, and the cutting erosive action by the angle function in equation (1-7).

$$ER = (10^{-9}\rho_{wall})E(\theta) \tag{1-6}$$

$$E(\theta) = K(Hv)^{k1}\left(\frac{V_p}{V^*}\right)^{k2}\left(\frac{d_p}{d^*}\right)^{k3}[\sin(\theta)]^{S_1(Hv)^{q1}}\{1 + Hv[1 - \sin(\theta)]\}^{S_2(Hv)^{q2}} \tag{1-7}$$

Tabakoff and Grant model for ductile materials presented in equation (1-8), is one of the few models to consider the restitution component of the particle angle and velocity. This is the resultant velocity and direction after impact. The angle function and velocity function for this equation are given by (1-9).

$$ER = K_1 f(\beta_1)(V_{1T}^2 - V_{2T}^2) + f(V_{1N}) \tag{1-8}$$

$$f(\beta_1) = \left[1 + k_2 k_{12}\sin\left(\frac{\pi\beta_1}{2\beta_0}\right)\right]^2 : \; f(V_{1N}) = k_3(V_1\sin\beta_1)^4 \tag{1-9}$$

The Det Norske Veritas DNV RP 0501 is an erosion model for ductile materials and has been proposed by DNV [47]. This model has been applied to include, the empirical values for titanium and fiberglass-GRP in addition to steel. The angle function is given in equation (1-11).

$$ER = K_s f(\alpha)\left(\frac{U_p}{U_{ref}}\right)^n \tag{1-10}$$

$$F(\theta) = \sum_{i=1}^{8} A_i\,\alpha^i \tag{1-11}$$

There are some general considerations that must be highlighted when evaluating predictive models:

- The erosion rate in existing models, is represented by a wide range of units, and it is not intuitive to compare results from one to another.
  - kg m^{-2} s^{-1} • mm yr^{-1} • m s^{-1} • m kg^{-1} • kg kg^{-1} • mm^3 kg^{-1}
- A large number of erosion models contain mixed units
- Some are made dimensionally sound by assigning an arbitrary unit to the material constant.

The Salama model, for predicting wear in pipelines, presented in Salama [48] and shown in equation (1-12), is an example of the use of mixed units in erosion model equations. In tyhis model, the erosion rate E_p is represented in mm kg^{-1}, The pipe diameter D (mm), particle diameter d (μm), velocity in m s^{-1}, density (kg m^{-3}) and the geometric constant S_p is assumed to be dimensionless.

$$E_p = \frac{1}{S_p}\frac{V_m^2 d}{D^2\rho_m} \tag{1-12}$$

Another such use of mixed units in a functional relationship between the variable parameters and the erosion rate, is the model presented by Gupta et al [49] shown in equation (1-13), and modified by Patil et al [50], as shown in equation (1-14). The erosion rate E_w represented in mm/year however, the dimensional units of V are in m s^{-1} and particle diameter in mm.

$$E_w = KV^{\alpha}d^{\beta}C_w^{\gamma} \quad (1\text{-}13)$$

$$E_w = KV^{\alpha}d^{\beta}\theta^{a}C_w^{\gamma} \quad (1\text{-}14)$$

In developing a new model, equation (1-6), Oka et al [44] and [45] describe the particle property factor K as a constant assigned with an arbitrary unit. This is also the case in the general model shown in equation (1-2). In this model the erosion rate is represented by the ratio kg/kg (i.e. mass loss of target material divided by the mass of particles impacting surface), in which the constant K is assigned the arbitrary units in the form of the inverse of the velocity function $(m\ s^{-1})^{-n}$, DNV GL [51].

1.4.3 Surface Measurement

Another method of determining the effect of solid particle erosion is to assess the damage caused to the surface using a metrological technique. Many studies evaluate the surface in order to determine the type of damage, and by extension, the mechanism through which erosion has occurred, evaluating the ploughing, cutting and deformation wear which the particles create on the target face. These mechanisms will be discussed in further detail in Chapter 2. Moreover, the surface can also be evaluated to determine the manner in which the particles affect the surface topography. Amongst other factors, the surface roughness can affect flow parameters in pipeline systems; the roughness has also been found to be a crucial factor in the development of corrosion [52].

A mechanical surface consists of three primary characteristics, the form, the waviness and the roughness. The form describes the general shape of the surface, examples of these could be the surface of a cylindrical object or a flat inclined surface. The difference between the waviness and the roughness is directly related to both the wave-length spacing as seen in Figure 1-18 and the practical application of the component [53, 54].

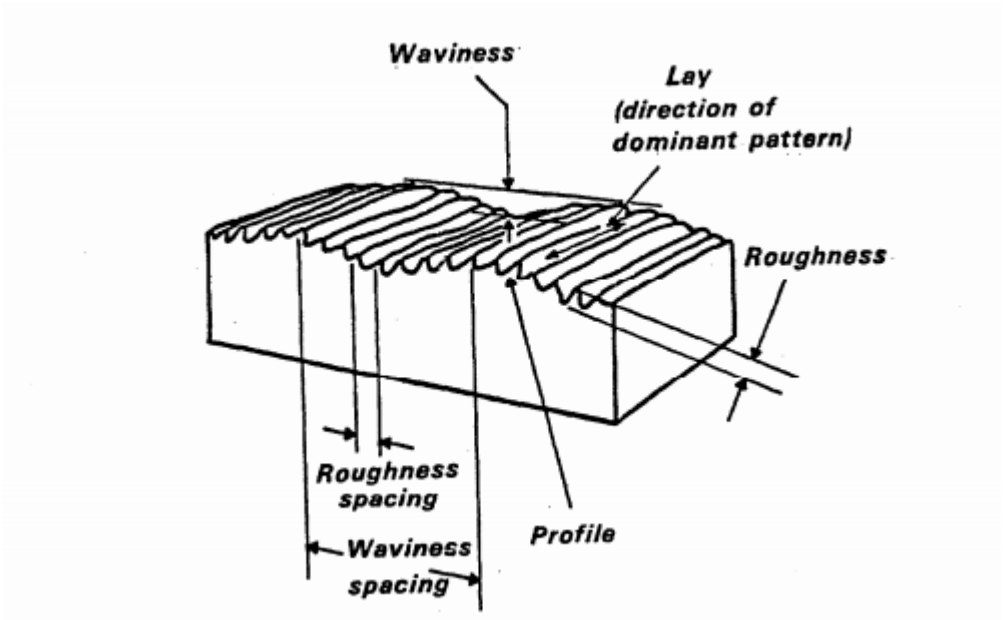

Figure 1-18 Surface characteristics and terminology [50]

The process of measuring a surface can be divided into three components:

- The fitting is the process by which the components shape is eliminated from the evaluation. The shape or form can be removed digitally, which is a tool that is available in post processing software, conversely this can also be removed by scanning an area small enough to eliminate the form wavelength.
- Filtering allows the waviness to be separated from the roughness, this is set by the cut-off wavelength. BS EN ISO 25178-3:2012 defines these values for aerial surface texturing.
- Thirdly is the method chosen for the analysis of the data captured, a vast quantity of parameters have been offered, the choice of parameter depends on the surface being analysed and the application for which the component is intended [55].

1.5 Motivation

The entrainment of solid particulates in the flow of oil/gas during the extraction process, creates a costly problem for the petroleum industry, as solid particle erosion can damage down-hole tubing, fittings, pipelines, valves and pumps. Furthermore, there are cost implications that can be attributed to production downtime, maintenance and damaged assets. In extreme cases, where erosion is occurring over an extended period of time, this could result in fatal safety and environmental problems, such as a blow-out and/or loss of well. The measures employed by industry are costly. The E/CRC [56], outlines some of these countermeasures to be the use of coatings, restrictions on production and limitation of flow velocities.

Although there has been a significant amount of work done in the field of erosion studies, there are aspect of research within this discipline that remain severely limited. The preliminary examination carried out in this undertaking has highlighted a number of key considerations. Firstly the study of solid particle erosion prediction, is highly dependent on empirical data. This is partly due to the large number of variables and factors contributing to the propagation of erosion. Secondly, there is still a gap in the understanding of the interdependence of the variables, and by extension how this interdependence changes with different target material and erodent combinations [12]. In particular, aqueous environments provide the preferred conditions for the enhancement of erosion degradation through the synergistic erosion-corrosion effect. Furthermore, as section 1.4.3 outlines, particle erosion directly impacts the surface topography, which in-turn can have implications on the fluid dynamics, as well as having an influence on the development of corrosion.

This work will explore aspects of erosion that are necessary in order to extend the understanding of this phenomenon. This will contribute to the ability of industries to predict erosion rate and develop predictive models for the improvement of systems susceptible to solid particle entrainment.

1.6 Research Aims

The aims set forth for this research study are specifically laid out below to ensure that the scope of work is planned in accordance with the established aims.

1. Analysis of solid particle erosion through a parametric investigation of the principle variables influencing material degradation.

2. Surface metrology based investigations of the surface texture morphology as a result of solid particle erosion.

1.7 Thesis Structure

This thesis is the written evidence of the body of work which has been carried out based on the research aims, and is divided into 6 chapters:

Chapter 1 sets the scene for the work being conducted, providing a general background of the petrochemical industry in relation to the use of pipelines as a means for conveyance. There is also an outline of the principle parameters identified in the propagation of solid particle erosion. Additionally, the research motivation and the success matrix, in the form of the primary aims, have also been outlined.

Chapter 2 comprises a detailed literature review covering a plethora of published works focused on the assessment of particle erosion. The literature review provides details of experimentation conducted, as well as the development of erosion models covering a period of over five decades. Moreover, the specific research objectives of this work have also been stated in this chapter.

Chapter 3 provides a detailed description of the approach taken in carrying out the current study. It outlines the experimental methodology and offers justification for the experimental process. This chapter describes the experimental setup and the equipment used along with an outline of the materials which have been selected for the erosion testing. It also provides details of the post experimental methods used to capture the results.

The details of some of the principle erosion parameters and their effect on the erosion rate have been presented in Chapter 4. This chapter investigates the influence of velocity, particle size and exposure time on the erosion rate of the target material. This chapter also offers a modified erosion model which includes the influence of particle size as an influencing prediction parameter.

Chapter 5 details the approach taken in investigating the morphology of the target material surface texture. It provides a description of the manner in which the material surface responds to being eroded in an aqueous environment. It outlines the manner in which surface texture changes based on changes on particle size, flow velocity, time and impact angle.

A full description of the realisation of the research aims, as well as a summary of the achievement of the research objectives, has been presented in Chapter 6. This chapter also gives a summary of the limitations of this work and a set of recommendations for future work.

The following chapter details the literature review which has been conducted in the field of solid particle erosion.

Chapter 2 LITERATURE REVIEW

In order to get a full understating of the current state of solid-particle erosion research, a detailed review of published literature has been presented. This chapter offers a chronological approach to the development of erosion research and an evaluation of the potential gaps that exist in this field of study. In an effort to achieve the established research aims, the scope of the research has been defined and a list of objectives identified based on the evaluation of the literature survey.

2.1 Mechanisms of Erosion

Bitter [15] addressed the theory of material erosion through the mechanism of repeated deformation. Bitter developed a mathematical model for the prediction of wear through the mechanism of deformation, derived from the St Venants theory of elastic wave propagation in two colliding bodies and the balance of energy equation. Bitter [15] determined that the energy required to subject the material to plastic deformation is proportional to the mass (M) of the impacting particle, and developed equation (2-1). In which K is the velocity component required to initiate erosion and is generally considered to be zero for ductile materials, δ is the specific energy for deformation (J mm^{-3}).

$$W_D = \frac{1}{2}\frac{M(V_p \sin\alpha - K)^2}{\delta} \tag{2-1}$$

Bitter [16] further focused on the mechanism of cutting wear erosion which predominates the material degradation process when the impact angle of the impinging particle is small. For cutting to occur bitter suggest that both a perpendicular velocity and a velocity parallel to the material surface act in concert to create a penetrating and scratching action on the surface of the material. Two equations were developed based on two possible conditions: in which the particle continues to have a horizontal velocity after impact, the other in which the particle's horizontal velocity tends to zero, that is, all of its kinetic energy in the parallel is absorbed upon impact.

The study further suggests that material erosion is a combination of both plastic deformation and cutting, with the predominating mechanism being determined by the angle of impact and the material ductility and can be determined through the following equations.

$$W_{c1} = \frac{2MC\,(V\sin\alpha - K)^2}{\sqrt{V\sin\alpha}}\left(V\cos\alpha - \frac{C(V\sin\alpha - K)^2}{\sqrt{V\sin\alpha}}Q\right) \tag{2-2}$$

$$W_{c2} = \frac{\frac{1}{2}M\left[V^2\cos^2\alpha - K_1(V\sin\alpha - K)^{3/2}\right]}{Q} \tag{2-3}$$

A study by Neilson and Gilchrist [57] looked at both analytical and experimental approaches to solid particle erosion, the experimental work set out to simplify the mathematical models developed by [15, 16], while seeking to correlate the analytical work to experimental data. The experimental setup used aluminium oxide (210 μm) and glass sphere (475 μm) particles, to bombard a selection of sample materials: Aluminium, Glass, Perspex, and Carbon (graphite plates).

The study assessed how changes in the angle of attack, velocity and particle properties specifically shape and hardness affected the erosion rate of a material, based on the material properties. The work carried out, allowed for the development of two models, equations (2-4) and (2-5), of erosion wear which revolve around the particle having either a small or a large impact angle, in which ϕ and ε are constants representing the cutting and deformation wear respectively.

$$W_1 = \frac{1/2MV^2\cos^2\alpha\ \sin n\alpha}{\varphi} + \frac{1/2M(V\sin\alpha - K)^2}{\varepsilon} \qquad \alpha < \alpha_0 \tag{2-4}$$

$$W_1 = \frac{1/2MV^2\cos^2\alpha}{\varphi} + \frac{1/2M(V\sin\alpha - K)^2}{\varepsilon} \qquad \alpha > \alpha_0 \tag{2-5}$$

The study correlated work done previously, finding that there were two forms of erosion which contribute to the overall wear of the surface; deformation and cutting wear. The study unearthed some key factors that had not been previously considered; at a normal impact angle with speeds of 120 m s^{-1} to 192 m s^{-1} the aluminium sample experienced a gain in mass due to the deposition of aluminium oxide on the surface before surface degradation begins as seen in Figure 2-1. It further recognises that a reduction in the impact angle resulted in a large weight loss for the same number of impacting particles.

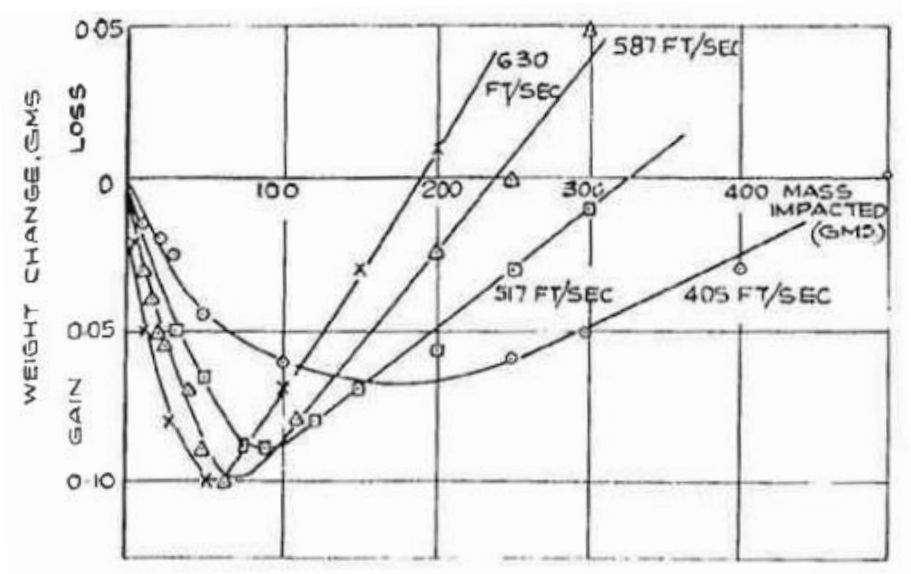

Figure 2-1 Weight change of an aluminium sample as a function of impacting mass of aluminium oxide particle at a normal angle of impact and vary speeds

Hutchings and Winter [58] conducted experiments to analyse the mechanisms of damage that result in metallic erosion. The experimentation used spherical steel balls of 9.5 mm to impact a metallic surface at velocities that ranged from 100 m s^{-1} to 356 m s^{-1}. The studies determined that the impacting particle creates a crater on the surface of the material, the resultant is a trifold cascade of events:

- Some of the material adheres to the surface of the impacting particle due to adhesive forces between the impact wall and the particle.
- Some of the disturbed material is entirely removed from the surface.
- The remaining disturbed material is left as an overhanging wave like formation.

In a study presented at the Royal Society of London, Hutchings et al [25] present further findings from the study. Figure 2-2 shows the manner in which the surface was damaged based on different impact angles between 10^{o} and 35^{o}. The study is purely based on analysing the erosion mechanism on a ductile material using single impact scenario to determine mechanism of damage, specifically focusing on the damage caused by spherical impact particle. There was no consideration for other parameters such as different particle shape or size, nor was repetitive bombardment analysed.

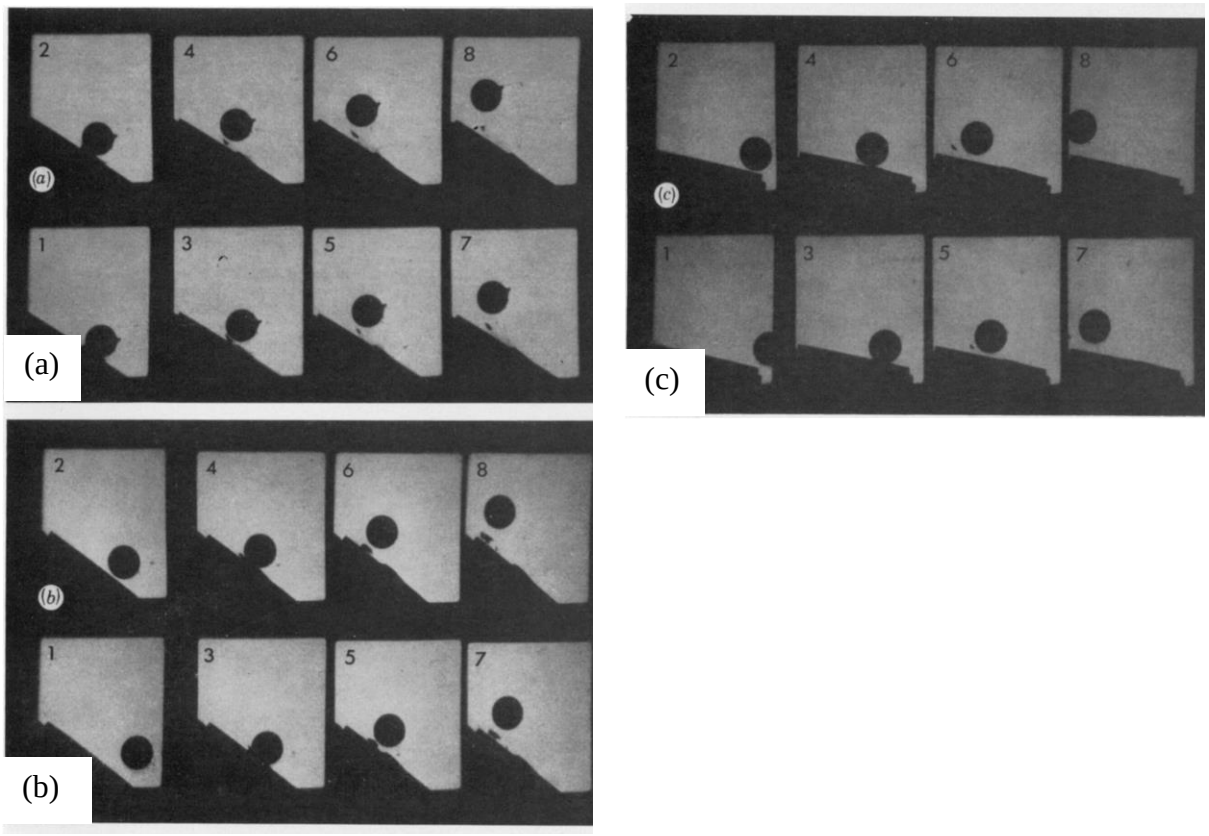

Figure 2-2 High speed camera images of a spherical particle impact on the surface of a metal. At angles of (a) 30^{o} (b) 35^{o} (c) 10^{o} [25]

Andrews [59] conducted numerical studies on solid particle erosion mechanisms in ductile materials. The results of the analysis focused on improving erosion prediction models through the concept of impact zones, which allows for the flux of the particles to be taken into account. The mathematical model highlights two limits necessary for the initiation of erosion namely:

- A minimum number of particle impacts must occur
- A minimum frequency of particle impacts must occur within the impact zone

These limits, Andrews [59] suggest are the main drivers behind the incubation time between particles striking the surface and the onset of metallic erosion, as was shown by Neilson and Gilchrist [57] in the initial weight gain of aluminium. The model does not take into consideration the medium in which the particles are suspended, nor does it consider the potential interaction between particles as the flux increase.

Bellman and Levy [60] conducted an experimental study on the mechanisms of solid particle erosion, in ductile metals using the sequential erosion technique. The study aimed to observe the process of erosion under more realistic erosion conditions, using multi-impact method as opposed to the single particle impact approach which had been previously investigated. This investigation, employed the use of a jet stream to deliver particles of silicon carbide at a rate of 0.1 g s^{-1} to an aluminium surface at a velocity of 30.48 m s^{-1}. An outline of a combined mechanism for erosion is presented including the effect of particle rotation on the angle of impact, however the study did not take into account the effect that the particle medium would have on the impact rate or impact angle on the surface of the metal.

A study carried out by Salik and Buckley [61] on the effect of mechanical surface and heat treatments on the erosion rate, revealed two essential findings. The study used two distinct type of erosion particles; round particles in the form of glass beads and crushed glass with sharp edges. These particles, bombarded the surface of aluminium 6061 samples with the graphical results shown in Figure 2-3. The study determined that the mechanical surface treatment and the surface roughness had minimal impact on the erosion rate. The discussion offered that this finding, could be as a result of the initial erosion that wears down the first layer of material. The study further established that the wear rate resulting from the impingement of the crushed glass was far greater than that of the glass beads, highlighting the fact that the particle shape is a major variable in the propagation of metal erosion. There was no measurement of the flow rate or speed of the particles in this evaluation.

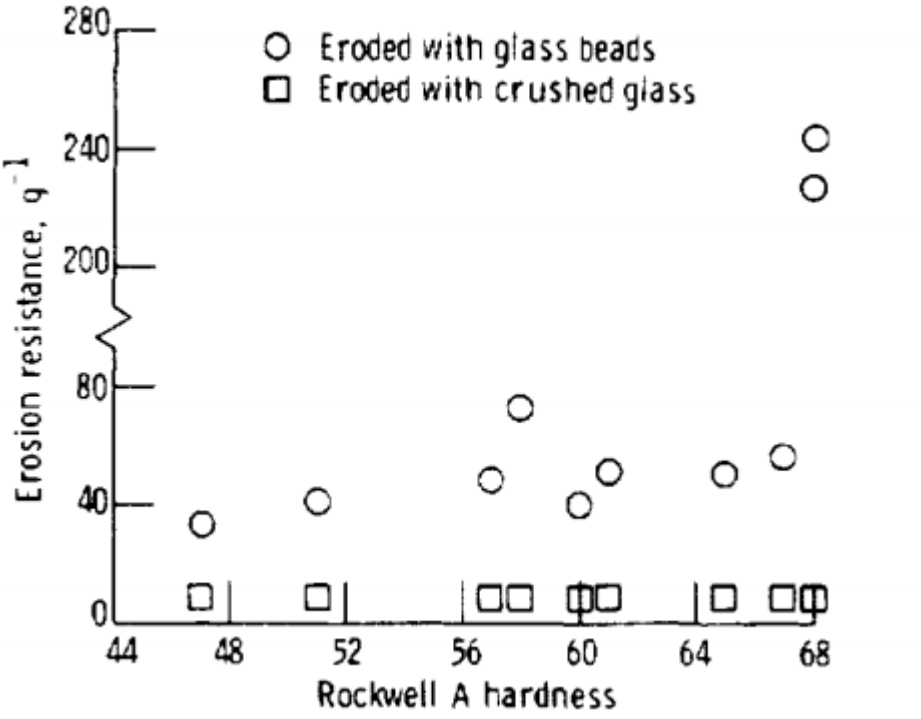

Figure 2-3 Graphical representation of the erosion resistance against the hardness of the target wall when eroded by crushed glass and the glass beads

Andrew and Horsfield [62] carried out an experimental study to assess the particle-particle interaction during the erosion process. This was theorised as a possible reason for the apparent decrease in the erosion rate seen in earlier works. The study found that in the low flux range (this range was not defined), the reduction in the erosion rate cannot be attributed to collisions between particles, as insufficient collisions occur when particles are projected at a target in a free stream of air. The study did not assess the effect of inter-particle collisions at high flux, the study also did not extend to include other mediums of particle transport.

The experimental work conducted by Rickerby and Burnett [63] focused on the erosion of titanium nitrite coated metals. The study assessed the effect of glass beads (blunt) and alumina grit (angular) on both a thin layer (1 µm) and a thicker layer (10 µm) of TiN on samples of stainless steel and mild steel. The results outlined the effect of the erodent shape on the surface coating and determined, that the thicker coating of TiN was more readily damaged by the blunt erodent than the angular alumina grit. When compared to the study by Salik and Buckley [61], this finding shows that the coating responds in the contrasting manner to the uncoated surface when evaluating the erosion rate as a function of particle shape.

Time dependent analysis of particle erosion, have predominantly been assessed in high velocity applications through the use of jet impingement rig. In these tests, surfaces are generally only exposed for a relatively short duration of time. Rao and Buckley [29] suggest that significantly lower flows and particle velocities may require longer erosion test time in order to achieve a steady state of erosion rate. A study by Randall, Clark and Wing [21] graphically mapped out the response of P110 Steel, which is an API high grade steel, in a viscous environment being eroded by Silicon Carbide (SiC) particles. The resultant graph when plotted against the exposure time, clearly shows a changing gradient within the time intervals evaluated. As such the assertion made by Tilly [30], that steels attain a steady state of erosion rate immediately, depends largely on the exposure conditions.

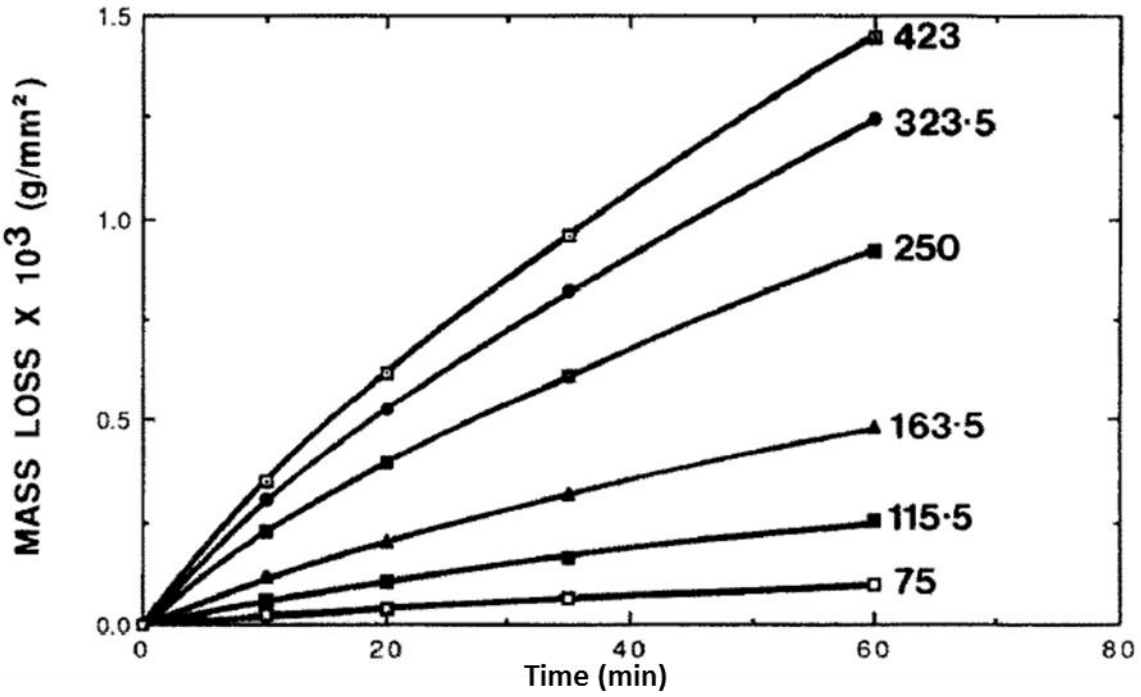

Figure 2-4 Time based progression of mass loss per unit area for P110 steel in diesel oil eroded by 1.2 wt.% SiC at 18.7 m s^{-1} [21]

2.2 Predictive Models for Erosion

Gupta et al [49] carried out a two-part slurry erosion study, in which an erosion test pot was used to examine the erosion rate, while a flow loop was employed to predict the location of wear for both steel and brass. The test pot evaluation, was carried out using three parameters, flow velocity from 3.92 m s^{-1} to 8.06 m s^{-1}, solid particle concentration of 15% and 25%, as well as particle sizes of 112.5 µm and 223.5 µm. A thorough discussion was outlined for the prediction of wear based on velocity, particle size and concentration. A plot of the results obtained for the wear of brass is shown in Figure 2-5. Using equation (2-6), which describes the functional relationship of these three parameters to the erosion rate, a regression analysis was used. The method of least squares was applied to the experimental results in order to determine the values of the empirical constants k, m, n and p. This was completed for the prediction of erosion wear in both brass and mild steel under the given conditions. These equations are shown below (2-7) and (2-8). This study did not assess the effect of multi-sized slurry on the erosion rate, nor did it discuss the potential impact of exposure time. Moreover particle attrition, in the recirculating rigs was also not evaluated

$$E_w = kv^m d^n C_w^p \tag{2-6}$$

$$E_{w\,brass} = 0.178V^{2.4882} d^{0.291} C_w^{0.516} \tag{2-7}$$

$$E_{w\,mild\ steel} = 0.223V^{2.148} d^{0.344} C_w^{0.556} \tag{2-8}$$

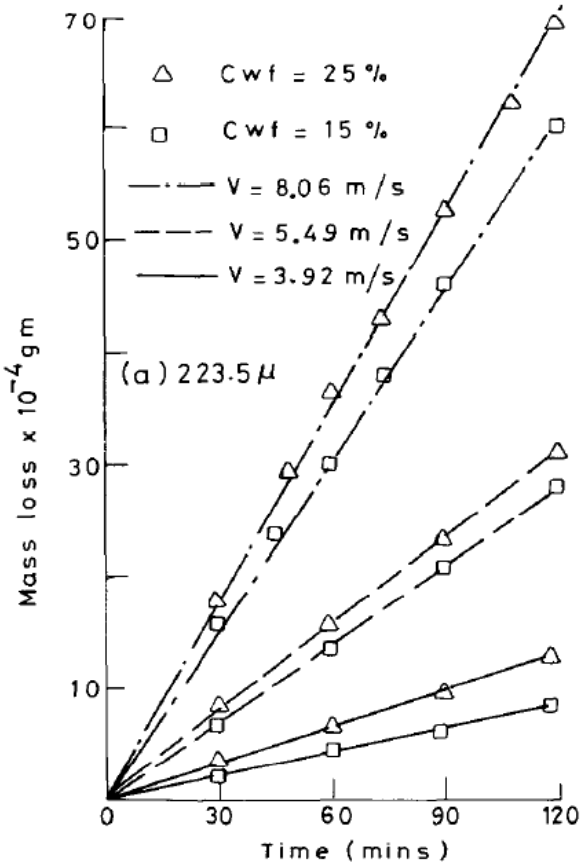

Figure 2-5 Mass loss of brass as a function of time, eroded by tailings from copper mine [61]

A study carried out by Clark and Wong [26] assessed the effect of the angle of impact and the particle energy on erosion of a range of brittle materials, ductile materials and polymers using Silicon Carbide as the erodent. The study was conducted at speeds of 9.35 m s^{-1} and 18.7 m s^{-1}, with particle size ranging from 136 µm to 772 µm. Cylindrical samples were used with the leading 180º providing the reference for the impact angles from 90º to 0º. The total wear was discussed in terms of the individual contribution of deformation and cutting wear. Using the mathematical model offered by Bitter [15, 16] equation (2-1), to predict the deformation wear and associated energy, a thorough discussion was presented, detailing the specific energy required to erode an array of different target materials. In an earlier study Lynn, Clark and Wong [21] assessed the effect of particle size on erosion rate, for particle sizes between 20 µm and 550 µm. Results were offered, on the change in erosion efficiency, erosion rate and impact velocity as a function of the particle size. Both of these studies were conducted using dilute slurry in a diesel oil viscous medium, with equi-sized particles. Neither study assessed the impact of multi-sized particle slurry, nor how the erosion rate would be impacted in a less viscous medium.

Clark [64] conducted a comparison study, of solid particle erosion in different fluid mediums, specifically gas (air) and liquid (diesel oil). Both investigations were conducted in an erosion test pot with the configurations displayed in Figure 2-6. The discussion provided a thorough analysis of the damage mechanism, based on the velocity and angle of impact of the particle. A direct comparison was presented between the flow velocity and particle velocity for both mediums. However, the study is limited to assessing a single particle size, of the glass bead erodent.

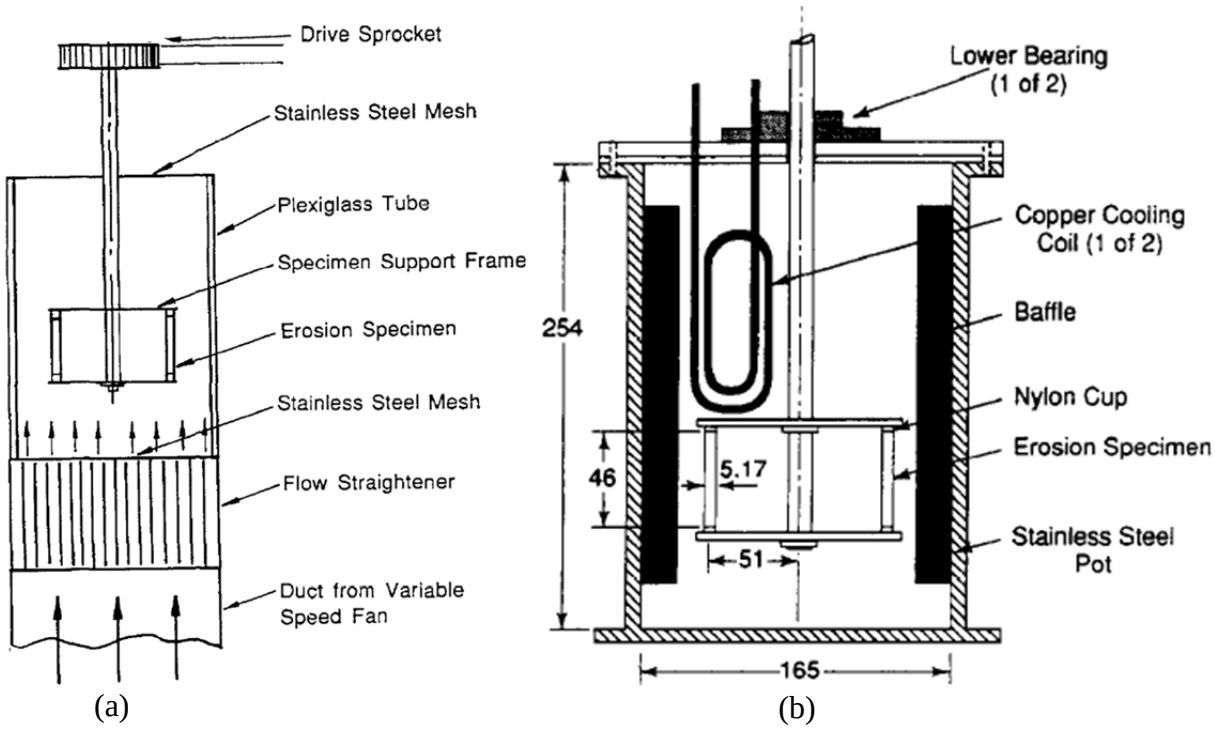

Figure 2-6 Schematic of erosion test rig for air suspended (a), and oil suspended particles (b) [21]

Mishra et al [40] carried out an experimental study to investigate the characteristics of solid particulates in a liquid medium at long radius pipe bends. The work focused on determining the distribution of multi-sized, solid particles (zinc tailings) at the pipe bend and the manner in which the change in the outer radius of the bend affect the solid distribution and by extension the erosion rate. A detailed discussion was presented outlining the distribution of particles based on size and deposition speed at varying bend radii. The study does not present details of the impact angles nor does it assess particle shape as a parameter.

Edwards et al [65] undertook a study of solid particle erosion in elbows and plugged tees, using Computational Fluid Dynamics, through a solver commonly known as CFX. This study allowed for the assessment of both direct impingement and indirect impingement, caused by the momentum of the fluid carrying the particle into the target wall, and the turbulent fluctuations within the bulk fluid flow respectively. Moreover, this study improved on previous works by including the effect of the squeeze film as well as both the normal and tangential restitution effect to the particular velocity upon rebounding from the target wall. The discussion, provides a quantitative comparison of the erosion rate and location of maximum erosion for three configurations; elbow, long radius elbow and plugged tee. The erosion ratio model employed, represented by equation (2-9), (2-10) and empirical constants in **Error! Reference source not found.**, does not take into account the influence of particle size on the erosion rate.

$$ER = AF_s V^n f(\theta) \quad (2\text{-}9)$$

$$f(\theta) = \begin{cases} a\theta^2 + b\theta & \text{for } \theta \leq \alpha \\ x\cos^2\theta \sin\theta + y\sin^{-1}\theta + z & \text{for } \theta > \alpha \end{cases} \quad (2\text{-}10)$$

Table 2-1 Empirical constants for carbon steel erosion model in equation (2-9) and (2-10) [65]

Constant	Value
A	$1.559B^{-0.59}x10^{-7}$
α	π/12
a	-0.384
b	0.227
x	0.03147
y	0.003609
z	0.02532
n	1.73

Desale et al [66] carried out a study to improve the performance of the slurry test pot. This focused on determining the optimum configuration for particle dispersion while also assessing the effect of solid particle erosion as a function of impact angle and particle concentration. Previous configurations of the test pot attached a butterfly propeller to the main shaft that holds the samples. However, it was found that a separately installed pitched blade turbine operating in a down-pumping, counter rotating manner provides the best particle distribution while also minimising the relative radial velocity between the particle and the specimen. The effect of particle attrition was evaluated through the erosion of AA6063 by uni-sized silica sand (550 µm). It was found that changing the eroding mixture every hour has the least adverse effect on the erosion rate, while running a specimen in a mixture for a period of 4 hours unchanged results in a lower erosion rate. This study did not quantify the mass loss of the erodent over the time intervals, as such the actual effect of attrition at the one hour time period was not assessed.

Gandhi et al [67] conducted experimental investigations on the dependence of erosion wear on three parameters; velocity, particle size and solid concentration. The study was focused on the erosion damage in parallel flow, for velocities ranging from 3.2 m s^{-1} to 8.18 m s^{-1} and particle size from 223.5 µm to 890 µm and concentration values of 0.2, 0.3 and 0.4 by weight (wt.%). The results obtained, showed the predominant wear pattern in parallel flow to be cutting wear. This work further quantified the effect of flow velocity on the wear rate of the target material. Further experimental work by Gandhi et al [68] extended their previous investigation to include the effect of the surface orientation and by extension particle impact angle on the erosion rate. The study was done with zinc tails as the erodent in concentrations of 20 wt.% and 40 wt.% by weight, with the test piece varying in angles from 15^o to 90^o in an erosion test pot Figure 2-7. A thorough discussion of the results was outlined, detailing the relationships between the erosion rate and the impact angle, particle flux and velocity. The study is limited to zinc as the eroding material, and does not address the potential effect of eroding with multi-sized particle slurry. Furthermore, neither the particle shape nor the particle sharp changes through attrition are addressed.

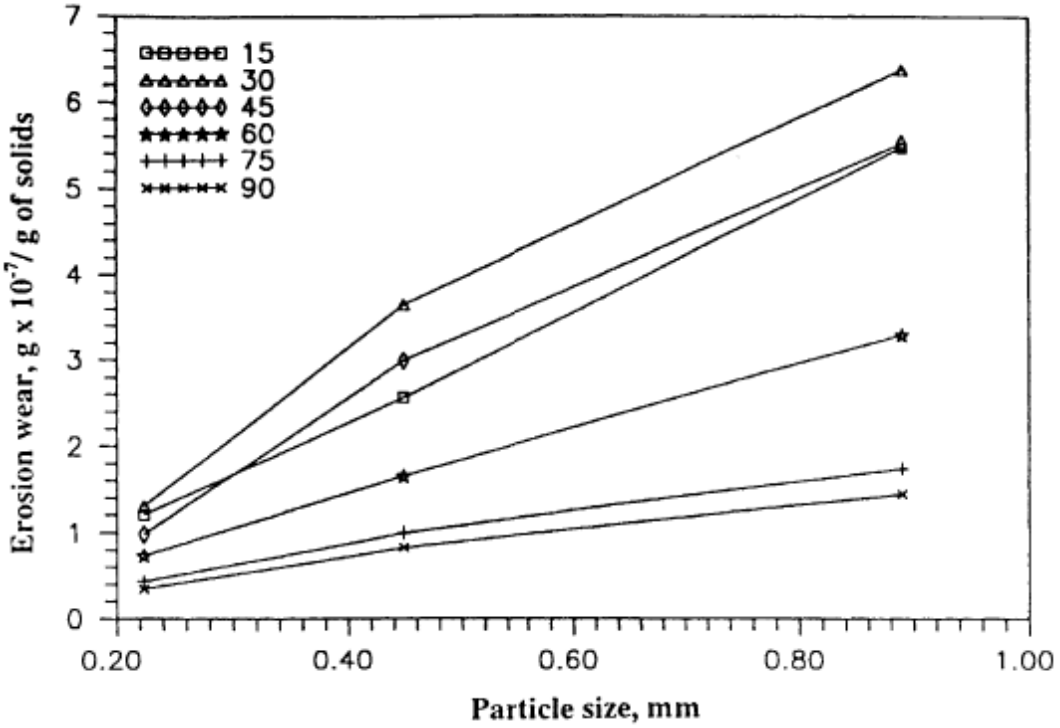

Figure 2-7 Variations in the erosion wear as a function of particle size [65]

Clark [27] produced a qualitative study of the effect of the squeeze film of a liquid in the phenomenon of erosion. A discussion was presented that detailed the approach and considerations that have to be given, to the quantitative impact of the squeeze film effect on key erosion parameters such as the impact velocity and the angle of impact. The review is limited to assessing the squeeze film effect.

Wood et al [69] conducted an experimental study and computational analysis on erosion wear in pipelines, assessing both straight sections of pipe and bends. Similar to Mishra et al [40], the test sought to determine the particle distribution in the duct. This was done experimentally with the use electrical resistance topography. The discussion of results focused on the agreement between the CDF prediction and the experimental results, as well as the location and mechanisms of localised wear (maximum) along the surface of the duct. The study did not assess nor quantify the effect potential stratification of multi-sized particles in a pipe system.

Zhang et al [70] investigated, through experimentation and CFD, solid particle erosion using both water and air as the bulk medium. The study extends previous works by assessing both the fluid velocity as well as the particle velocity through the use of Laser Doppler Velocimeter (LDV). The study examined several erosion models in order to determine the most appropriate for the given conditions. The discussion, found both the E/CRC model and the Oka model represented by equation (1-3) and (1-6) respectively, provide the most comparable results to the experimental work. The Tulsa angle function is given by equation (1-4) with the value of (A) found empirically for carbon steel, listed in Table 2-2. The angle function for the Oka model is represented by equation (1-7), which has two parts; one representing the damage caused by normal impingement angle, the other representing damage at all other impact angles. The empirical constants are set out in Table 2-3(2-2). The study found that the particle velocity is significantly lower than the fluid velocity, with large variations existing in velocity among the particles. There is no assessment of the temporal attribute of the erosion rate, and the evaluation is limited to silica flour and silica sand.

Table 2-2 Values of A for i=1 - 5 for carbon steel based on the E/CRC model [70]

A_1	A_2	A_3	A_4	A_5
5.4	-10.11	10.93	-6.33	1.42

Table 2-3 Values of empirical constants for the Oka model [70]

s1	s2	q1	q2	K	k1	k3
0.71	2.4	0.14	-0.94	65	-0.12	0.19

Desale et al [71] conducted a study on the erosion of an aluminium alloy subject to slurry erosion, at a fluid velocity of 3 m s^{-1} and solid concentration of 20 wt.%. The study focused on, determining the mechanisms of erosion and the change in erosion rate, as a function of particle size (37.5 µm and 655 µm) at orientation angles of 30º and 90º. The discussion detailed the contributing factors, which result in an increased erosion rate as the particle size increases, highlighting, the associated particle kinetic energy attributed to the removal of mass from the surface. SEM micrographic images are presented, however, these are limited to a qualitative view of the eroded surface. The study is limited to assessing the effect of particle size and does not examine the interrelation of particle size and other key parameters.

Mohammadikhah and Abdolkarimi [72] carried out a study of solid particle erosion on pipeline bends using CFD modelling based on the Langrangian Framework. The focus of the study was to determine the erosion performance, of an industrial sized pipe bend of a gas booster station, in which solid particulates of black powder, impinge the material surface. The study employed the use of the Rosin-Rammler distribution function for multi-sized particles, ranging from 125 µm to 2360 µm. In order to determine the erosion rate, a User Defined Function was employed, combining the Tulsa model with the Huser and Kvernvold model represented by equation (2-11). In this model n=2.6, Fs= 0.2 (fully rounded particles), B= Brinell Hardness, and the angle function F(α) is offered in equation (1-4) with empirical constants presented in Table 2-4. The analysis presented, shows a correlation between the flow velocity, particle size and the angle of impact particle size. In particular, the study shows how these variables affect the location at which the particles impact the surface of the pipe bend. The study compared the predicted particle distribution information with published experimental data, however this was not offered for the erosion rate analysis. The model used to predict erosion wear does not account for the particle size effect on the erosion rate.

$$ER = 1559B^{-0.59}F_s v^n F(\alpha) \qquad (2\text{-}11)$$

Table 2-4 Values of A for i=1 - 5 for the angle function [72]

A_1	A_2	A_3	A_4	A_5
0.047	0.00049	-4.7e-005	6.8e-007	-3e-009

Zheng et al [73] conducted experimental studies into the erosion-corrosion resistance of alloys. The experiment was conducted in 10 wt.% H_2SO_4 solution with a solid particle concentration of 15%. The discussion outlined the impact of improving corrosion and erosion resistance on the erosion-corrosion synergism, however, the study is severely limited as it only assesses the flow velocity's contribution to the erosion-corrosion synergy.

In carrying out experimental work on the erosion-corrosion resistance of engineering materials, Rajahram et al [74] used natural uncrushed silica sand as the impacting particle, within a slurry test pot. The study included a range of pH solutions as seen in Figure 2-8. The particle parameters included a range of particle sizes described as fine medium and coarse, as well as a series of solid particle concentrations. The investigation focused on the erosion-corrosion synergistic trends, and mapped out a transition regime for the crossover between corrosion dominant, corrosion-erosion damage, to an erosion dominant, erosion-corrosion wear regime. The work does not assess the impact of particle attrition, nor does it address the influence of flow and impact angle on the erosion and erosion corrosion synergy.

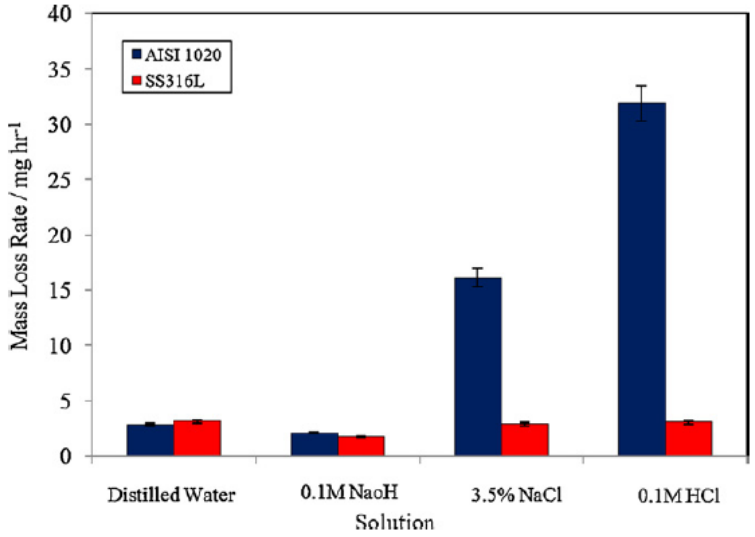

Figure 2-8 Comparison of erosion and erosion-corrosion rates in different solutions [71]

2.3 Surface Profiling

A study carried out by Islam and Farhat [75] assessed erosion wear of API X42, employing the use of aluminium oxide as the erodent, at high abrasive feed rate and high velocities. This study used the jet impingement method with air as the bulk fluid, striking the specimen at 30°, 45°, 60° and 90°, at speed between 35 m s^{-1} and 80 m s^{-1}. The discussion presented an analysis of the effect of velocity and impact angle and the cross comparison of these parameters. Moreover, surface topography was used to analyse the wear depth at different angles and exposure times. Figure 2-9 shows the development of a surface scar as the exposure time is increased.

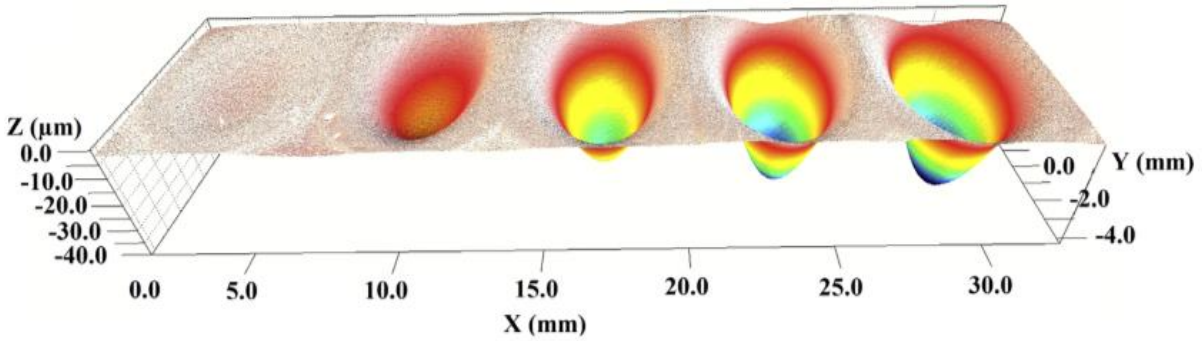

Figure 2-9 Shows that wear damage caused on the material surface with exposed to the impinging flow for 10 s and up to 420 s, at a velocity of 36 m s^{-1} [72]

The surface was further analysed using Scanning Electron Microscope (SEM), which allowed the investigators to assess the manner in which erosion was taking place throughout the material surface. Figure 2-10 shows four images with distinct mechanisms of erosion taking place. The study is limited to depth assessment and the qualitative assessment of the erosion mechanisms and does not evaluate the surface texture of the target material.

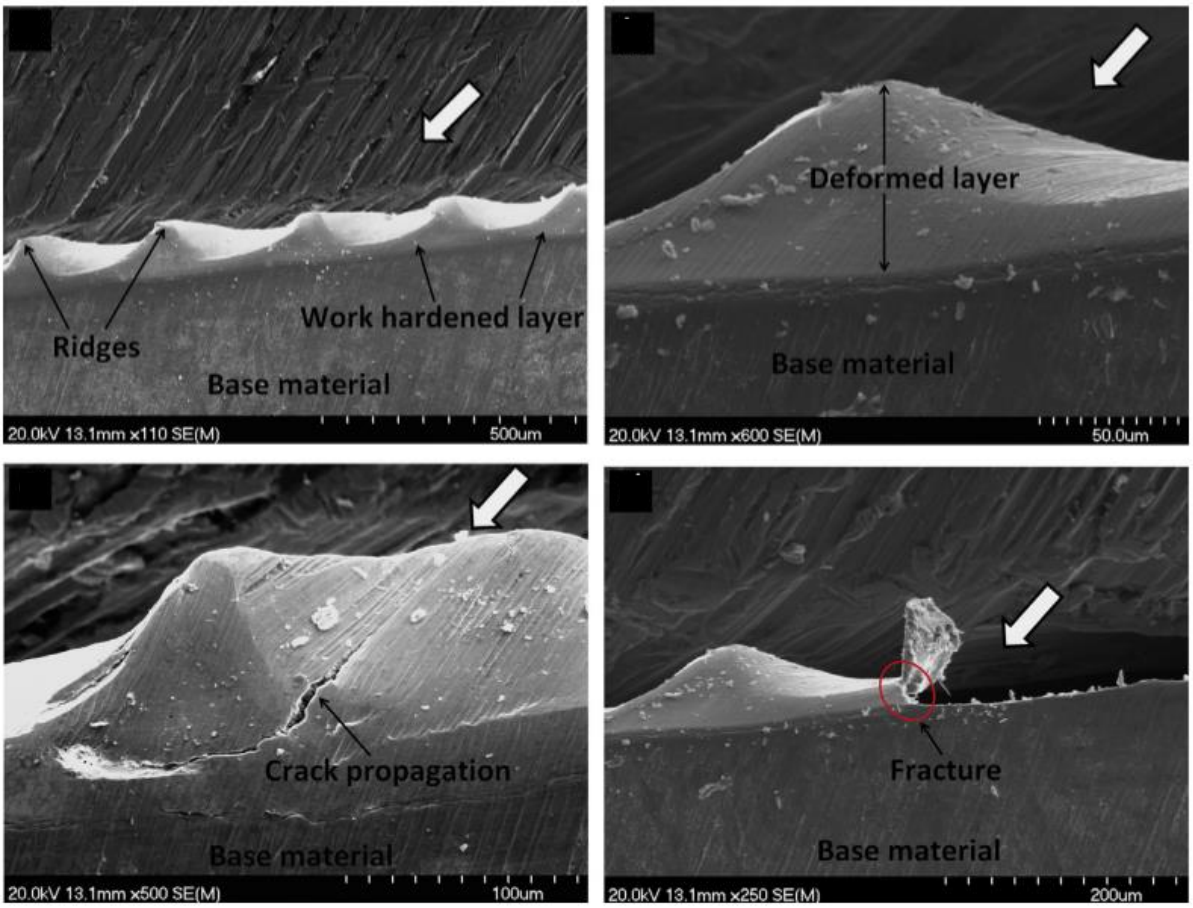

Figure 2-10 SEM images of surface damage, displaying different mechanisms of erosion wear taking place, the arrow in the images represents the direction of flow [72]

Laguna Camacho et al [76] investigated the damaged caused to the surface of a soft annealed stainless steel AISI 304 by angular shaped silicon carbide (SiC) particles, using a compressed air jet impingement rig. The experimentation was carried out at four incident angles 20º, 45º, 60º and 90º, the discussion focused on the surface damage which occurred at 45º and 60º, providing a comparison of the transition in the mechanisms of erosion occurring at each angel. Magnified photographs were taken throughout the target surface revealing the different types of erosion incidents taking place, with results similar to Islam and Farhat [75], showing deformation, cracking and fracturing taking place. Furthermore, an investigation into the change in surface roughness was presented, and found that the surface roughness increased when eroded at both 45º and 60º. Figure 2-11 shows the profiles examined and determined the roughness value to be 280 nm and 321 nm at 45º and 60º respectively. The study did not assess the surface roughness with respect to the time domain, nor did it assess this in an aqueous bulk flow.

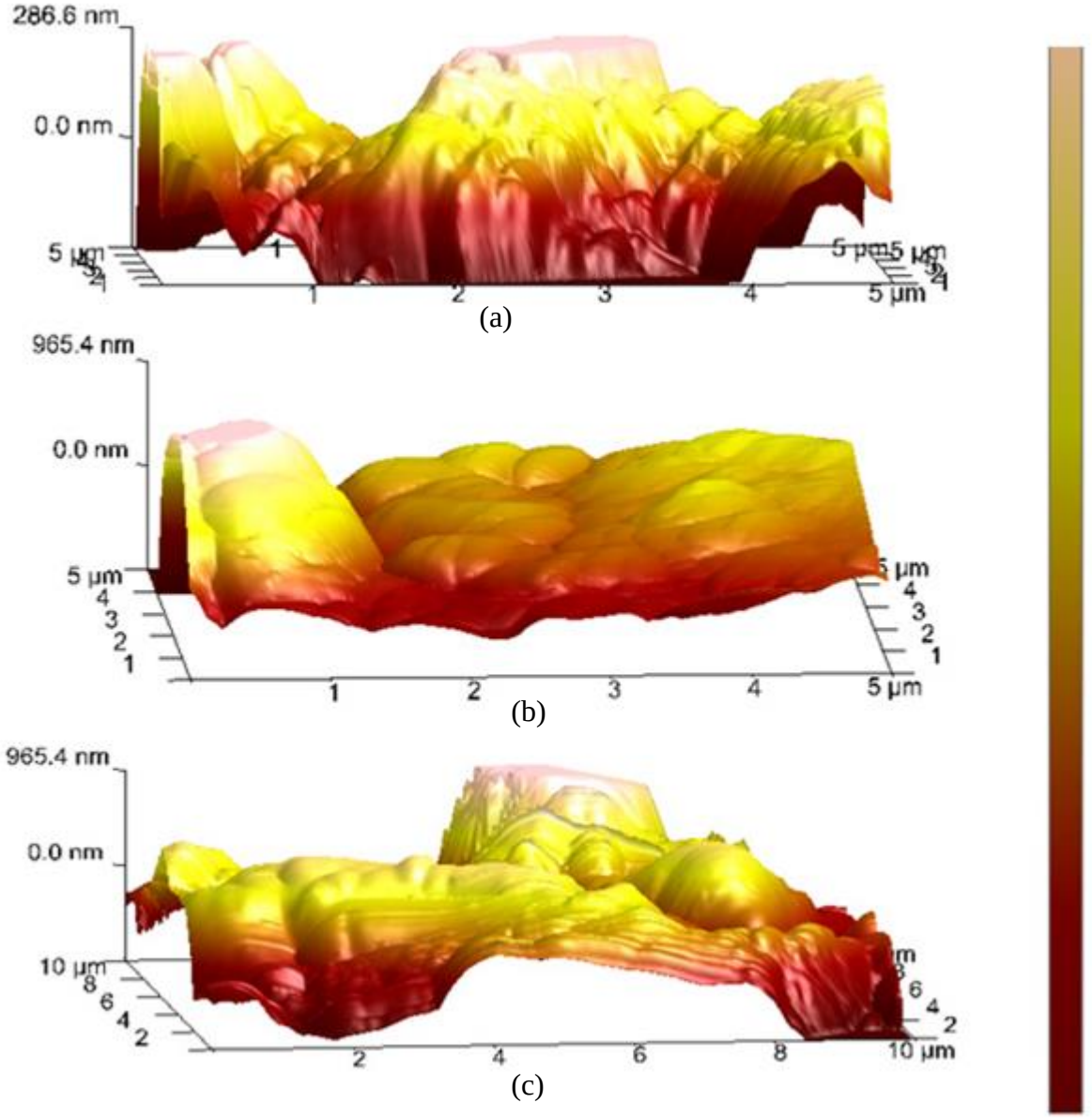

Figure 2-11 Surface profiling of AISI 304 (a) uneroded (b) 45° and (c) 60° [73]

A study by Patel et al [77] assessed the erosion of uncoated stainless steel SS304 when subjected to air jet erosion by a stream of alumina particles at 40 m s^{-1}. The analysis was conducted on both, weight loss through gravitational measurement and on the surface deformation, with the use of SEM and Energy Dispersive X-ray Analyser (EDAX). The EDAX analysis of the surface composition found the presence of the Al and O, this s due to the erodent being imbedded into the material surface during impingement. When eroded at 30° SS304 exhibits an incubation period, followed by an acceleration in the erosion rate, before finally attaining steady state. After reaching steady state the erosion rate at 30° was found to be higher than that at 90°, it must also be noted that the material attained steady state immediately at 90°. The EDAX analysis also showed a higher presence of Al and O when eroding at 30°, this could have contributed to the lower weight loss at the onset of erosion. A detailed discussion of the surface was presented however this was not assessed from a surface texture nor a surface texture morphology perspective.

2.4 Summary of Literature Review

What has become apparent from the review of preceding works in this field is that, although it has been studied extensively, there is a great deal that is not yet understood about solid particle erosion. All of the literature reviewed are in agreement on one fundamental aspect of solid particle erosion, and that is the nature in which a combination of erodent, target material and environment will behave is not universally applicable. This is further evident through the non-existence of a universal erosion model.

2.5 Scope of Research

The work completed in this field assess the damage caused by a limited range of eroding materials, silica sand predominantly appears as the natural erodent in most studies assessing erosion in an aqueous environment. This work will employ the use of Olivine which is a naturally occurring mineral which is abundant in rock formations. There has been limited research carried out assessing erosion with the use of olivine. It would also be beneficial to assess its comparability to silica in erosive aqueous environments.

When the surface of a material is eroded, it undergoes several changes due in large part to the work being done by the impinging particles. Surface imagery has been extensively reviewed in an effort to analyse the manner in which erosion takes place, however, the investigation of the change in surface topography as a result of slurry erosion is an area that has not been explored in literature, but will be investigated in this work.

It is also necessary to address erosion in relation to the time dependent domain. Some works state that time is not a factor in the erosion of steels, however from the review of literature this observation does not hold true in all circumstances. It is therefore essential to address this parameter of erosion under the current conditions.

Some of the popular models that are employed in erosion prediction neglect the effect of particle size, as such this work will seek to address the interdependence of the velocity and multi-sized particles while also offering an alternative erosion model.

2.6 Research Objectives

Following on from the research aims which have been detailed in section 1.6, the literature review was conducted in order to determine potential gaps in existing knowledge and areas of further work required in this field. Following from this, the work to be conducted has been divided into several objectives described below:

1. In an aqueous environment, establish the influence of flow velocity and multi-sizes particles on the erosion rate of EN3B
2. Determine the temporal nature of eroding EN3B in an environment containing angular olivine particles
3. Propose a new erosion model based on the Zhang/Tulsa: E/CRC model of erosion
4. Topographically investigate the morphology of the target surface when eroded at different at incident angles and particle sizes
5. Provide a quantitative analysis of the change in surface texture as a function of exposure time and flow velocity

The next chapter outlines the methodology employed in this study, in order to satisfactory achieve the aforementioned research objectives.

Chapter 3 EXPERIMENTAL MODELLING

In investigating the erosion wear using an erosion test pot rig, both gravimetric analysis and surface profile scanning have been employed. This chapter outlines the general methodology, processes and analysis of the work carried out, detailing the apparatus as well as the experimental methodology used. Also included is an assessment of the inherent limitations and assumptions which are made, and the safety considerations in conducting this experimental work.

3.1 Target Material

Owing to its desirable properties carbon steel is the material of choice for the manufacture of oil and gas pipelines. Its strength, toughness, ductility, weldability and its availability make it the ideal material for this application. Despite its poor resistance to corrosion it is readily satisfactorily protected from corrosion by coating and also through the use of cathodic protection [78].

The material selected for the study is a bright mild steel, EN3B (BS970:1991 070M20), which is a general application mild steel. The general composition of EN3B is outlined in Table 3-1. The dimensions of the samples used in this study are rectangular prisms measuring (WxHxL) 10 mm x 5 mm x 45 mm. A thorough cleaning of the metal surface was done using a clean spirit followed by distilled water. The samples were then allowed to air dry.

Table 3-1 Composition of EN3B mild steel

	Composition %				
	C	Mn	Si	P	S
EN3B	0.16-0.24	0.5-0.9	<0.35	<0.05	<0.05

3.2 Erodent

The erodent which has been selected for this work is olivine obtained from SandGrit, Eastfield Road, South Killingholme, Immingham, which is a naturally occurring magnesium iron silicate mineral that is commonly found in igneous rock formation [79]. The olivine supplied are angular particles with a Mohs hardness between 6.5 (982 Hv) and 7 (1161 Hv), a specific gravity of 3.3 and have a bulk density of 1600-1900 kg m^{-3}. The olivine of AFS30 Grade, with a chemical composition as listed in Table 3-2.

Table 3-2 Chemical Composition of Olivine

	Chemical Composition %			
	Al_2O_3	MgO	SiO_2	K_2O
Olivine	0.8	49.25	42.06	0.07

Data sheet in Appendix II

3.2.1 Particle Size Distribution Study

AFS30 grade contains particles in a size range from 200 μm to 1 mm. In order to gauge the proportion of any given particle size in the bulk material a mechanical sieve particle size distribution analysis is conducted. In order to attain a representative sample of the olivine, the stockpiling method was used. To allow for two independent studies of 1000 g each, 2000 g of material was taken from four locations around the stockpile.

Hand sieving method was used for this process, using eight different sieve sizes ranging from 200 μm to 850 μm:

1. 1000 g of olivine particles were sieved through an 850 μm sieve, 200 g at a time to ensure proper sieving. Sieving was actioned until further sieving allowed no additional olivine to filter through the sieve.
2. The retained material was placed into a measuring bowl:
    a. Some material naturally remained trapped in the sieve, this was brushed out of the sieve onto a collecting mat and counted as part of the retained material.
3. A balance was used to measure the mass of the olivine retained, this was then recorded on a log.
4. The olivine that successfully passed though the sieve was then sieved through a 700 μm sieve, with the same process as 1 and 3 above being carried out.
5. This was repeated for each of the remaining sieve sizes.
6. Steps 1 through to 5 were then repeated for the second 1000 g of olivine.

The results of both studies were averaged out and recorded in Table 3-3 below.

Table 3-3 Averaged measured and calculated values from solid particle size distribution study

Sieve Opening (μm)	Mass of sand retained (g)	Percentage of mass retained (%)	Cumulative Percentage retained (%)	Percentage Finer (%)
850	17	1.7	1.7	98.3
710	73	7.3	9	91
500	92	9.2	18.2	81.8
400	616	61.6	79.8	20.2
300	141	14.1	93.9	6.1
280	0	0	93.9	6.1
212	49	4.9	98.8	1.2
200	10	1	99.8	0.2
Total Retained Mass (g)	998			
Initial Mass	1000			

To determine the possible error in the analysis the percentage mass loss to sieving is calculated, 0.2% is an acceptable variance from initial total mass to retained total mass [80].

$$\text{Mass loss to sieving} = \frac{\text{Initial Mass} - \text{Total Retained mass}}{\text{Initial Mass}} \text{x} 100 = 0.2\% \qquad (3\text{-}1)$$

Figure 3-1 is a graphical display of the information outlined in Table 3-3, from which it can be seen, that approximately 80% of the olivine are sized from 300 µm - 500 µm, while relatively few particles remain in the region above 800 µm. It can also be seen from Figure 3-2 that over 60% of the olivine particles, pass through 500 µm opening but remain on the 400 µm opening.

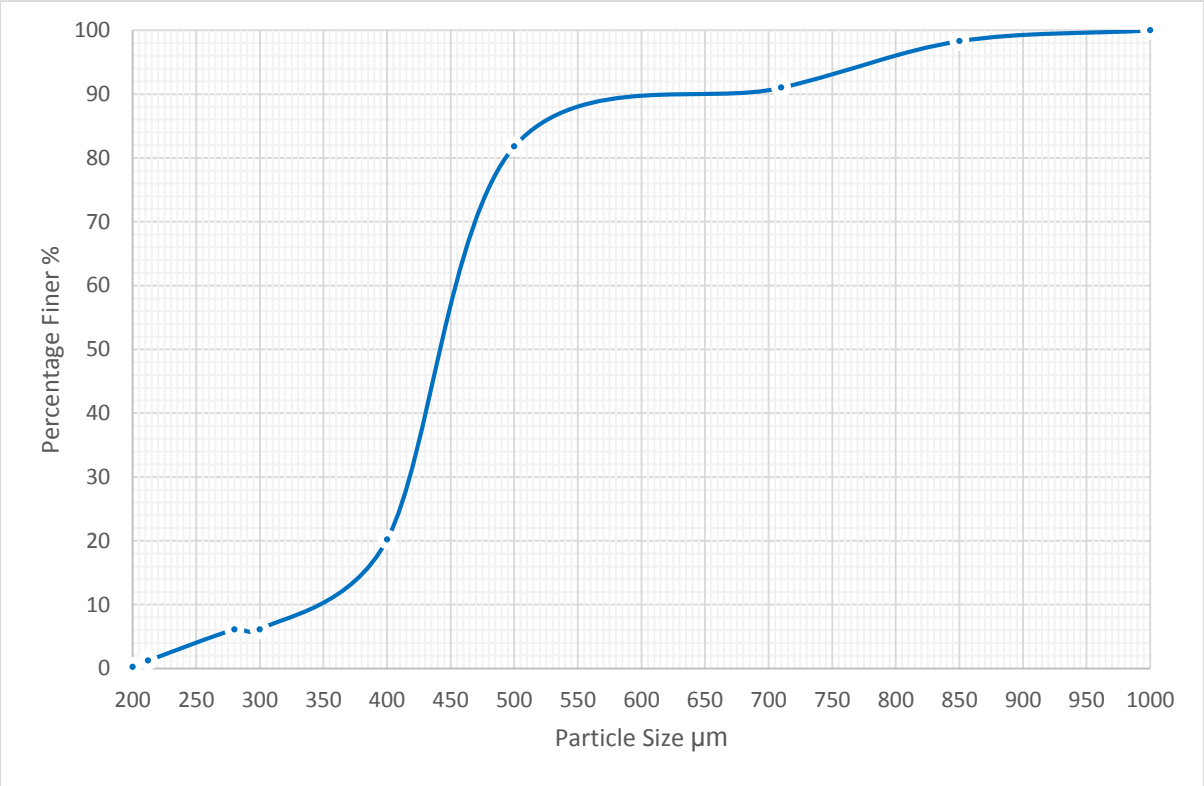

Figure 3-1 Cumulative fraction of particle sizes

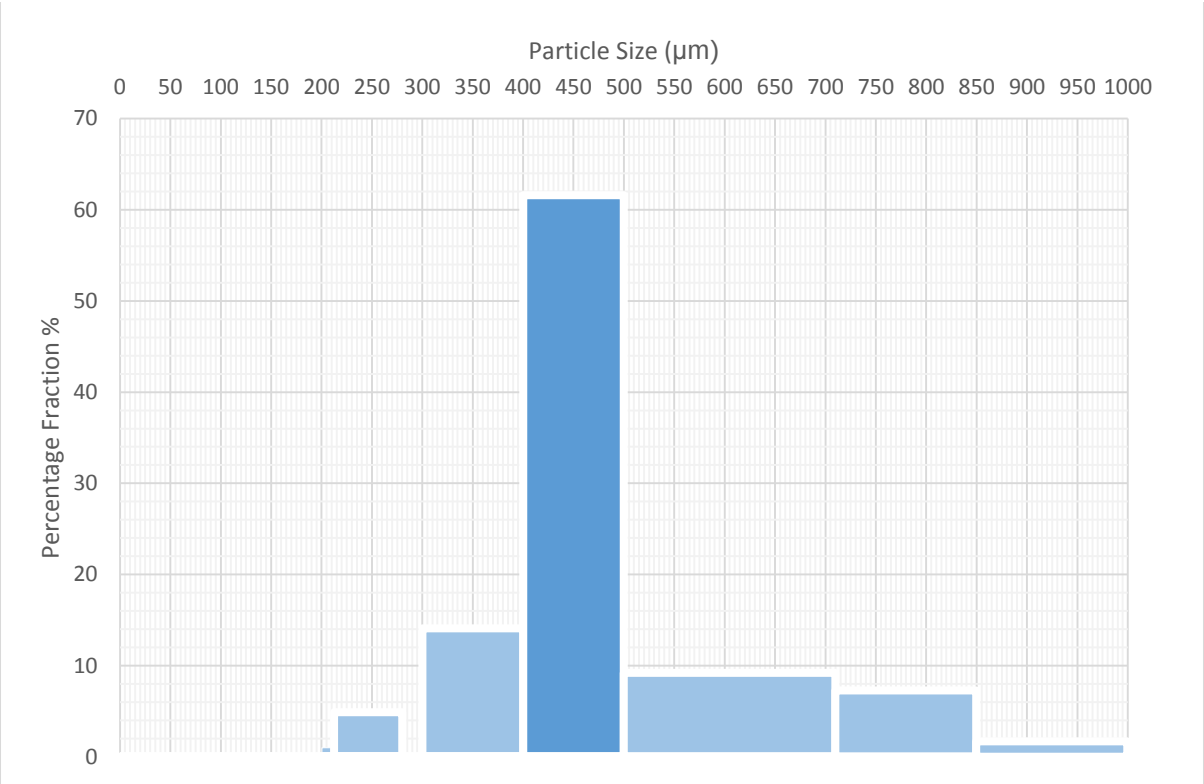

Figure 3-2 Percentage fraction distribution

3.3 Experimental Methodology

3.3.1 Slurry Pot Tester

In order to conduct the solid particle erosion experimentation, an erosion test pot rig was constructed with the general design based on the details in section 1.4.1. A full CAD model schematic of the system is displayed in Figure 3-3. The mixing tank is fabricated from 4 mm thick acrylic tubing with a 170 mm out diameter. The base, top flange and cover are all made from polycarbonate which has a high impact strength. The design allows for two specimens to be eroded at a time, with specimens being held between two carbon-steel sample holders as shown in Figure 3-3, both contain a slots in which ABS 3D printed inserts are fitted. These inserts allow for quick change over when different angles are needed, they also aid in the prevention of corrosion at the contact points. The samples are placed in the holders at 180^{o} apart to minimise the effect of wake.

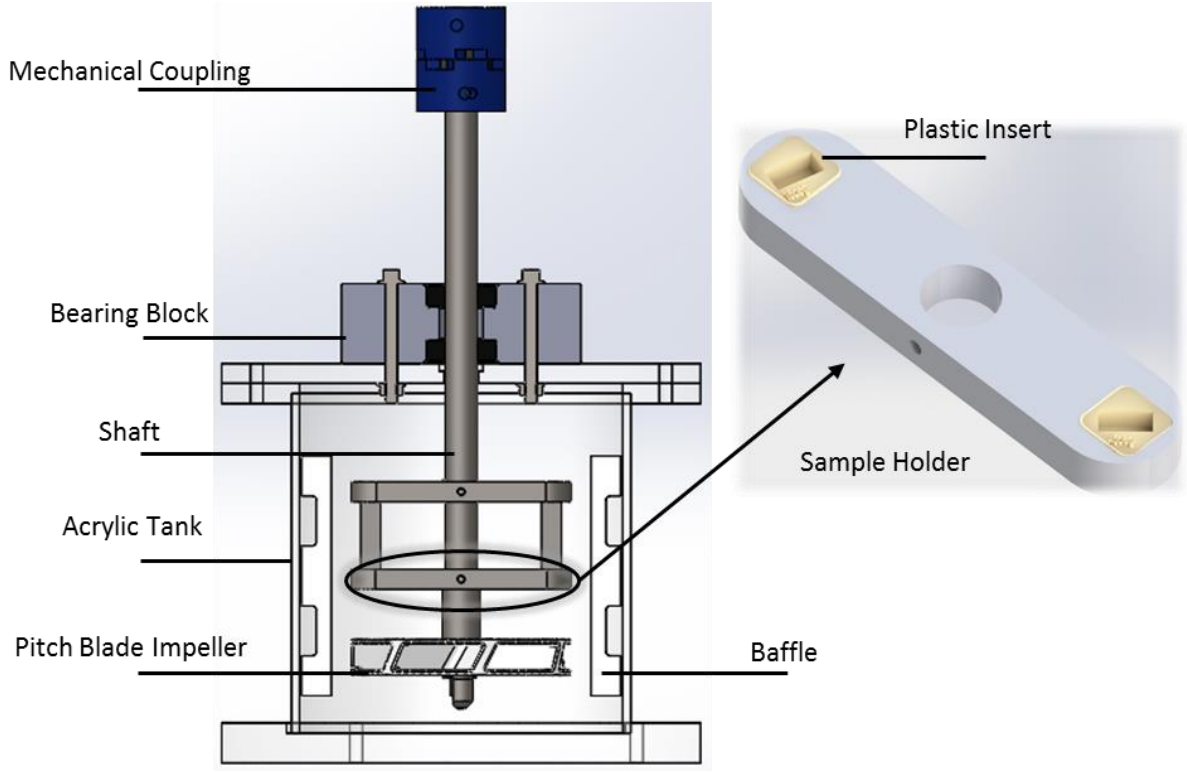

Figure 3-3 Schematic of erosion test pot

In mixing vessels with a centre mounted impeller shaft, both vortexing, as well as a swirling effects ensue; causing the entire bulk fluid to move almost in unison [81]. This results in poor mixing, and in the case of solid particles poor suspension. In order to prevent this from occurring, a four baffle arrangement has been used in the mixing tank. The baffles eliminate the swirling effect, and allow for good particle dispersion. Alongside the use of baffles, a pitched blade impeller, which is effective in vessels where there is low clearance from the bottom of the tank, has been used. This promotes better dispersion and good suspension as it generates flow in the axial direction. A study conducted by Desale et al [66] determined that a pitch blade impeller operating in a down pumping regime, provides more efficient particle dispersion within an erosion test pot. As such, this was chosen as the mode of operation for these experiments. Pictures of the experimental setup are displayed in Figure 3-4.

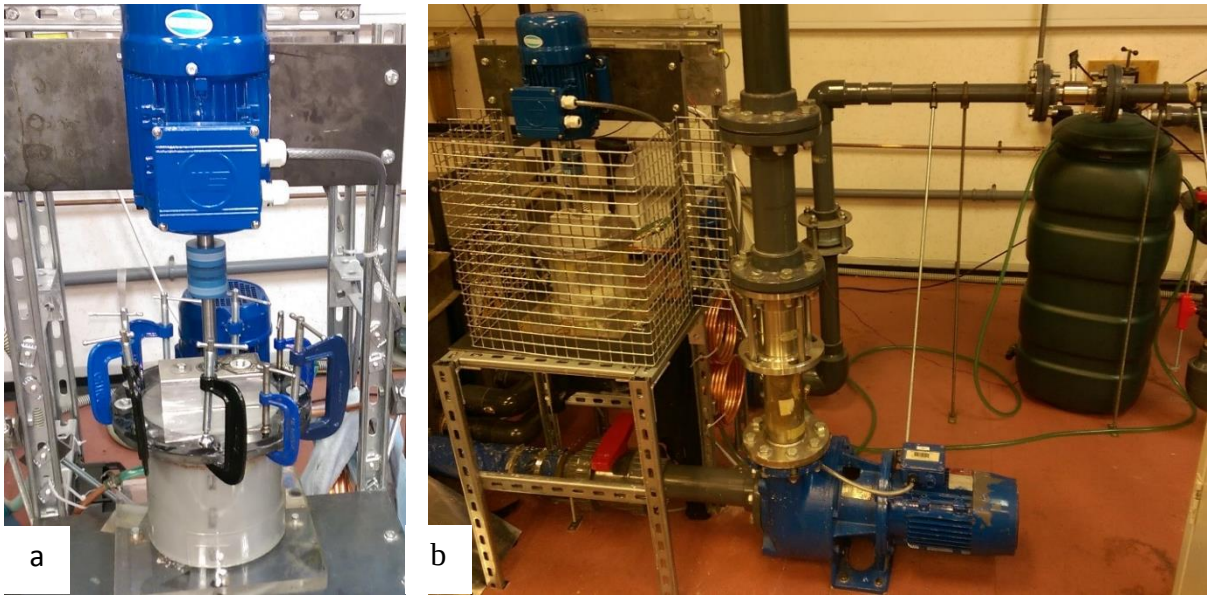

Figure 3-4 Erosion test rig setup (a) test pot (b) full rig setup

Two rubber seals are used in the test pot, one v ring seal on the inside of the tank which seals against the cover face, the other is a rotary seal on the outside of the cover as a secondary seal. The rig is powered by a variable speed inverter drive, which is a single-phase to three-phase device, 0.55 kW to 0.75 kW 230 V, which in turn powers a Marelli 0.75 kW 4-Pole three-phase induction motor. The output of the motor when connected to the variable speed drive is outlined in Table 3-4.

Table 3-4 Summary of Motor Continuous Output When Using Variable Speed Drive

Continuous Output: When motor is powered by Inverter Drive				
Frequency (Hz)	75	50	25	5
Velocity (rpm)	2145	1430	715	143
Power (kW)/(HP)	0.75/1	0.75/1	0.32/0.43	0.038/0.05

During the preliminary tests conducted, it was found that the temperature of the fluid in the mixing tank, increased from 21^{o} C to just above 55^{o} C when operating at 1200 rpm, and increased to over 75^{o} C when operating at 1800 rpm. Although these ranges of temperature have a minimal effect on the erosion rate of the target material, this can have an adverse effect on the integrity of the tank which is an operational and safety concerns. Moreover the increased temperature, also affects the operating life of components such as, the bearings and seals. Temperature regulation was achieved through the use of a copper coil, positioned at the upper section of the test pot, water was circulated through the coil from a reservoir to a heat sink. This setup allowed for the temperature to be maintained below 36^{o} C; Figure 3-5 shows the full set of the thermal control system. The temperature map in Figure 3-6, shows the temperature variations of the multiphase mixture, with respect to time, at 1800 rpm. During continuous runs ranging from five hours to eight hours, the reservoir's water was drained and replaced at intervals of approximately two hours. This proved to be appropriate in maintaining the desired operating temperature within the test pot.

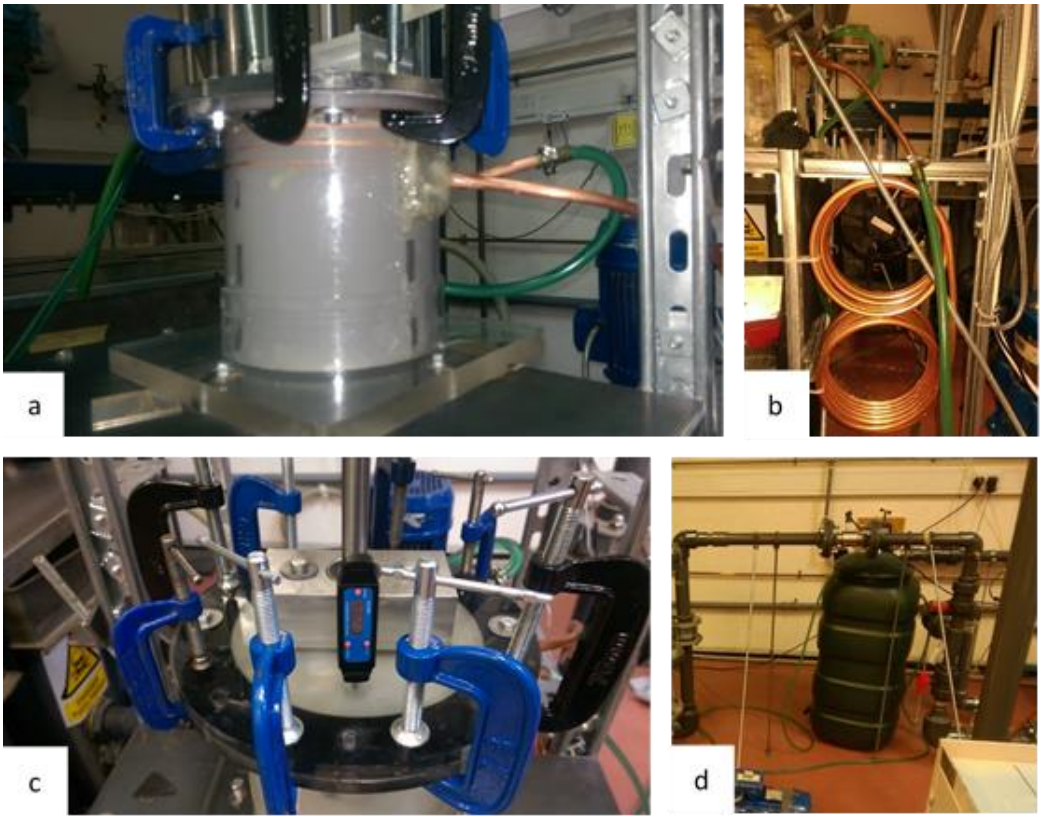

Figure 3-5 Thermal control setup (a) copper coil inside the mixing tank (b) cooling coils with forced convection (c) thermometer (d) reservoir tank

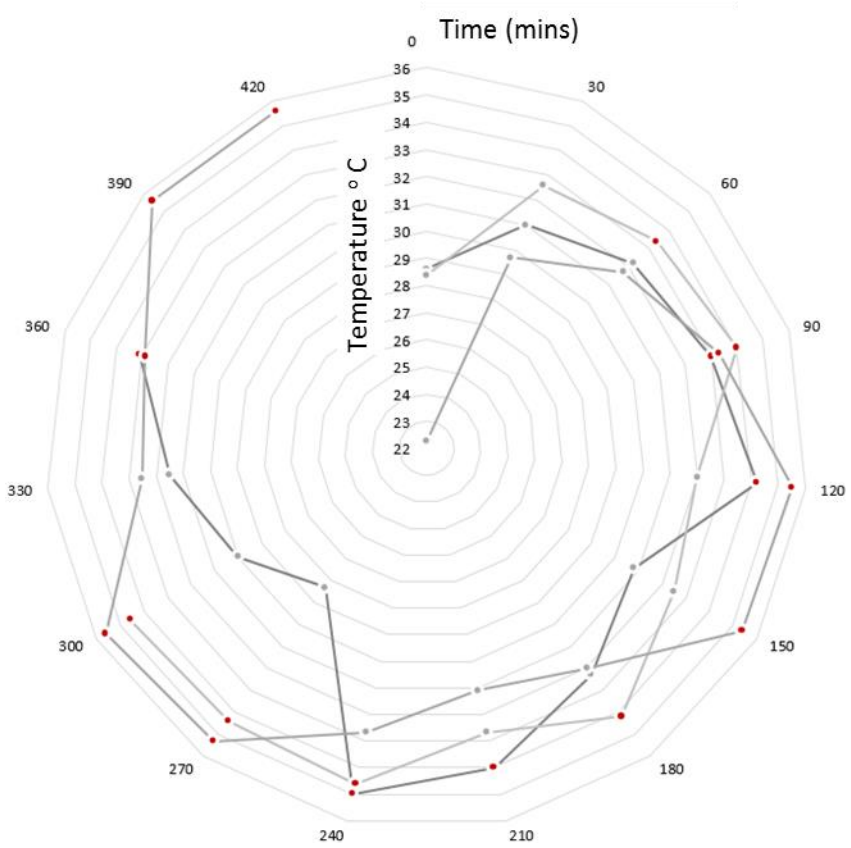

Figure 3-6 Temperature map of test pot with three runs at 1800rpm

3.3.2 Surface Measurement

Prior to conducting erosion testing, the specimen surface is topographically measured in order to obtain a baseline analysis of the profile. This is achieved through the use of optical three-dimensional surface metrology using an Alicona InfiniteFocus microscope. The InfiniteFocus system, applies the principle of focus variation, from which it produces a 3D dataset. This describes the process by which, the optical lens's focal plane is moved over the target surface capturing an image as the surface area comes in focus, as Figure 3-7 illustrates. This is achieved by defining a focal range, through which the system will capture a scan of the surface at intervals through this z plane [82].

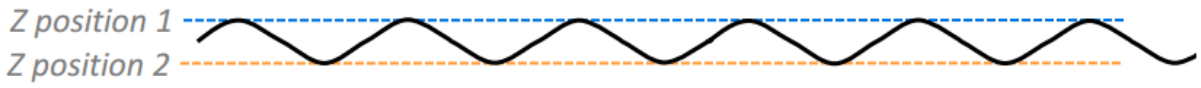

Figure 3-7 Lower and Upper limits for the capture of surface profile [79]

For this analysis, a 10x zoom lens is used, the objectives details are outlined in Table 3-5. The sample is placed on the platform which is moved in the x and y direction while the head is moved in the z direction until the sample comes into focus. The z range is then defined based on the upper and lower sample surface heights. The sample has an aerial surface area of 10 mm x 45 mm, however, the area defined for the analysis is the central zone, of area 6 mm x 41 mm. A corner unit was installed on the platform to ensure consistent datum for measurements, as shown in Figure 3-8 . The Alicona, progressively takes images (size: 1429 x 1088 (μm^2) of the entire defined surface area and subsequently stitches the images together to form a complete data set of the surface. Post erosion; surface measurements are again taken of the sample, covering the same region as the initial scans, this is done at each time interval being evaluated. Alicona's post processing software is then used, to capture the surface parameters, of the uneroded and eroded surfaces.

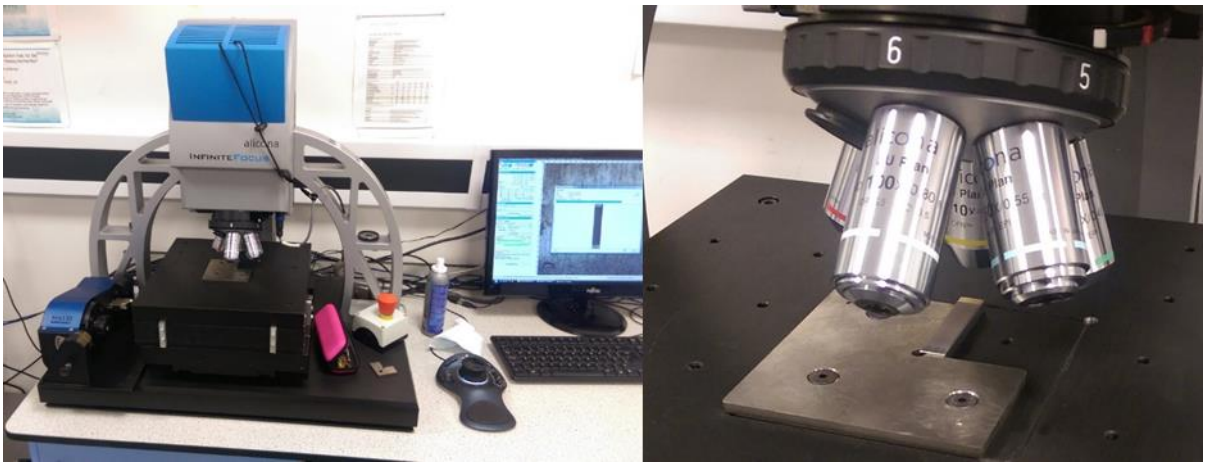

Figure 3-8 Specimen on the Alicona platform, with the corner locator in place

Table 3-5 Primary objectives details for the Alicona infinitefocus at 10x optical zoom

Objectives Details: 10x optical lens				
Field of view x (µm)	Field of view y (µm)	Vertical resolution low /high speed (nm)	Optical lateral resolution (µm)	Sampling distance (µm)
1429	1088	100 /2000	1.1	0.88

3.3.3 Gravimetric Measurement

The samples were weighed pre-erosion and post erosion; these gravitational measurements were conducted using an OHAUS Galaxy 110 digital balance (Figure 3-9) with a measurement range down to 0.1 mg. The weight of each sample measured six times with the extreme upper and lower values being ignored. Four readings were recorded, from which the average was taken.

Figure 3-9 Digital scale

3.3.4 Post-Test Handling

When samples are removed from the test pot, and left to sit for a relatively short period of time, a propagation of corrosion can be seen throughout the surface. This can lead to erroneous weight measurements, and can also affect the surface texture profile of the sample being evaluated. As such, upon being removed from the test pot, post erosion, the samples are immediately and thoroughly cleaned, dried and vacuum sealed.

3.4 Safety

The general risk assessment as outlined by the university is located in Appendix III

The next chapter details a discussion on the effect of the erosion variables on the erosion rate of EN3B being eroded by olivine, It also presents a study on the effect of particle attrition and particle friability.

Chapter 4 EVALUATION OF TIME, VELOCITY AND MULTI-SIZE PARTICLE EFFECT

This chapter outlines the actions conducted in determining the effect of fluid velocity, multi-sizes particles and time on the erosion rate. A qualitative and quantitative analysis, of the effect of the recirculating nature of the rig on the initial particle properties has been presented. The results of the experimentation and a detailed discussion is presented showing the relationship between velocity, particle size and erosion rate, as well as the temporal nature of eroding the target material. Moreover, this chapter offers a novel erosion rate prediction model that can be used to determine the erosion rate under the stated conditions.

4.1 Methodology

A series of experiments have been conducted in order to determine the manner in which EN3B would perform in an erosive aqueous environment over a period of time. The fluid used in the mixing tank is tap water which contains 10.3 mg Na/l, 12.5 mg Ca/l and a pH of 7.9 based on the 2015 period report for water in Huddersfield centre [83]. The tank has a total capacity of 3.51 litres, but was filled to a level just above the top line of the baffles to a fill of 2.9 litres. The concentration of olivine used in this evaluation is 10% by weight, which is considered the upper limit of a dilute slurry. A full array detailing the experiments conducted can be seen in Table 4-1. The motor rpm settings of, 900, 1200 and 1800 (rpm) are equivalent to a linear velocity of, 4.241 m s^{-1}, 5.654 m s^{-1} and 8.482 m s^{-1} at the centre of the specimen, that are placed at a 90^{o} orientation to the flow. In practical applications, the particles entering the bore in an oil well are not of a single size, as such, multi-size particles have been used in three distinct particle size ranges, labelled small, represented as (s) 90 µm – 280 µm, medium, represented as (m) 280 µm - 500 µm and large, represented as (l) 500 µm – 1 mm.

Preliminary tests were conducted over a period of eight hours and these revealed that there was negligible difference in the erosion rate of EN3B at four and eight hours. As a result, the study was conducted over a shorter period of time. These initial experiments also revealed that at the end of a four-hour run the olivine would be severely degraded, with a significant amount of the erodent being powdered into the water. Section 4.1.1 details the manner in which this particle degradation was addressed.

Two samples were placed in each experimental run with the test times running for a period of three hours with the samples being weighted at intervals of 30mins. Tests were conducted three times for all test parameters and the mass loss was taken as an average of all three sets of results. Gravitational measurements were conducted as outlined in section 3.3.4, and were recorded before and after each experiment. Due to the wear experienced by both the sample holder and the inserts, as shown in Figure 4-1, the inserts were also changed every few hours as required. Despite replacing the inserts, it was found that the exposed area varied slightly over the duration of the experimentation as such each specimen was individually measured to determine the area exposed to erosion from which the mass loss was normalised to the indented exposed area.

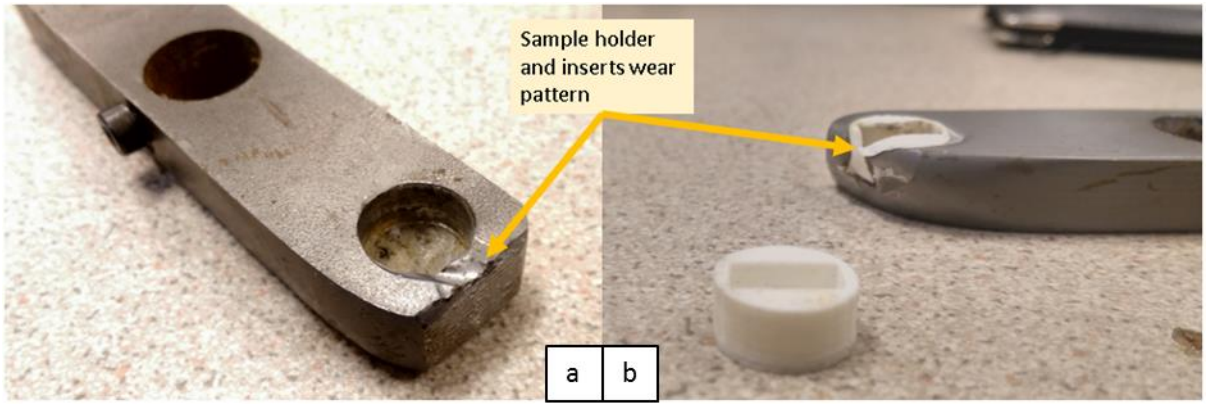

Figure 4-1 (a) Sample holder showing initial flow erosion at outer edge (b) Erosion of sample holder and insert

The impeller Reynolds number N_{Re} for the mixing vessel has been calculated for the lower and upper limits of impeller speeds (900 and 1800 rpm), and was found to be $1.8x10^{5}$ and $3.6x10^{4}$ respectively.

Table 4-1 Array detailing experiments conducted

Time (hr)		0.5			1			1.5			2			2.5			3		
Sand Size		s	m	l	s	m	l	s	m	l	s	m	l	s	m	l	s	m	l
Velocity (rpm)	900					✓													
	1200		✓	✓	✓	✓	✓		✓	✓	✓	✓	✓		✓	✓	✓	✓	✓
	1800		✓	✓		✓	✓		✓	✓		✓	✓		✓	✓		✓	✓

4.1.1 Particle Attrition and Friability

In pipelines delivering multiphase flow with solid particulates, there is a continuous supply of fresh particles entering the system. These particles are not subjected to a great deal of particle-wall impacts, nor particle-particle impacts, thus retaining their initial physical characteristics at the moment of impact. One of the great advantages of using a pipe flow loop as described in section 1.4.1 is the diminished effect of particle attrition. Contrastingly, a test pot recirculates a given mass of particles under continuous impact condition over a set period of time. This results in a considerable amount of particle-particle and particle-wall impacts. This inherent limitation of, attrition, in the erosion test pot process, manifests itself through the break-up and the dulling of sharp angular particles.

Owing to the fact, that attrition is minimal in a pipeline system, but is magnified in an erosion test pot, the consequence of particle attrition in the experimental process, results in incorrect assumptions and predictions being concluded. To minimize the impact of particle degradation on the experimental results, it is crucial to appreciate the amount of attrition taking place. A study by Desale et al [66] assessed the effect of particle attrition on erosion rate, by varying the replacement interval of a sand-water mixture. This study was conducted at a shaft speed of 404 rpm which equated to a linear flow velocity of 3 m s^{-1}. The results of this study are shown graphically in Figure 4-2, where it was found that the mass loss deviates greatly when the interval is four hours, compared to the baseline of one hour. When the interval is reduced to two hours, although the erosion rate is lower than the baseline there is not a significant deviation over a three hour period. This study is incomplete in assessing the degradation of the sand particulates, as it can be surmised that if the baseline is set to ten minute intervals, the mass loss at intervals of one hour will deviate significantly from the baseline.

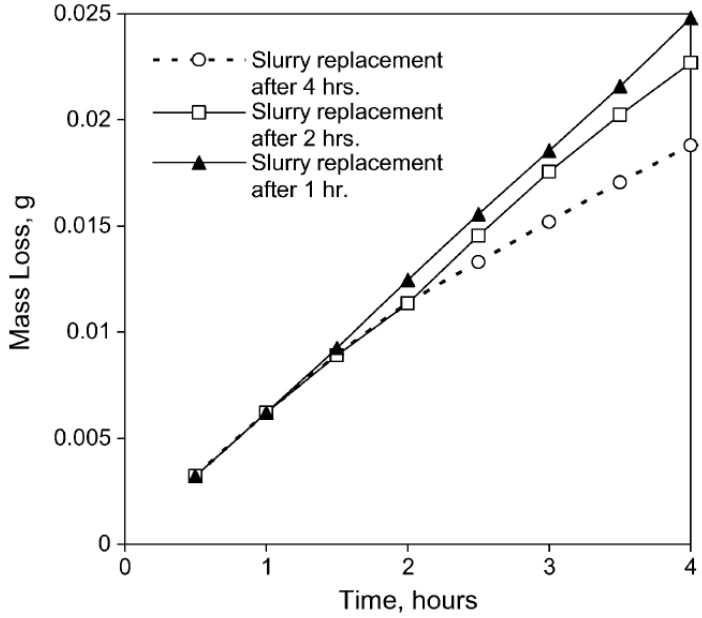

Figure 4-2 Mass loss as a function of the mixture replacement intervals for particle attrition study [63]

It is necessary, particularly when using multi-sized particles, to quantify the rate at which particles within a given diameter grouping, degrade and fall below the given range. This allows for adequacy of the time interval chosen to be quantitatively validated, using the initial mass as the baseline. The study was conducted at 1200 rpm, which equates to a flow velocity of 5.654 m s^{-1}. The medium-particle size range (280 µm - 500 µm) was used, at an initial mass of 300 g for three experimental runs, conducted at periods of one, two and four hours. Upon completion, the solid particles were captured in a cloth filter, they were then dried and sieved. The particles retained in the sieving process, were weighed, and the mass recorded in Figure 4-3. The percentage decrease by mass, in the particle size after one hour of use is 15%. This becomes a percentage decrease of 30.33% after 2 hours, and falls to almost half of the initial mass when the mixture is used continuously for a four hour period.

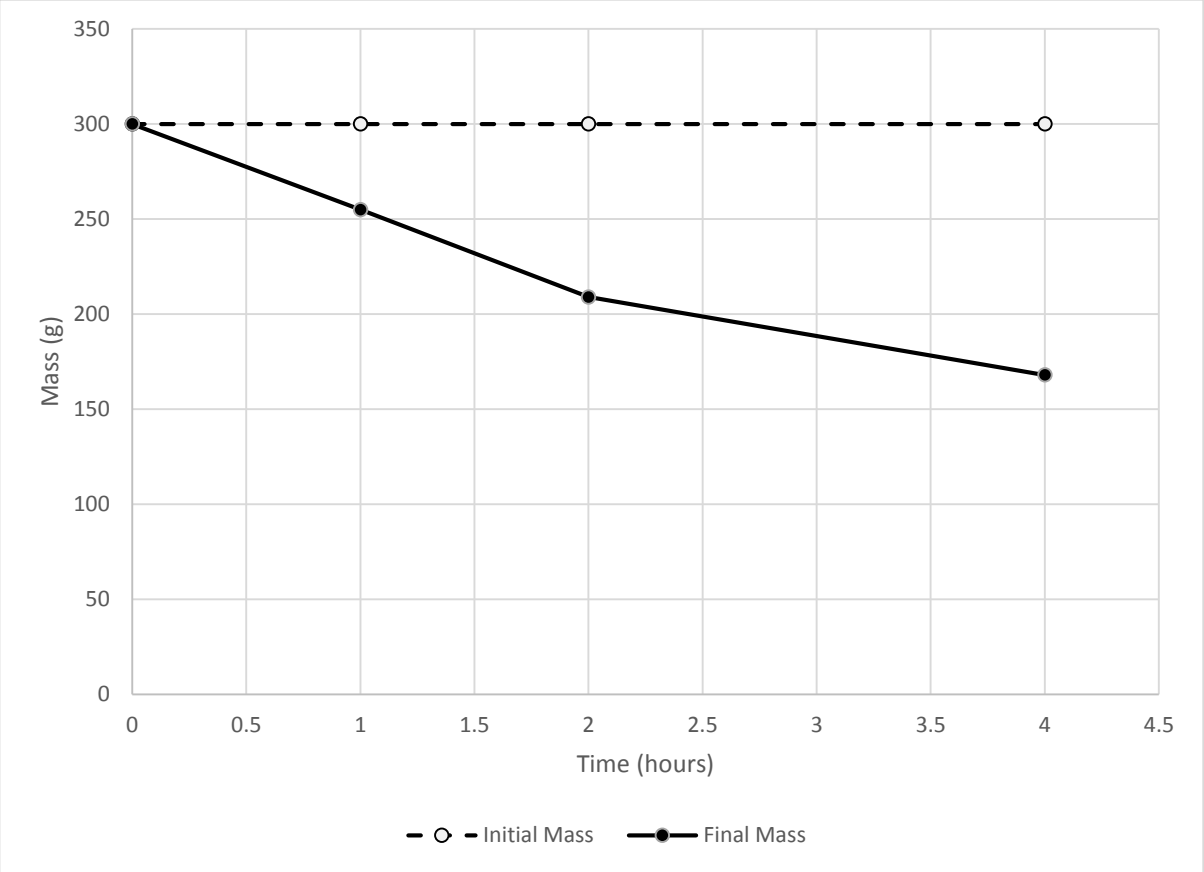

Figure 4-3 Change in mass of olivine which remained within the desired particle size range after a period of 1, 2 and 4 hours at 5.654 m s^{-1}

The significance of particle shape, as a factor in the development of erosion wear has been presented in previous chapters. Therefore, in addition to quantifying the particle break-up, it is equally essential to take into account, the change in particle shape as the experiment progresses. This study provides a qualitative assessment of the change in particle shape, after a period of one hour. Figure 4-4(a), shows unused, clearly defined, sharp angular olivine particles in the size range 280 µm – 500 µm. Figure 4-4(b), shows particles used for one hour of erosion at speed of 5.654 m s^{-1} (1200 rpm). It can be seen that although there is some rounding, the particles have largely retained their angularity. Furthermore, chipped/powdered olivine can be seen throughout the image with some adhering to the particle surface.

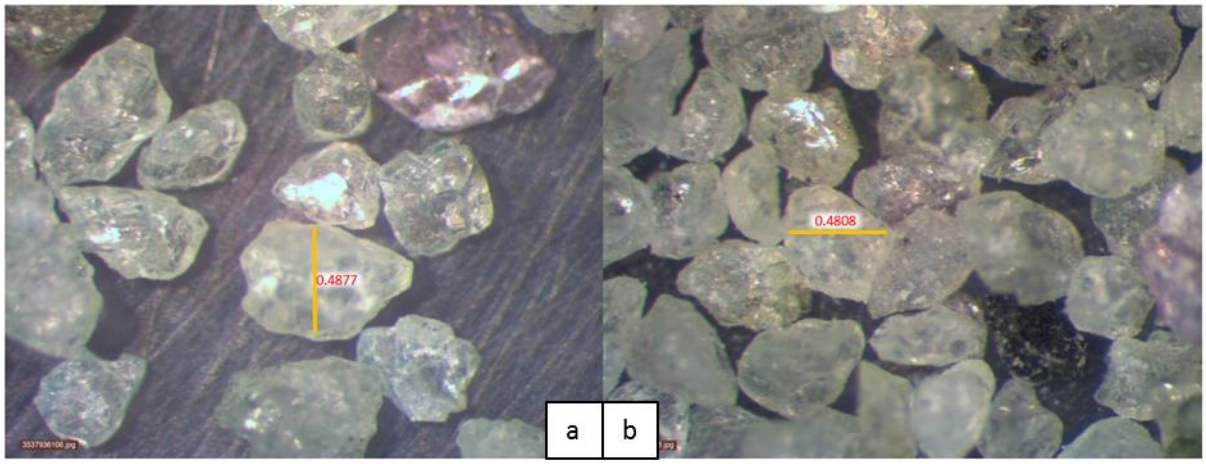

Figure 4-4 Magnified 280 µm -500 µm olivine (a) pre-erosion, (b) post-erosion, one hour at 1200 rpm (5.654 m s^{-1})

Figure 4-5 displays olivine particles in the size range of 500 µm -1 mm, being evaluated after being eroded at 1200 and 1800 rpm for a period of one hour. Figure 4-5(a) shows pre-erosion olivine particles, having clearly defined angularity. In Figure 4-5(b), which is after one hour of eroding fat 1200 rpm, it can be seen that although the particles have some rounding, it is not substantial. However, effect of attrition is pronounced when the olivine particles are run for the same time period at the higher velocity of 1800 rpm, Figure 4-5(c) shows more significant rounding, retaining only minor angularity. From this, it can be established that one hour is the extreme upper limit of the time interval that can be used in the evaluation

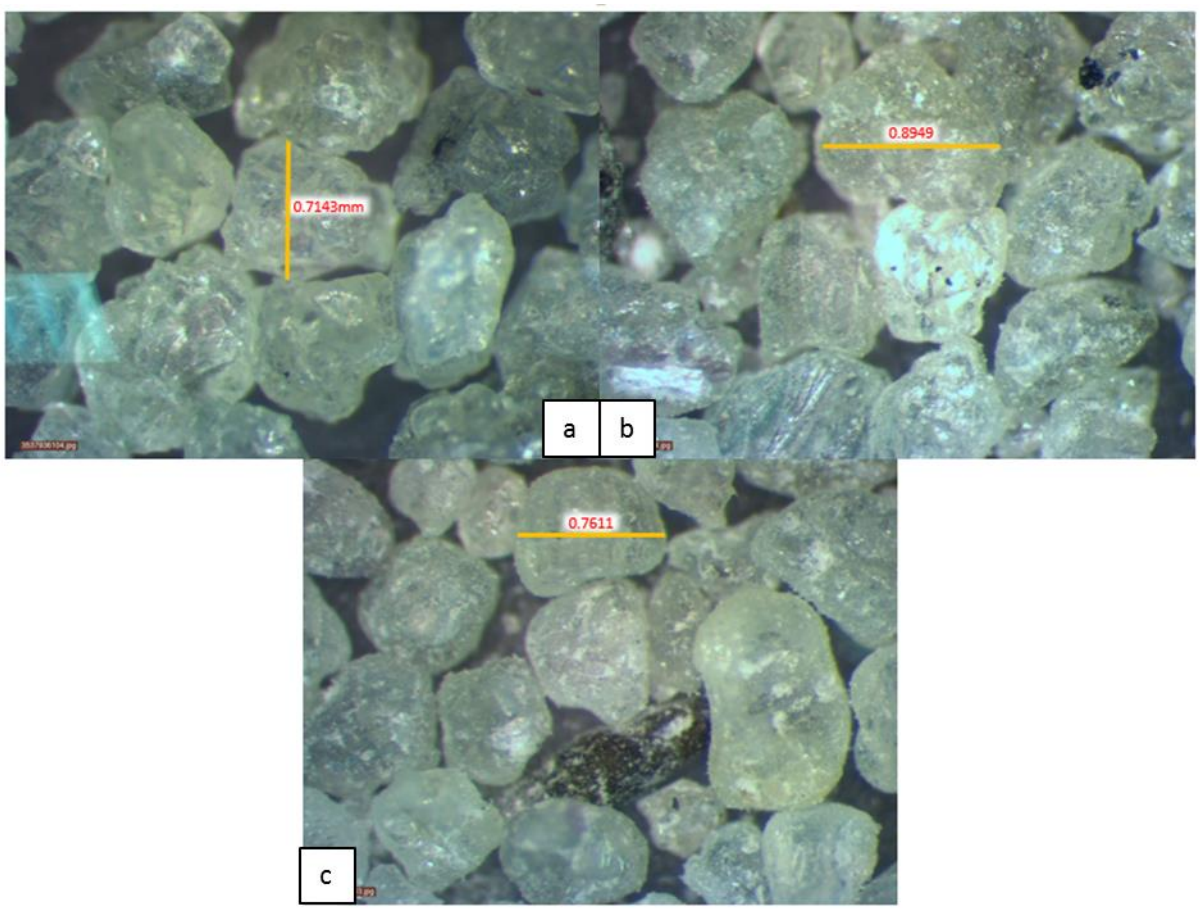

Figure 4-5 Magnified 500 µm-1 mm olivine (a) pre-erosion (b) post-erosion, one hour at 1200 rpm (5.654 m s^{-1}), (c) post-erosion, one hour at 1800 rpm (8.482 m s^{-1})

4.2 Results and Discussion

4.2.1 Influence of Velocity

As outlined in the section 4.1 the experimentation was conducted at three distinct velocities. Figure 4-6 outlines the results of the normalised mass loss for the three multi-sized particle ranges, plotted as a function of the flow velocity. The graph shows that at each particle size range, as the fluid velocity increases the mass loss of the target material also increases, however this is not a linear relationship. When comparing the average of the mass loss, for all three particle size ranges at 4.241 m s^{-1}, against the average of the mass loss at 8.482 m s^{-1}, the material experiences a 400% increase in the mass loss. This response to the velocity change, parallels findings in literature; Rajahram et al [74] details the same trend when eroding AISI 1020 Carbon steel with uncrushed silica sand in sodium hydroxide (NaOH).

The values of mass loss have been obtained through gravitational measurements, as described in section 4.1. Errors in the gravitational measurements have been minimised through, the process of recording the weight loss four times and taking the average of these. Each experimental run was conducted three times, and the error bars in the graph displays the standard deviation error which exists in the results from the experimental runs conducted. It can be seen that the deviation error is more significant at the higher velocities, however, the compact nature of the cluster of results provides confidence in the processes repeatability.

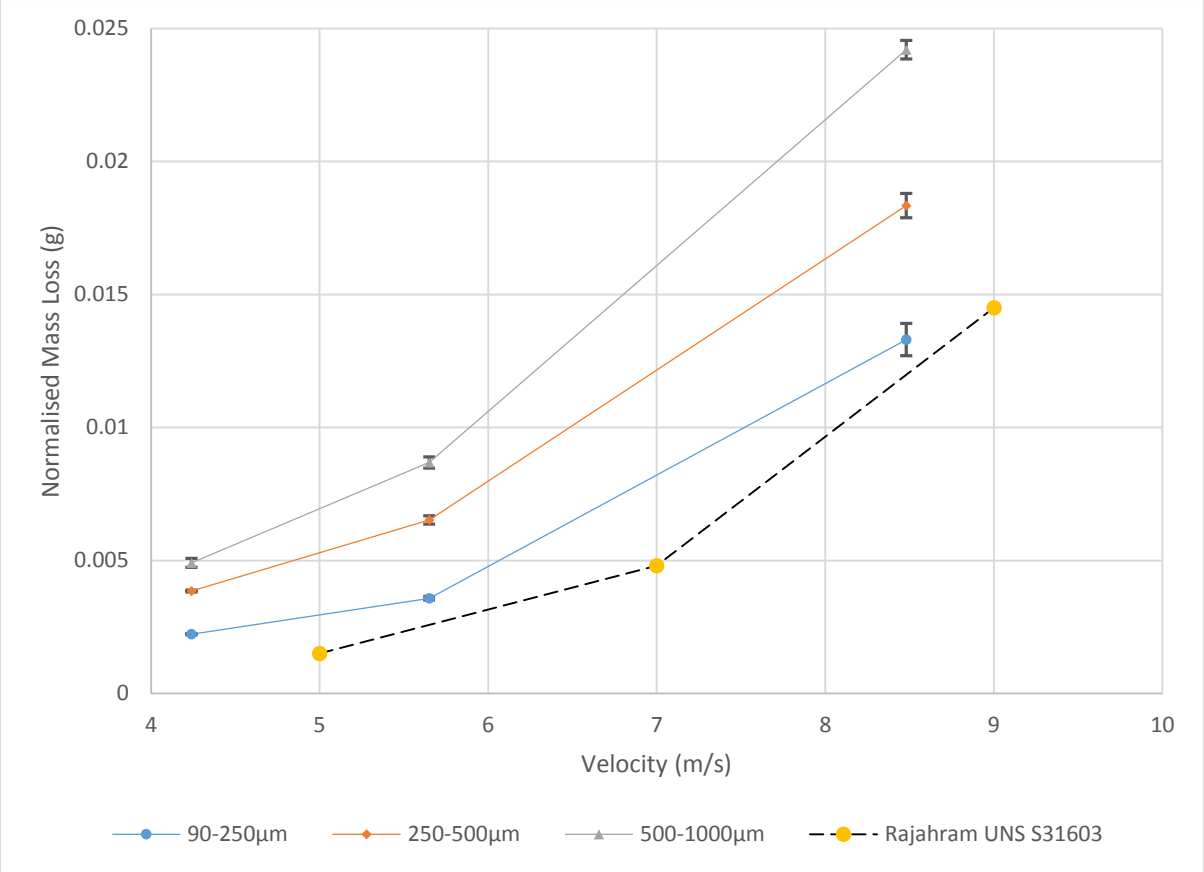

Figure 4-6 Experimental results of erosion on EN3B carbon Steel by sharp angular olivine 10 wt.% concentration at 60 mins

Figure 4-6 also provides a comparison between the current experimental results and those of Rajahram [22]. Representing the mass loss of a stainless steel eroded by silica sand, at a particle concentration of 3 wt.% and particle size of 294 µm. This comparison shows, that along with the general trend of the mass loss being the same, the results are comparable when factoring the differences in concentration and particle size to the current study. This provides confidence that when assessing solid particle erosion of steel as a function of velocity, olivine provides comparable results to those of silica sand.

It can be seen that for the larger particle sizes at any given fluid velocity, the mass loss is significantly higher, this will be discussed in further detail in the next section. The link between the particle kinetic energy and the erosion rate has been detailed by Lynn et al [21] and Clark et al [26], and concluded that the rate of energy dissipation of a particle is proportional to the erosion rate of the target material. The increase in the mass loss can be directly attributed to the available kinetic energy contained by the particle as a result of the higher particle velocity at impact. As outlined in section 1.3.4, the relationship between the mass loss and the velocity is not always a squared relationship, by virtue of the complex interdependence of flow variables.

In this experimentation, the specimens are placed at a 90^{o} orientation, however, the actual impact angle of each particle, and by extension, the manner in which this changes with velocity, is not identified. What has been identified, however, is that the impact angle is not uniform through the entire target wall face. This becomes apparent when analysing the surface profile of the samples. In Figure 4-7 a surface profile of a test sample eroded for six hours can be seen. It shows greater wear towards the outer edge of the sample. This is due in part, to greater velocity further away from the centre of the test pot, moreover, this can be attributed to the flow divergence which occurs, from the stagnation line towards the outer edge of the target wall. This in-turn changes the initial trajectory of the particle thus impacting the wall at an angle other than normal.

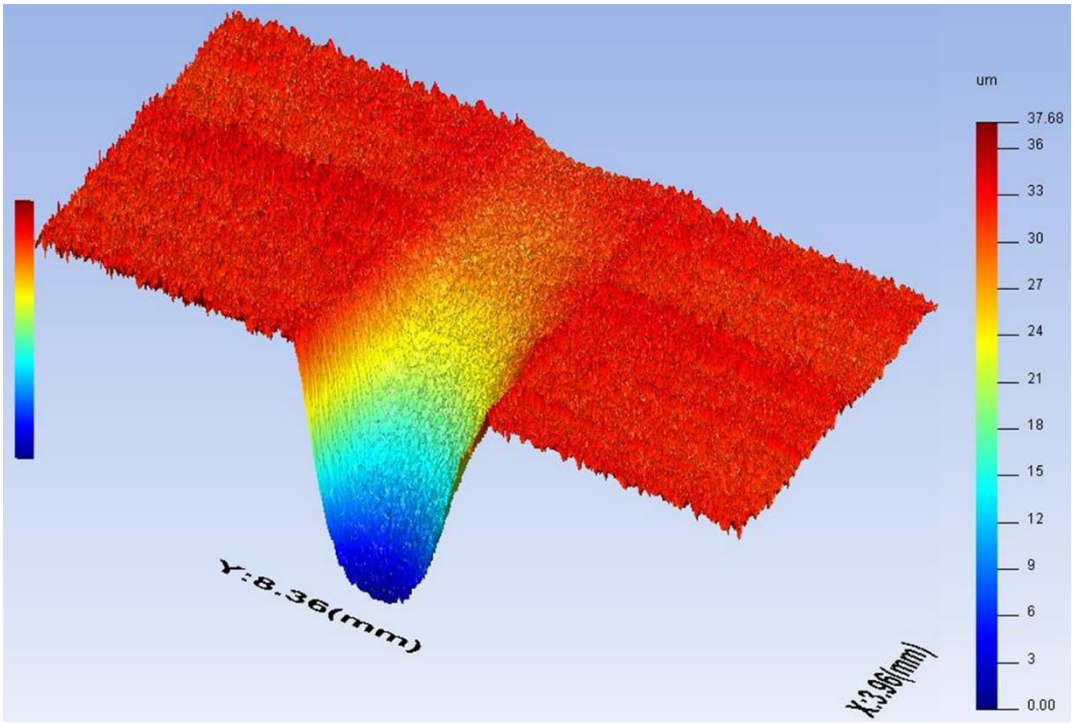

Figure 4-7 Surface texture and profile of specimen, after six hours of erosion at a concentration of 10 wt.% at 90^{o} orientation

4.2.2 Influence of Particle Size

The effect of the particle size range on the erosion rate has been graphically illustrated in Figure 4-8, which displays the erosion rate in kg m^{-2} s^{-1} as a function of the particle size. The response of a target material to a change in the erodent size varies significantly depending on a number of factors. Changing the erodent, the erodent shape or even the erosion testing equipment can provide a significantly different response. In the case of EN3B in an erosive aqueous environment, using an erosion pot tester, with olivine at 10 wt.% concentration. The erosion rate shows an ever-increasing trend as the particle size range is increased, between the sizes of 90 µm and 1 mm, when subjected to multi-sized particle impingement.

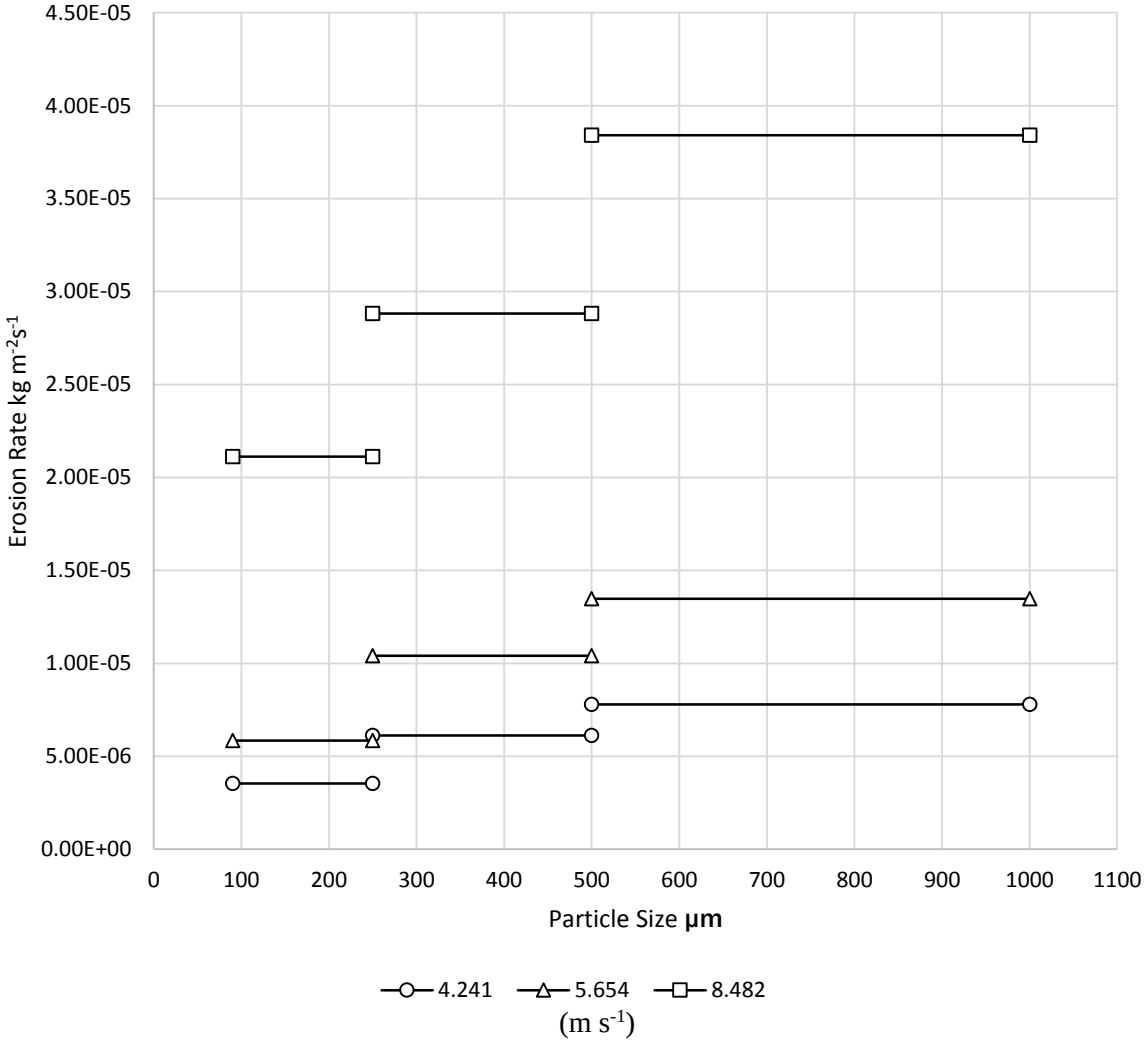

Figure 4-8 Experimental results of erosion on EN3B carbon Steel by sharp angular olivine 10 wt.% concentration at 60mins of exposure time

At the velocities being evaluated, the smaller particle size range (90 µm to 280 µm), exhibits a significantly lower erosion rate than the larger sizes of particles. Table 4-2 is a tabulated dataset showing the percentage increase in the erosion rate as the particle size increases. It can be inferred that the change in the erosion rate is greater when the particle size is increased from small to medium, than when it is further increased from medium to large, except at 8.482 m s^{-1} where there is parity in the percentage increase. When considering the percentage increase in the erosion rate from the small to large size, for 4.241 m s^{-1} and 5.654 m s^{-1} the erosion rate

increases by 120.1 % and 130.3 % respectively. However, at a speed of 8.482 m s^{-1} the percentage increase is 86.6 % which is a significantly lower increase than was seen at the lower speeds. A possible explanation for this, is that the effect of particle attrition, particularly, with respect to the rounding of angular particles, is more significant at the higher velocity. This has the effect of producing a lower erosion rate than would otherwise be generated, had the particles remained angular.

Table 4-2 Percentage increase in erosion rate with the increase in particle size for each reference velocity

Linear Velocity m s^{-1}	Particle Size	280 µm to 500 µm	500 µm to 1 mm (l)
4.241	90 µm to 280 µm (s)	72.70%	120.07%
	280 µm to 500 µm (m)	x	27.43%
		280 µm to 500 µm	500 µm to 1 mm
5.654	90 µm to 280 µm	79.07%	130.29%
	280 µm to 500 µm	x	28.60%
		280 µm to 500 µm	500 µm to 1 mm
8.482	90 µm to 280 µm	35.94%	86.61%
	280 µm to 500 µm	x	37.27%

A study by Lynn et al [21], evaluating the erosion of steel by 1.2 wt.% SiC in an erosion test pot, concluded that there is a limiting value at which the erosion rate stops increasing with the increase in particle size. This occurs when the collision efficiency reaches unity, and the effect of squeeze film and flow divergence are negligibly small. Other works as detailed in 1.3.2 find, that beyond this limiting value any further increase in particle size has a regressive effect on the erosion rate. This could be due to particle-particle interactions or potentially increased friability of particles. Most of these studies explored particles in a narrow-size range, representing equi-sized particles. However, the present work investigates several multi-sized particle ranges.

One of the contributing factors to the effect of the particle size on the erosion rate is that of collision efficiency, which describes the ratio of particle impact on a given area over a period of time. As the particle size decreases, the effects of liquid drag overcome the particles inertia and the particle then has a tendency to conform to the divergent flow of the fluid [18]. This collision efficiency increases as the particle size increases which accounts for the increase in erosion rate with size, alongside the increase in the kinetic energy dissipation at impact.

Multi-sized slurries, offer a particular complexity as it relates to describing the particle size, Figure 4-8 avoids the use of a nominal size but rather shows the size banding for each study. Gandhi and Borse [84] assessed the accuracy of using a nominal size of the particles as a representation of the slurry, and found that the results deviated by up to 45% when compared to a comparable uni-sized slurry. Ghandi and Borse [85] extended this understanding, and proposed the use of the weighted mass particle size, d_{wn} as seen in equation (4-1). This is a description of the size distribution by weight in a given slurry. N is the number of divisions which have been made within the size band, f_i is the mass fraction of each size group and d_i is the nominal diameter of the upper and retaining sieve (lower sieve).

$$d_{wn} = \left\{ \sum_{i-1}^{N} f_i \, d_i^3 \right\}^{1/3} \quad (4\text{-}1)$$

In order to determine the weighted mass particle size for each size range the information gathered from the particle size distribution in section 3.2 was used. This information provided enough data points to determine the d_{wn} for the large and medium particle size ranges. For the smaller particle size range an additional particle size fraction was carried out, which determined the particle mass fraction between 90 µm and 280 µm. The representative particle size for each size range, is shown in Table 4-3, while Figure 4-9 shows the erosion rate versus particle size using the nominal size, determined through the use of the weighted mass particle size for each slurry size range. Using d_{wn}, as in Figure 4-9, provides more practical data when evaluating the erosion rate as a function of particle size for multi-sized particle slurries.

Table 4-3 Weighted mass particle size for multi-sized particle ranges used in slurry

Size Range	90 µm to 280 µm	280 µm to 500 µm	500 µm to 1 mm
Weighted mass Particle Size (m)	0.000195	0.000435	0.000732

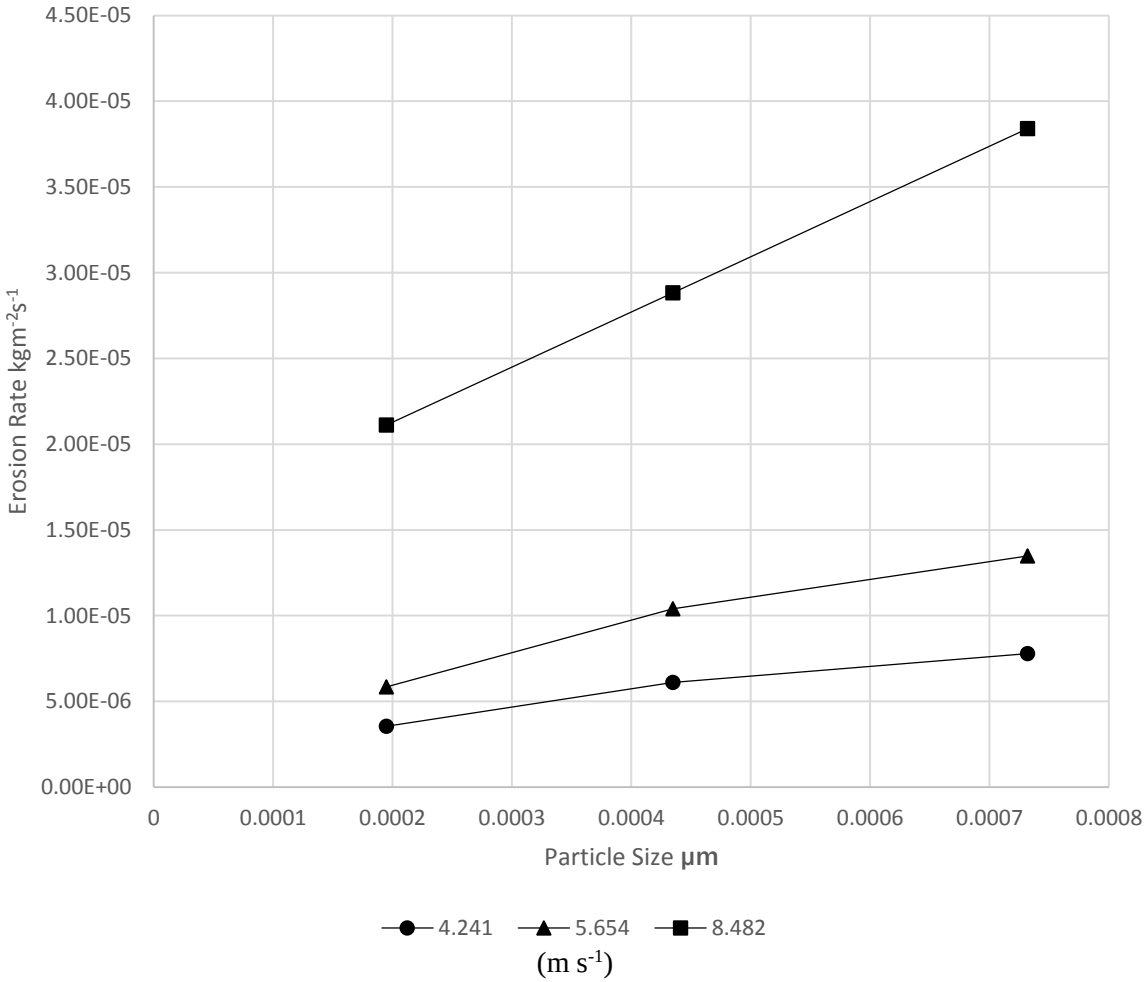

Figure 4-9 Variation in erosion rate as a function of particle size using the weighted mass particle size method

4.2.3 Effect of Exposure Time on Erosion Rate

The temporal nature of solid particle erosion has been discussed albeit to a limited degree in section 1.3.5 as well as in the literature review found in Chapter 2. It has been understood through the studies conducted over the years that the manner in which a target wall erodes with respect to time varies significantly across test conditions. For this analysis, an erosion test pot was used to determine the progressive nature of eroding EN3B mild carbon steel in an aqueous environment using multi-sized olivine particles at a suspension concentration of 10 wt.%. The results of this study found that the erosion rate is relatively constant from the onset of the test with no distinguishable pattern which suggests a changing erosion rate over a period of time.

A study conducted by Gadhikar et al [86] assessed the time dependence of erosion. Figure 4-10 is an illustration of the results, from which it was found that when mild steel is eroded by sand over a 16-hour period, there exists a period of incubation followed by an acceleration of the erosion rate up to a peak value, a subsequent deceleration period, followed by the attainment of a stead state, all occurring within the first six to eight hours. This study was carried out at a specimen velocity of 120 rpm using uni-sized particles. It must be noted that the grade of steel, the type of sand, and the process by which the study was carried out have not been described in the study. Furthermore, the time intervals between the replacing and replenishing of the eroding mixture for not offered.

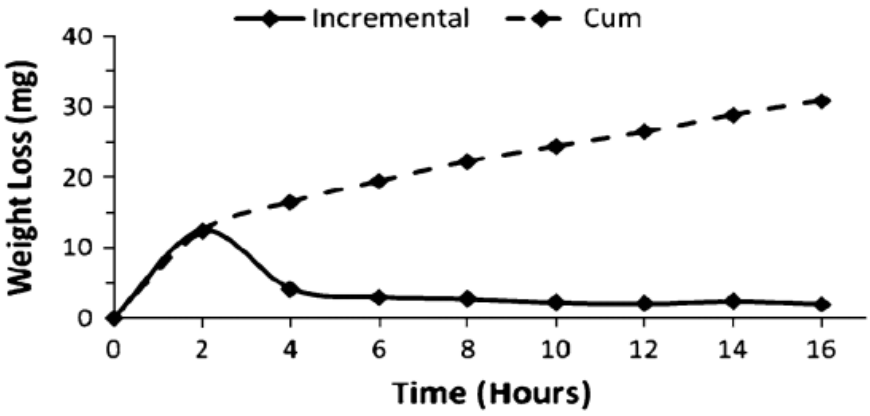

Figure 4-10 Variations in weight loss as a function of time for mild steel erodes by sand [83]

As described in section 4.1, preliminary experiments were conducted and found negligible difference in the erosion rate at four hours and eight hours, therefore, the time period assessed in this study range from thirty minutes to three hours. The graphical results of this study have been presented in Figure 4-11 and Figure 4-12, the mean values for the multiple experimental runs at each time interval returned slight variation in the results. The uncertainty in the values has been quantified by the standard deviation error shown in the error bars in both plots. The 30 minute readings seem to be more susceptible to fluctuations with all four plots relaying this same trend. This could be down to the experimentation process, particularly the process or changing the eroding mixture at 1 hour intervals. Taking the mean of each dataset, and evaluating the percentage difference from the data points, the largest percentage difference was found to be 2.6 %, with the average percentage difference across all four data sets being 1.1%. This can be taken as negligibly small changes in the erosion rate, hence, immediate steady state is achieved. The results are in agreement with a number of studies including, [32], [49], [87] and [75], which all found the erosion rate to reach a steady state from the onset, albeit, all covering a different scope i.e velocity, target material, eroding material, equipment.

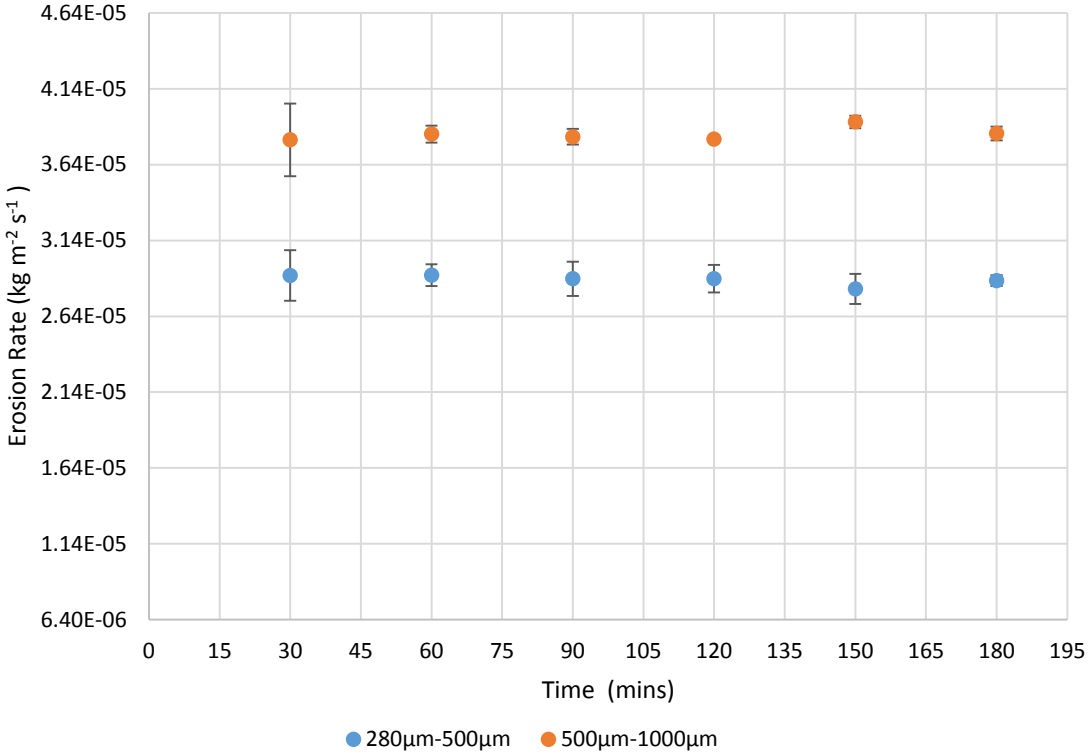

Figure 4-11 Erosion rate of EN3B as a function of time, for (280 to 500 and 500 to 1000) µm at 8.482 m s^{-1}

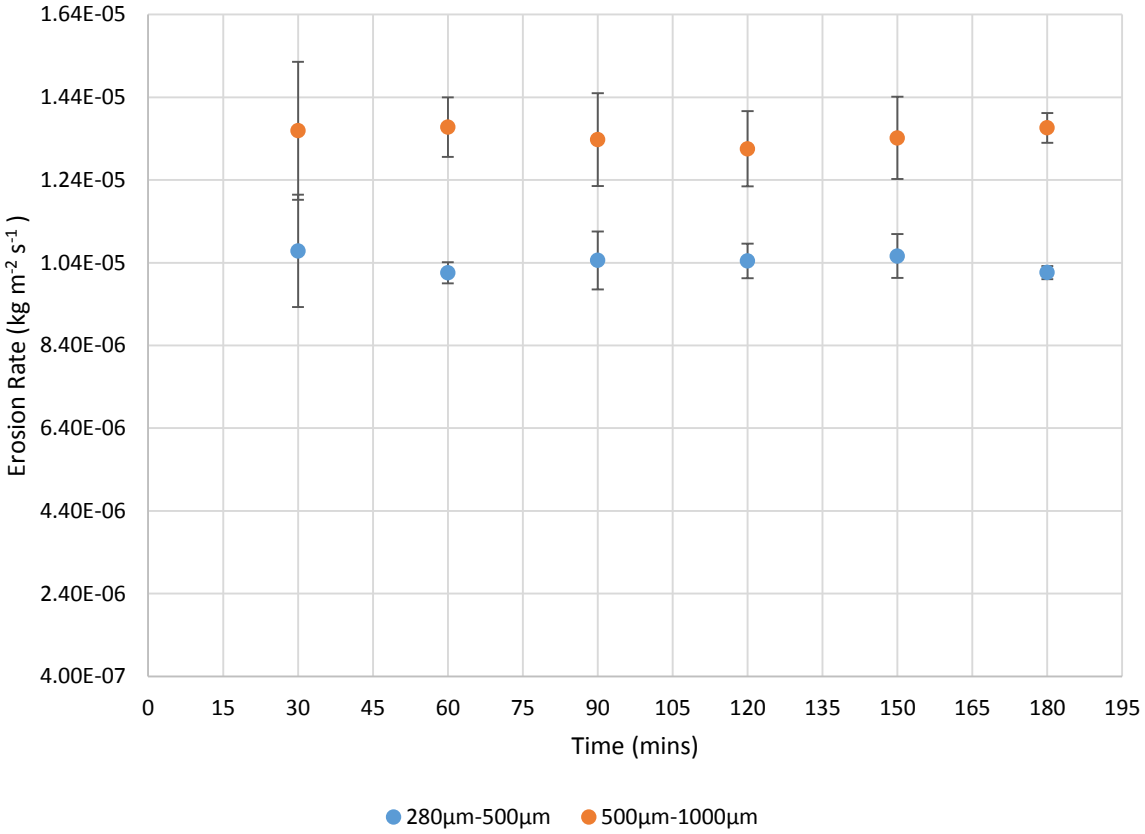

Figure 4-12 Erosion rate of EN3B as a function of time, for (280 to 500 and 500 to 1000) µm at 5.654 m s^{-1}

4.2.4 Modified Model for Erosion Prediction

Computational fluid dynamics has proven a vital tool in the field of particle erosion prediction as it provides both, quantitative and qualitative benefits in the form of erosion rate prediction, while also highlighting data such as the location of erosion wear. This section provides the process taken in developing the erosion prediction model.

The Erosion and Corrosion Research Centre is one of the premier bodies conducting experiments, gathering field data and carrying numerical modelling in the field of solid particle erosion. The body of work which has been produced under this umbrella has offered a number of erosion models all based on the principal E/CRC model also referred to as the Tulsa model equation (1-3). Equations (1-4) and (1-5) show several different angle functions which have been proposed, while other modifications of the E/CRC model include the Ahlert model equation (2-9) and the Zhang model (4-2). One of the principle conclusions made by Parsi et al [12] is the fact that erosion models are too conservative. Furthermore, of the twenty-three erosion equations reviewed in that study, only ten contained the particle diameter as a contributing variable.

$$\mathrm{Er} = 2.17 * 10^{-7}(\mathrm{HB})^{-0.59}\mathrm{V}^{2.41}(\mathrm{f\theta})\mathrm{F_s} \tag{4-2}$$

The novel erosion rate prediction model being proposed in this study, is based on modifying the Tulsa/Zhang model in equation (4-2), by incorporating the effect of multi-size particle diameter, using the weighted mass particle size, as described in section 4.2.2. For this work, several functional relationships have been adopted; the angle function (fθ) for carbon steel provided by Zhang et al [70], the material hardness function ($B^{-0.59}$) as given by the Alhert in Edwards et al [65] and the influence of particle shape 1, 0.52, and 0.2 for angular, sub angular and rounded particles respectively.

In order to ensure that the equation remains dimensionally unchanged, a non-dimensional particle size function has been offered. The functional relationship between the erosion rate and the particle size for multi-sized particle slurry has been established, as an exponential relationship of the weighted mean particle size of the slurry (d_{wn}), divided by the pipe/test-pot diameter (D), as shown in equation (4-3).

$$\mathrm{Er} \propto \left(\frac{\mathrm{d_{wn}}}{\mathrm{D}}\right)^{\mathrm{x}} \tag{4-3}$$

A log-log, multiple variable regression analysis, was conducted on the dataset of experimental values with an R square value of 0.972069. The model describes, the functional relationship of the erosion rate as a function of velocity, particle size, impact angle, particle shape and material hardness. The predictive model is offered in equation (4-4), along with the adopted angle function relationship established in the Zhang/Tulsa model (equation (1-4)), and the associated empirical constants for the angle function and shape function shown in Table 4-4.

$$\mathrm{Er}\left(\frac{\mathrm{kg}}{\mathrm{kg}}\right) = 1.036 * 10^{-7}(\mathrm{B}^{-0.59})\mathrm{F_s}(\mathrm{f\theta})\mathrm{V}^{2.35}\left(\frac{\mathrm{d_{wn}}}{\mathrm{D}}\right)^{0.56} \tag{4-4}$$

$$\mathrm{f}(\theta) = \sum_{\mathrm{i}=0}^{5} \mathrm{A_i}\,\alpha^{\mathrm{i}}$$

Table 4-4 Values of empirical constants of angle function and shape factor for erosion prediction model as provided by Zhang et al [70]

Value of A_i				
A_1	A_2	A_3	A_4	A_5
5.40	-10.11	10.93	-6.33	1.42
Shape Factor F_s				
Angular (sharp)		Sub Angular		Rounded
1		0.52		0.2

Figure 4-13 shows the difference between the erosion rates calculated through the model presented, and the results obtained through experimentation, converted to mm yr^{-1}. From Figure 4-13, it can be clearly seen that over 91% of the data fall within an uncertainty band of 20%, through a +12%/-8% error band for the empirical expression for erosion rate. Hence, the prediction model offered in this study, represents the erosion rate of steel in an aqueous solution, eroded by olivine with reasonable accuracy.

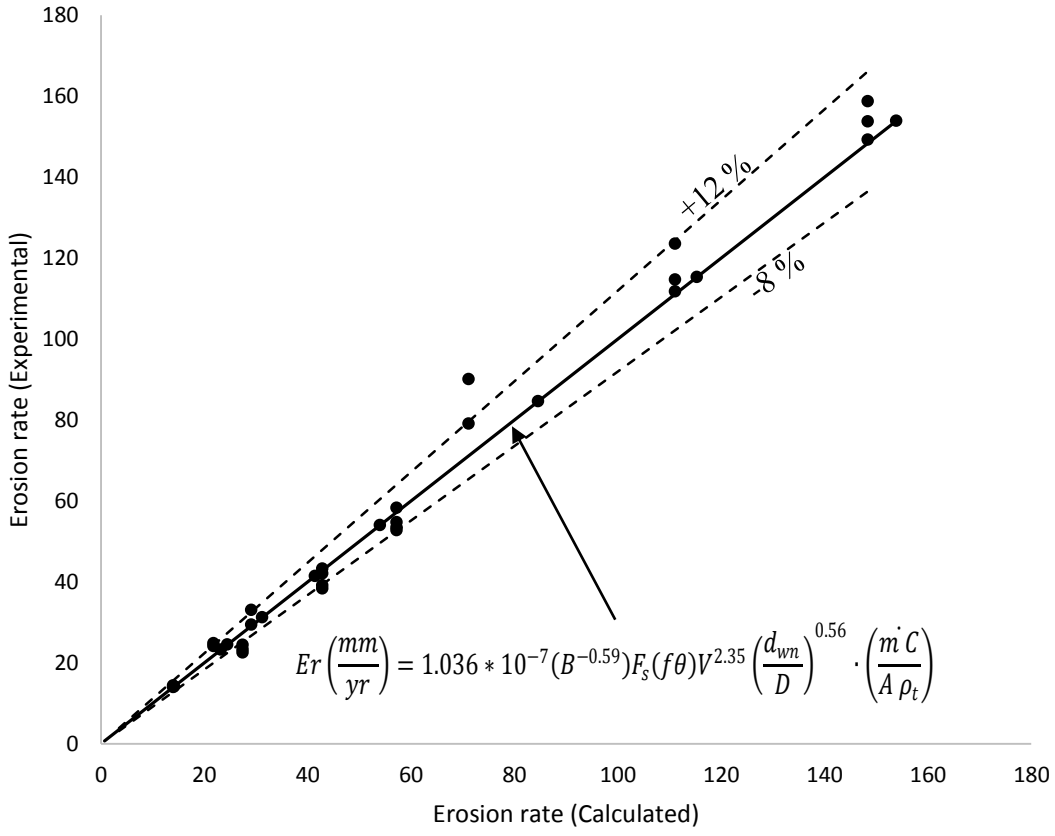

Figure 4-13 Erosion rate for carbon steel eroded by olivine

4.3 Summary of Work

A mild carbon steel EN3B and a naturally occurring mineral olivine have been used to assess the solid particle erosion rate in an aqueous environment. A slurry pot tester was used in order to perform experimentation at a solid particle concentration of 10 wt%. The influence of velocity, particle size and time on the degradation of a surface due to solid particle erosion have been evaluated and a new model has been proposed for erosion prediction. From this study the following deductions have been established:

1. Due to particle attrition, which is evident through both rounding and particle breakup, the slurry test pot has the potential to underestimate actually erosion rate. However, the hourly replacement of the eroding mixture has been found to be appropriate, for better result particularly at the high flow velocity this could be reduced.
2. Erosion increases with the increase in flow velocity, this has been observed to be an exponential relationship with the value of the velocity exponent n found to be 2.35.
3. Despite the use of a different erodent and the use of multi-sized particles the velocity exponent n has been found to be comparable to that found in literature for similar for steels.
4. In this study the value of n, has been evaluated for the entire data set, and has been approximated to a constant value, this is also the assumption made in other studies. However, when n is evaluated for the individual data sets constant velocity changing particle size, the value of n was found to change with particle size. However as outlined in section 1.3, and as offered by Clark [19], the relationship between velocity and particle size is complex. A direct relationship could not be established in this work, however further work can be conducted to examine the interaction between these two parameters.
5. For the multi-sized particles, an increase in the particle size has the effect of increasing the erosion. Both graphs shown in Figure 4-6 and Figure 4-8 show the particle size is not a negligible parameter in the evaluation of erosion. Although ignored in many erosion models, the particle size was found to have an exponential relationship with the erosion rate and the exponential constant x was evaluated to be 0.56.
6. In studies using equi-sized particles researchers have found a limiting particle size at which the erosion rate slows down and regresses as the particle size increase. In this application using multi-sized particles between 90-280, 280-500, and 500-1000 (µm), in an aqueous slurry, this was not observed.
7. Under the present experimental conditions, it has been determined that EN3B does not have a quantifiable incubation period, and attained a steady state erosion rate immediately, under the time intervals evaluated.
8. A new model has been presented and a User Defined Function has been written which can be hooked onto ANSYS Fluent to compare against other accepted models.

$$\mathrm{Er} = 1.036 * 10^{-7}(\mathrm{B}^{-0.59})\mathrm{F_s}(\mathrm{f\theta})\mathrm{V}^{2.35}\left(\frac{\mathrm{d_{wn}}}{\mathrm{D}}\right)^{0.56}$$

In the next chapter, a thorough discussion is presented on the results obtained by using a non-contact surface topography method, to assess the change in surface texture of the material surface as a result of being bombarded by the solid particles in the slurry test pot

Chapter 5 INVESTIGATION OF SURFACE TEXTURE BY SLURRY EROSION

This chapter details the process undertaken to both, erode the target surface as well the process undertaken to analyse the surface morphology. Moreover, this chapter provides a qualitative and quantitative assessment of the influence of velocity, time, multi-sized particle and impact angle on the change in surface roughness.

5.1 Methodology

In order to conduct the analysis of the surface morphology, erosion experimentation is conducted in a slurry test pot using water as the bulk fluid and angular olivine as the eroding mixture. The general procedure for the experimentation follows from the methodology outlined in sections 3.3 and 4.1.

In assessing the effect of orientation angle, parallel flow erosion which occurs at 0^o is not considered, however four orientation angles have been used and range from 15^o to 90^o. A full factorial evaluation has been conducted, and the principal variables investigated are the impact angle, which is taken as the orientation angle of the target wall to the flow, the flow velocity, particle size, and the exposure time. Details of the full factorial experiments conducted at each hour can be seen in Table 5-1, this was repeated for a second and a third hour. A solid particle concentration of 5 wt.% was used in this study.

Table 5-1 Table of experimentation conditions tested for the surface measurement analysis

Time	Size	Velocity	Angle (deg)			
Hours		rpm/m s^{-1}	15	30	60	90
1	280 µm to 500 µm d_{wn}0.000435 m	900/4.241	✓	✓	✓	✓
		1200/5.654	✓	✓	✓	✓
		1800/8.482	✓	✓	✓	✓
	500 µm to 1 mm d_{wn}0.000732 m	900/4.241	✓	✓	✓	✓
		1200/5.654	✓	✓	✓	x
		1800/8.482	✓	✓	✓	✓

The samples used contain an eroded zone flanked by two un-eroded zones at either end of the sample. The uneroded zones are the portions shielded by the plastic inserts, Figure 5-1(a) provides a visual of this arrangement and Figure 5-1(b) is the resultant topographical image. The specimen used have a footprint dimension of 10 mm x 45 mm with a depth of 5 mm. In order to prevent wear on the non-target walls of the sample, a housing was made for the sample to slot into. This takes the same general concept of that seen in Figure 5-2. For this study, a housing has been purpose made from resin, and arranged to ensure that only the target face of the sample was exposed during erosion.

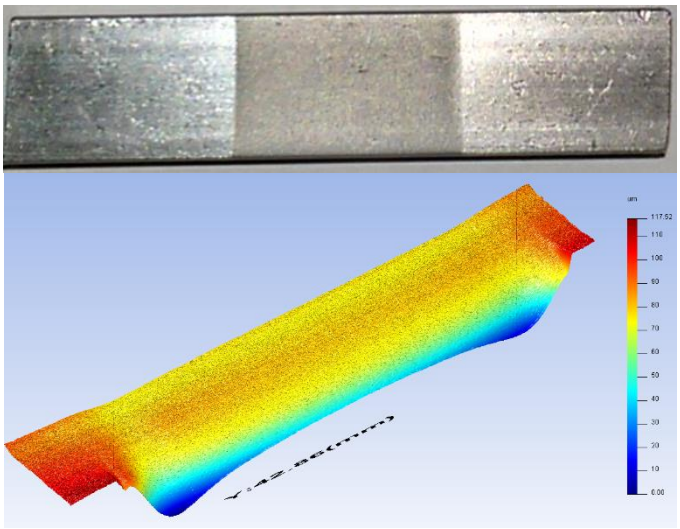

(a)

(b)

Figure 5-1 EN3B sample as eroded by olivine, showing both eroded and un-eroded sections

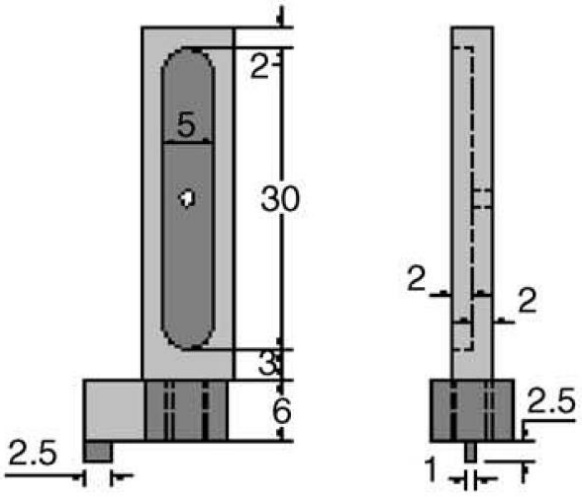

Figure 5-2 Sample housing as used in erosion test pot by Desale et al [63]

After each experiment the surface is profiled using optical three-dimensional surface measurement. As described in section 1.4.3, the distinguishing factor that separates roughness, waviness and form is the wavelength spacing, and the value of the cut-off wavelength is highly dependent on the application. Blunt and Jiang [53] provide a practical example of this in highlighting that the roughness of a component such as the axle of a motor vehicle, would in practical terms, be considered waviness or even form, when assessing a precision piece, such as the spindle of a watch.

In this study two standards have been applied to determine the appropriate settings required in order to both capture, and analyse surface roughness. The BSI Standard BS EN ISO 4288:1998 [88] defines the appropriate sampling length based on the average profile roughness Ra, Table 5-2 displays values extracted from the standard. For this evaluation, the average profile roughness values, both pre, and post erosion, fall between the 0.1 and 2 (µm) banding, which equates to a sampling length of 0.8 mm. The other standard used is the BSI Standard ISO 25178-3:2012 [89] that defines the nesting indices and appropriate sampling distance to use for surface texture mapping. The sampling length determined through the Ra parameter, is equivalent to the L-filter (λc) for the areal evaluation [90]. This L-filter nesting index is used to determine the range of values for the S-filter nesting index based on the BSI Standard as shown in Table 5-3. The S-Filter cut-off which is a noise filter, has to be at least five time the size of the sampling distance for image capturing. The optical lens used for this study is a 10x lens with an inherent sampling distance of 0.88 µm. Through the process of apply the standards, the sampling conditions used for this evaluation have been tabulated in Table 5-4.

Table 5-2 Roughness Sampling lengths for measuring Roughness parameters [88]

Ra (µm)	Roughness Sampling length (mm)
0,006< Ra≤ 0,02	0,08
0,02< Ra≤ 0,1	0,25
0,1< Ra≤ 2	0,8
2< Ra≤ 10	2,5
10< Ra≤ 80	8

Table 5-3 Relationship between L-Filter and S-filter nesting index for the given conditions [89]

L-Filter Nesting index value (mm)		S-Filter Nesting Index Value (mm)
0.8	Max	0.008
		0.0025
	Min	0.0008

Table 5-4 Sampling conditions applied in this study

Sampling length	F operator	Sampling Distance	S-Filter nesting index	L-filter nesting index
800 µm	Levelling	0.88 µm	8 µm	800 µm

One of the limitations of the Alicona software is its inability to scan over 100million surface points in one image field, as a result four steps of decimation were used. This form of down-sampling is used to reduce the number of data points stored to fall within the Alicona's capabilities.

Most surfaces, contain some element of form, this could be a functional geometric form, such as the cylindrical profile of a bullet or it could be non-functional such as a tilt or warping of the object. The samples being used have a slight bow which is largely unnoticeable to the naked eye, there is a significant height difference from one end of the sample to the other which is quite apparent once scanned. Figure 5-3 (a) shows the profile of a sample scanned, with the surface of interest changing from a height of -10 µm to -70 µm (approximately). In order to evaluate a functional surface devoid of geometric form, form removal is the first process that must be undertaken [91].

This F-operator extracts a set of data points from the primary surface to create a planar S-F surface leaving just the roughness and waviness profiles [92]. The virgin profile produced a height variance of 60 µm however the form removed profile shown in Figure 5-3(b) produced a height variance of approximately 2 µm.

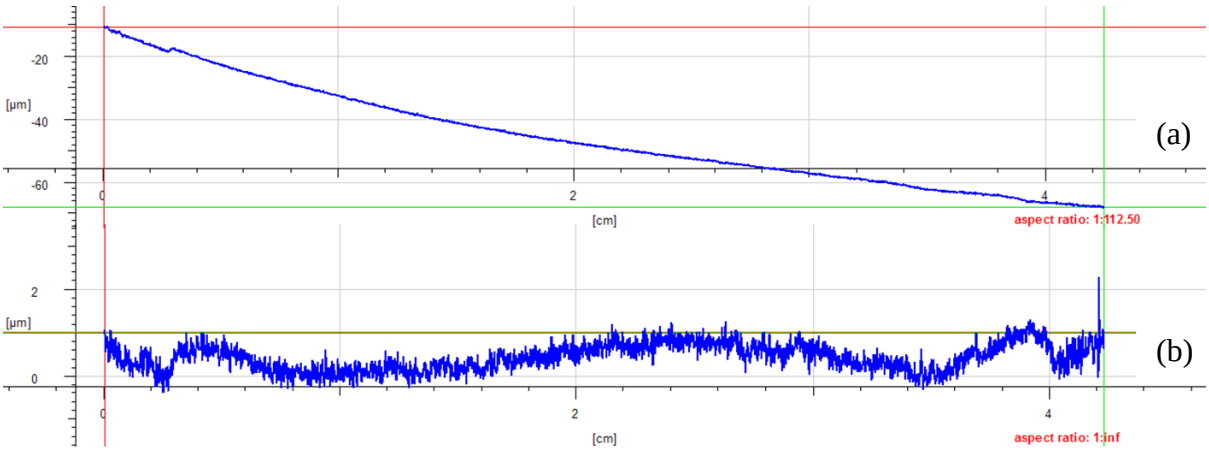

Figure 5-3 Form profile of sample (a) virgin dataset (b) dataset profile with form removal applied

The need to apply the correct cut-off filter, can be summarily visualised in Figure 5-4 and Figure 5-5. The former shows the profile roughness with a default λc cut-off of 8000 µm where the waviness profile has not been filtered out, while the latter is the profile roughness after a cut-off value of 800 µm showing the roughness waveforms.

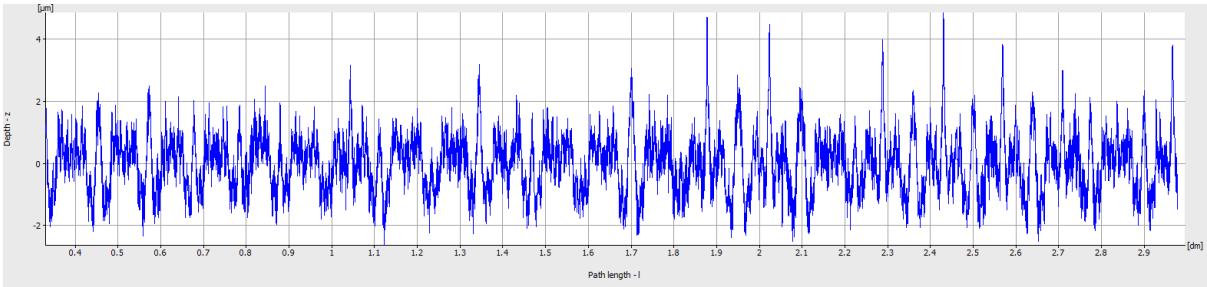

Figure 5-4 Frequency profile of waviness and roughness profile on sample surface with 8000 µm cut-off

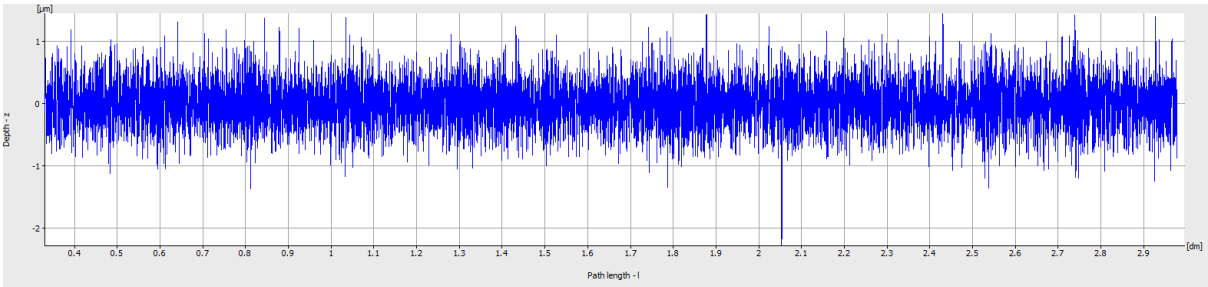

Figure 5-5 Frequency profile of roughness profile on sample surface with 800 µm cut-off

There are a host of different parameters that can be utilised in describing the texture of a surface. One of the most used is the Sa, which is the arithmetic mean of the absolute height of the peaks, valleys of the sampling domain. It has been described as the surface texture extension of the Ra (line parameter) however Blateyron [93] highlights the exclusion of the Sa from Blunt's and Jiang' SURFSTAND report [53] specifically to avoid it being used as the surface texture equivalent of the Ra. Sa is insensitive to discerning peaks or valleys which results in spatially dissimilar surfaces obtaining the same value of Sa [94]. In order to account for both amplitude and spatial changes a hybrid parameter is most appropriate. As such the primary parameter being used in this evaluation is the Developed interfacial area ratio S_{dr}, which describes the additional surface area of the textured domain compared to that of the cross sectional area of a planar surface of the same x,y plane. The S_{dr} can be represented mathematically by equation (5-1). The higher the frequency and amplitude of the peaks and valleys on a surface the large the value of S_{dr} conversely the S_{dr} of a planar surface is equal to zero [53].

$$S_{dr} = \frac{\sum_{j=1}^{N-1}\sum_{i=1}^{M-1} A_{i,j} - (M-1)(N-1)\delta x \cdot \delta y}{(M-1)(N-1)\delta x \cdot \delta y} \cdot 100\% \qquad (5\text{-}1)$$

The S_{dr} was determined by obtaining the roughness from ten random locations on the specimen, this was done for both the eroded and un-eroded sections. The mean of these readings and the standard deviation were calculated and the details of the results are presented in section 5.2.

5.2 Results and Discussion

5.2.1 Evaluation of Surface Roughness as a Function of Velocity and Particle Size

In evaluating the manner in which the surface texture changes with changes in the flow velocity, experimentation has been conducted at three velocities, in accordance with the procedure outlined in section 5.1. This section also assesses the surface texture changes with respect to the particle size, by which the experiments were conducted using two distinct multi-sized particle ranges, which are described throughout this chapter as medium, (M or d_{wn} 435 µm) and large (L or d_{wn} 732 µm). As each sample has a unique surface texture, this analysis does not describe the absolute surface texture before and after erosion, but rather, it evaluates the change in the surface roughness under the stated conditions, through the hybrid parameter S_{dr}. As a point of note, the results for the sample eroded at 90^o with the large particles has been omitted from the analysis.

The results obtained of the change in the developed interfacial area ratio, before and after erosion, can be seen graphically in Figure 5-6, Figure 5-7 and Figure 5-8, which are displayed as a function of the flow velocity at one, two and three hour erosion intervals respectively. When the surfaces of the samples are eroded, they all exhibit a lower value of S_{dr} which signifies a reduction in the roughness of the surface. The graphs, indicate a general trend in the behaviour of the surface texture as the velocity is increased, irrespective of particle size. This same pattern is seen at the two, and three hour erosion intervals. When the flow velocity is set to 4.241 m s^{-1} the change in S_{dr} is positive indicating a reduction in surface roughness from that of the uneroded surface. The average increase in ΔS_{dr}, when the velocity is increased from 4.241 m s^{-1} to 5.654 m s^{-1}, is 13.59 %. As such, a target wall eroded at 5.654 m s^{-1} produces a smoother surface than one eroded at a lower velocity. Conversely when the velocity is increased further, from 5.654 m s^{-1} to 8.482 m s^{-1}, ΔS_{dr} decreases by 13.54 %, which indicates an increase in the surface roughness compared to that generated at 5.654 m s^{-1}.

When assessing the individual data sets it can be seen that some exhibit a different response to the change in velocity than the universal trend; 90^{o}M at all three hours evaluated, 60^{o}M at the one and two hour intervals and 15^{o}L at two and three hour intervals, display a slightly different response to the change in the flow velocity from 5.654 m s^{-1} to 8.482 m s^{-1}. Despite this inconsistency and with the exception of 90^{o}M at the one hour interval, these datasets exhibit a significant reduction in the gradient from 5.654 m s^{-1} to 8.482 m s^{-1} compared to that from 4.241 m s^{-1} to 5.654 m s^{-1}. These anomalous values could be as a result of the process undertaken in determining the average surface roughness. The surface texture is not a uniform value through the entire sample which results in the need to measure the texture in multiple locations. The process of selecting ten random sample lengths could still yield values that are higher or lower than the overall surface roughness. This notwithstanding, the process has yielded a good appreciation of the trend in the change of the developed interfacial area ratio with respect to the changes in velocity.

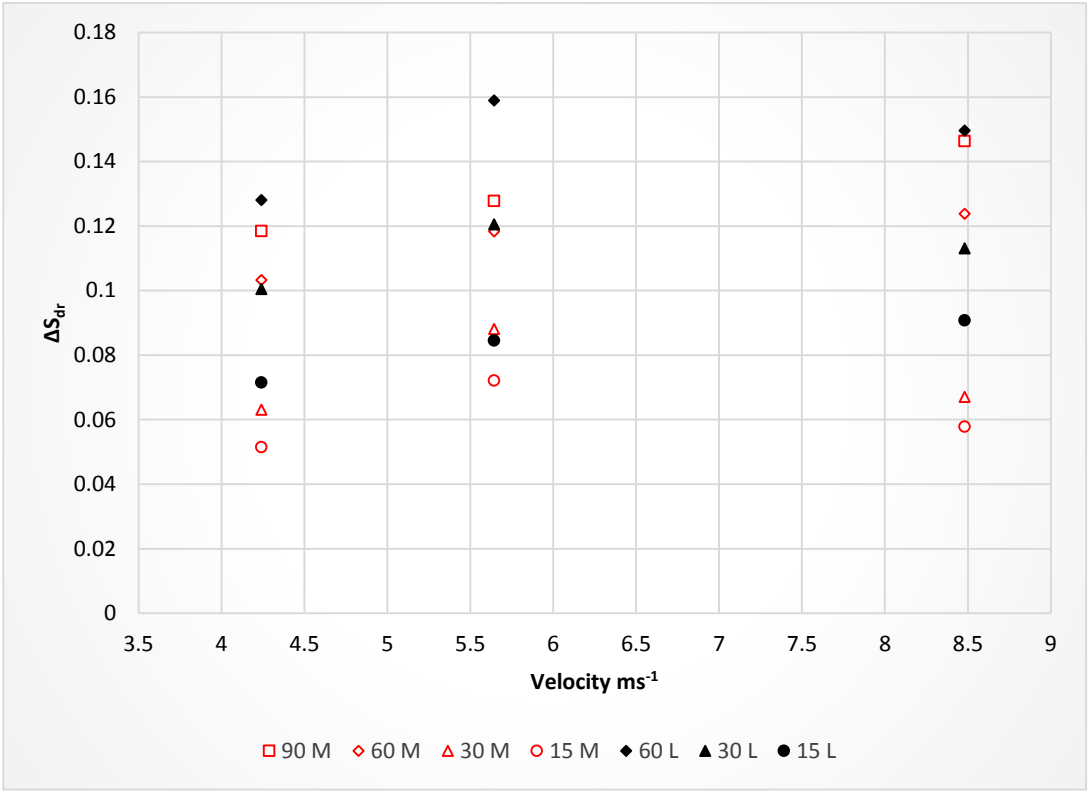

Figure 5-6 Change in developed interfacial area ratio as a function of velocity after one hour of erosion for the medium and large particle size ranges

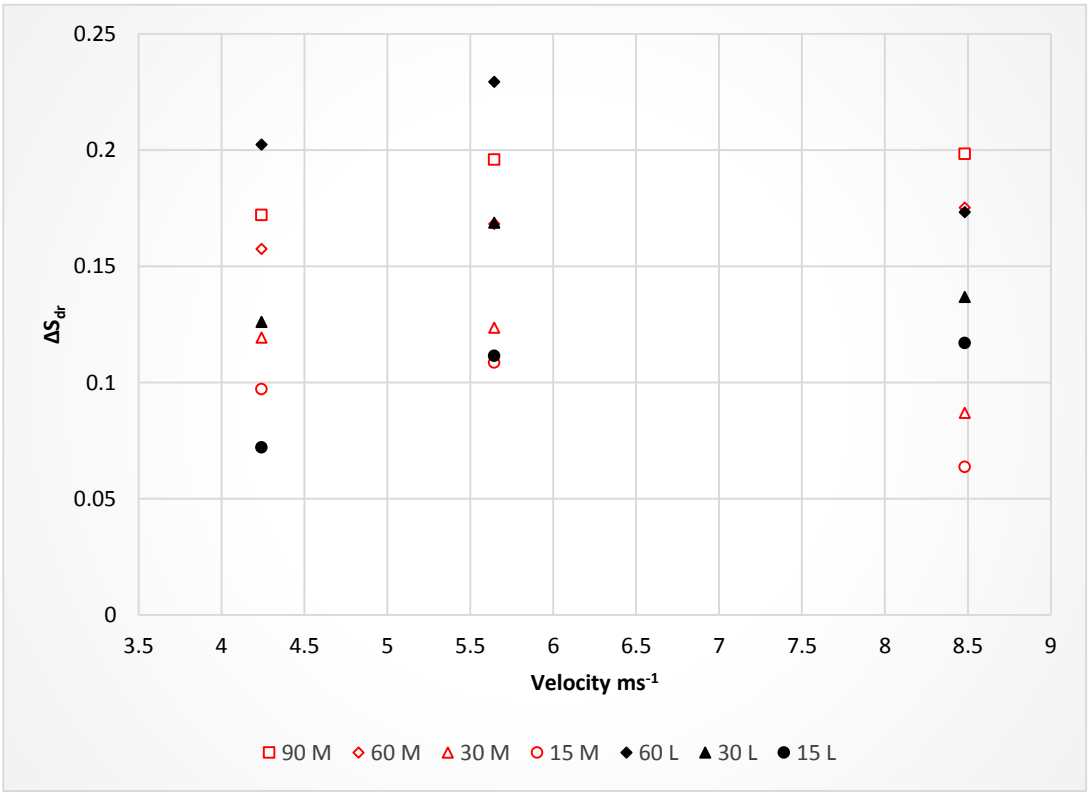

Figure 5-7 Change in developed interfacial area ratio as a function of velocity after two hour of erosion for the medium and large particle size ranges

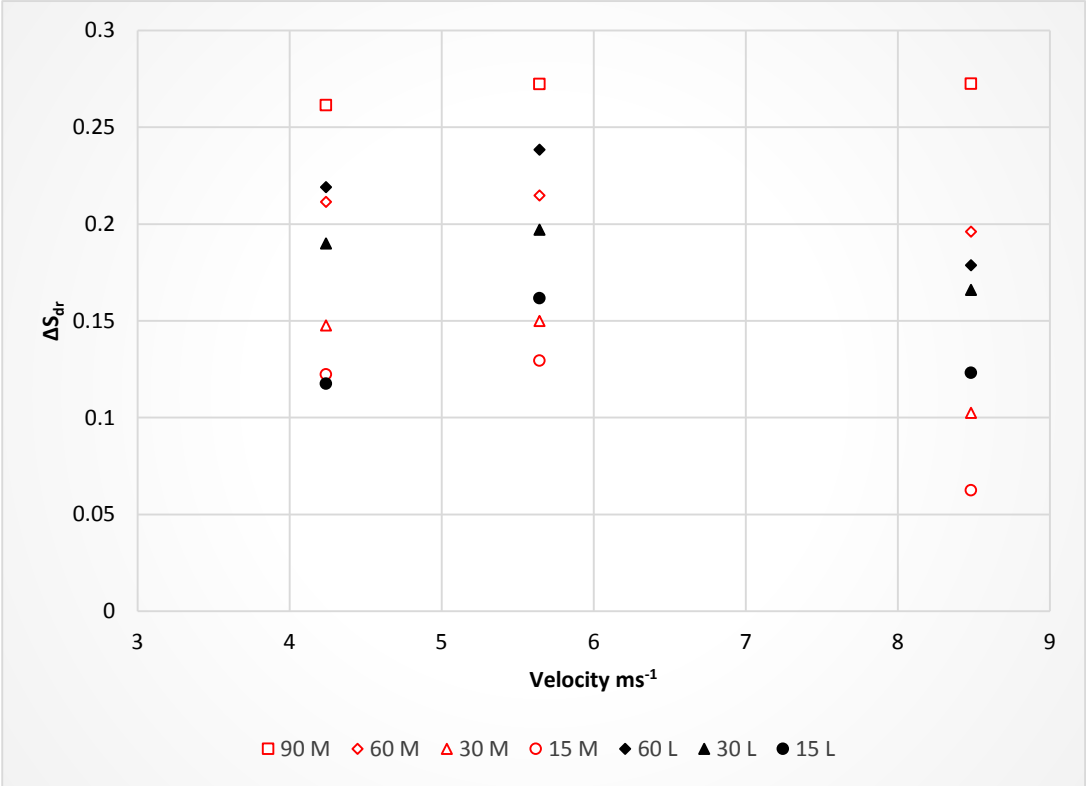

Figure 5-8 Change in developed interfacial area ratio as a function of velocity after three hours of erosion for the medium and large particle size ranges

A study conducted by Ćurković et al [95] assessed the behaviour to solid particle erosion of alumina ceramics, using both angular and rounded particles at different angles. The study detailed findings of the surface profile roughness as shown in Figure 5-9. It was concluded that the particle shape is a determining factor in the response of the surface roughness to changes in flow conditions. Although the study was conducted on a brittle material, it has nevertheless shown that a change in the erodent shape affects surface texture changes. It may be necessary to further evaluate the effect of the particle shape on surface texture for a ductile material, as the olivine particles used at 8.482 m s^{-1} tend to become significantly rounded as has been detailed in section 4.1.1.

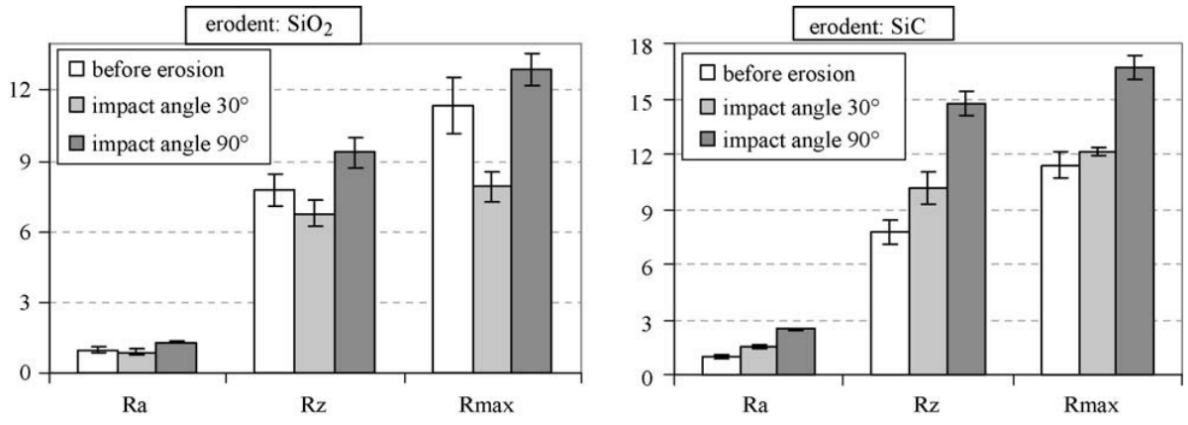

Figure 5-9 Variations in profile roughness parameters of rounded SiO2 and angular SiC [96]

The cache of images displayed in Figure 5-10(a-f) show the surface texture, optical images in pseudo-colour, for surfaces eroded at an orientation angle of 30^{o} for a period of 1 hour. Though this study is not evaluating the absolute value of S_{dr}, these optical images provide an awareness of the variance that exist in surface textures, and by extension, the relationship of, the amplitude and frequency of the peaks and valleys, to the developed interfacial area ratio. The surfaces in Figure 5-10(a-c) correspond to the velocities of 4.241 m s^{-1}, 5.654 m s^{-1} and 8.482 m s^{-1} respectively, eroded by the large olivine particles. Both (a) and (a) have been found to have similar values of S_{dr} of 0.181 and 0.180 respectively, they can be visually observed to have similar amplitude and spatial properties; while surface (c), has a higher amplitude and a significantly high frequency, and has been found to have an S_{dr} of almost 2.5 times that of surfaces (a) and (b).

From the graphical information presented in Figure 5-6 to Figure 5-8, the effect of the particle size on the surface morphology can be evaluated. It can be concluded, that the particle size is a significant influencing factor in the generation of surface texture in slurry erosion. Within the size ranges examined, the average difference between the medium size range and the large particle size range across all data-points, accounts for a 24.02 % increase in the ΔS_{dr}. Figure 5-10(c and f) show surfaces which have been eroded at the same velocity, however the former has been eroded by medium particles and the latter by the large particle. It can be seen, that there is a difference in the spatial distribution of the undulations, with the surface Figure 5-10(c) having a higher frequency of peak/valley distribution, while the surface in Figure 5-10(f) has a greater amplitude

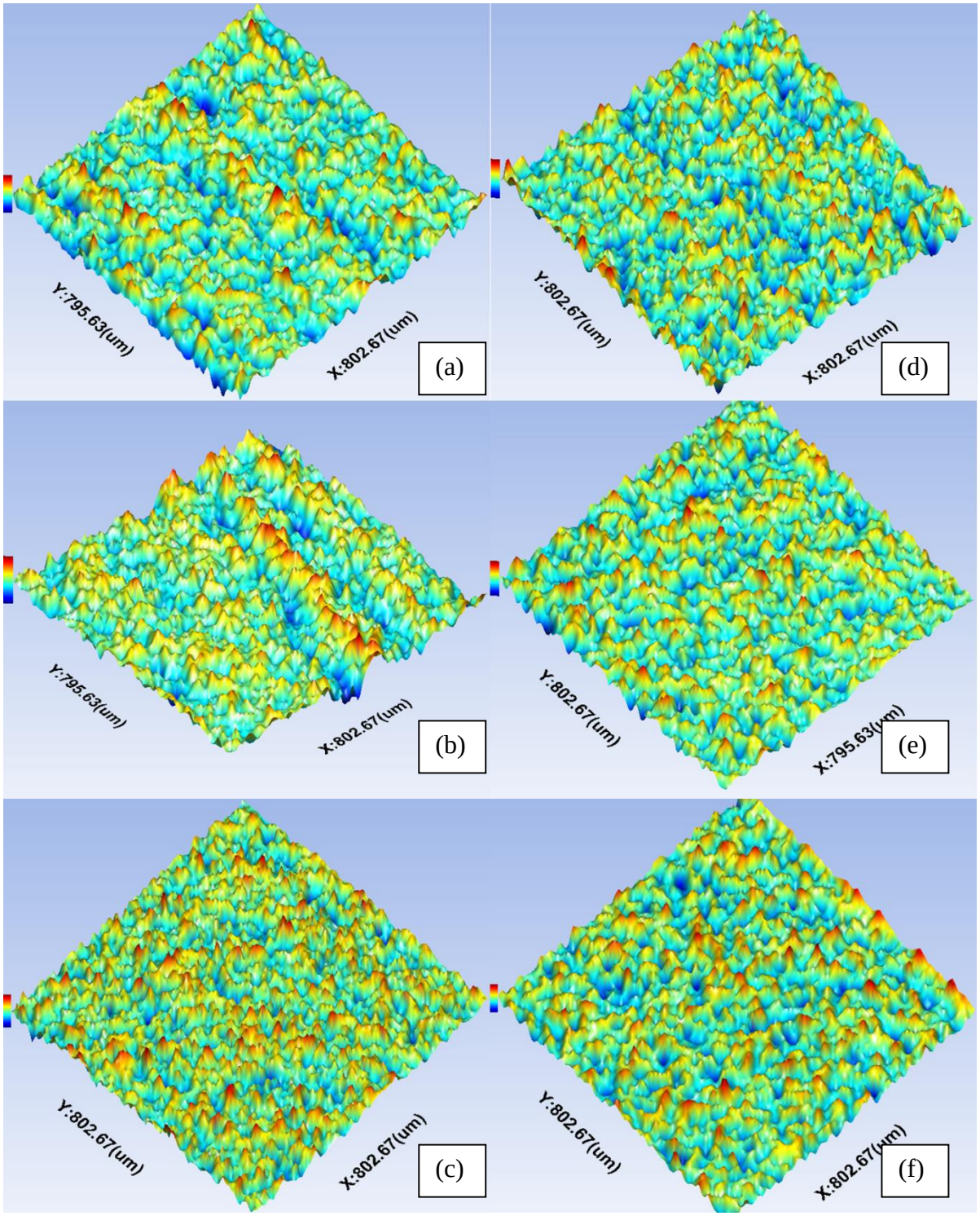

Figure 5-10 Surface texture at 30° for one hour (a) 4.241 m s^{-1} large particles (0.181 S_{dr}) (b) 5.654 m s^{-1} large particles (0.180 S_{dr}) (c) 8.482 m s^{-1} large particles (0.424 S_{dr}) (d) 4.241 m s^{-1} medium particles (0.203 S_{dr}) (e). 5.654 m s^{-1} medium particles (0.141 S_{dr}) (f) 8.482 m s^{-1} medium particles (0.199 S_{dr})

5.2.2 Evaluation of Surface Roughness as a Function Impact Angle

Solid particle erosion was conducted on the specimen at four impact angles, and the surface texture was measured and recorded and the difference between the uneroded and the eroded surfaces has been assessed. This section seeks to evaluate the response of the target surface to the changes in erosion parameters, while also quantifying the effect of the surface orientation angle to the generation of surface texturing. The results of the 90° sample eroded by the large particle size range at 5.654 m s^{-1} have been excluded from this evaluation

The work of Ćurković et al [95], addresses the change in roughness based on two impact angles using rounded and angular particles. This work concluded that the particle properties, such as, shape and size, not only affect the amplitude of the surface roughness, but also the behaviour of the material at different incident angles. This is illustrated in the graph shown in Figure 5-9. Further work by Avcu et al [96] on the morphology of a target surface subject to particle erosion, indicates that as a general trend, the surface roughness increases with the increase in velocity and impact angle. This was seen to hold true up to a limiting angle of 75° after which the roughness decreases up to 90° as shown in Figure 5-11. Both of these works were conducted at high speeds with air as the bulk fluid, with the former having been executed on brittle material, while the latter was performed on semi-ductile material. Both studies also evaluated the surface using a profile surface roughness parameter Ra, which is limited to profiling the arithmetic average height along a single path. As such it ignores the spatial properties, hence, the surface texture.

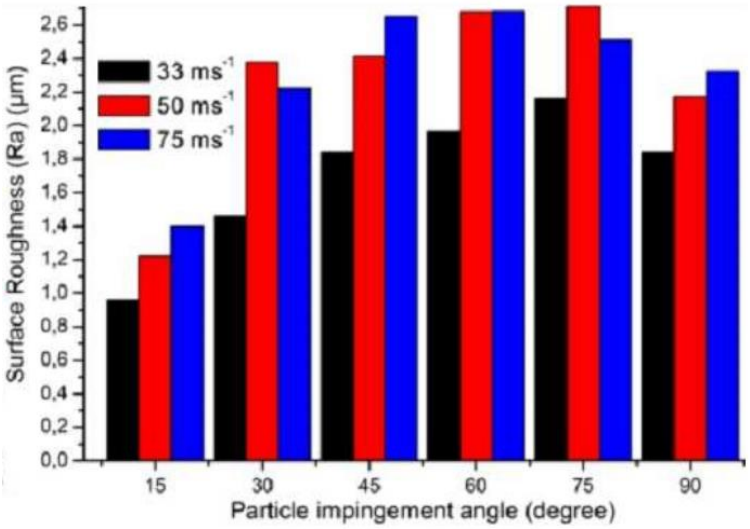

Figure 5-11 Chart of the variation in profile roughness Ra of Ti6Al4V based on impact angle and velocity [97]

The evaluation of the surface morphology with respect to impact angle has been assessed for three hours at one hour intervals, performed at three different flow velocities using two ranges of multi-sized particles. Figure 5-12 is a plot of the arithmetical mean height (Sa) as a function of the impact angle for a one hour and two hour period. This shows, that the change in surface roughness increasing proportionally to the increase in the impact angle, however, it achieves a maximum between 60° and 75°, after which it declines as it tends toward the normal impact angle. A study by Hamed et al [97] found a similar trend when studying the degradation of a turbine blade surface subject to dry erosion at a velocity of 91.44 m s^{-1}, as shown in Figure 5-13.

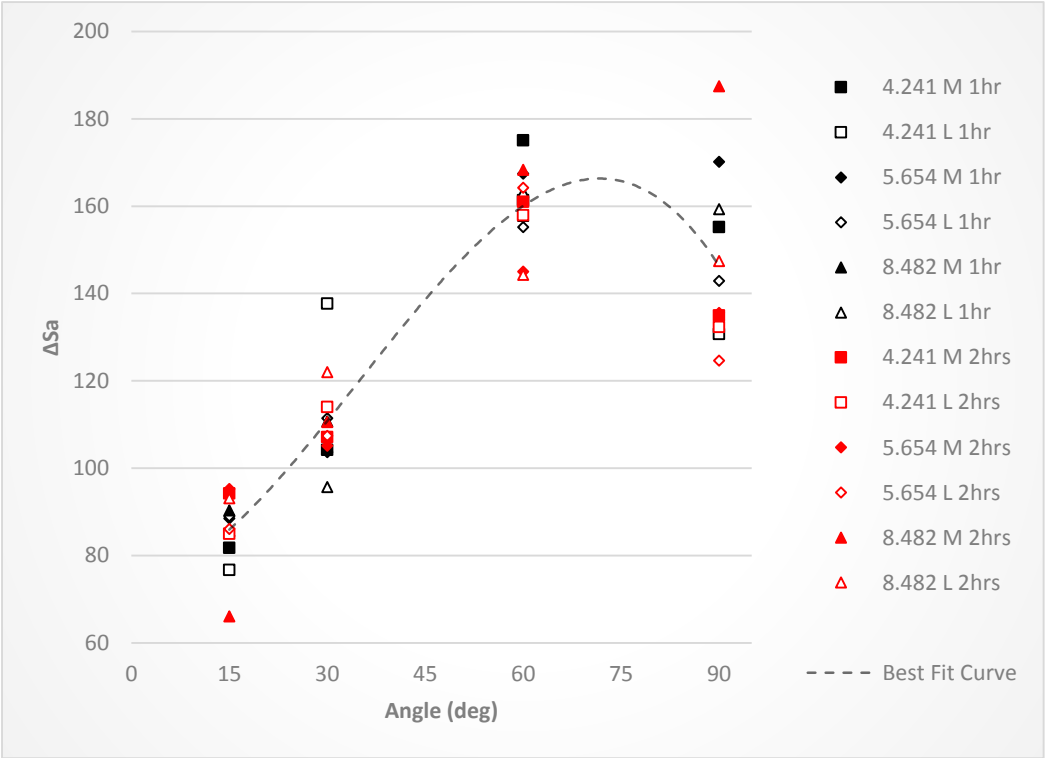

Figure 5-12 Change in the arithmetical mean height (Sa) as a function of impact angle after erosion at intervals of one hour and two hours

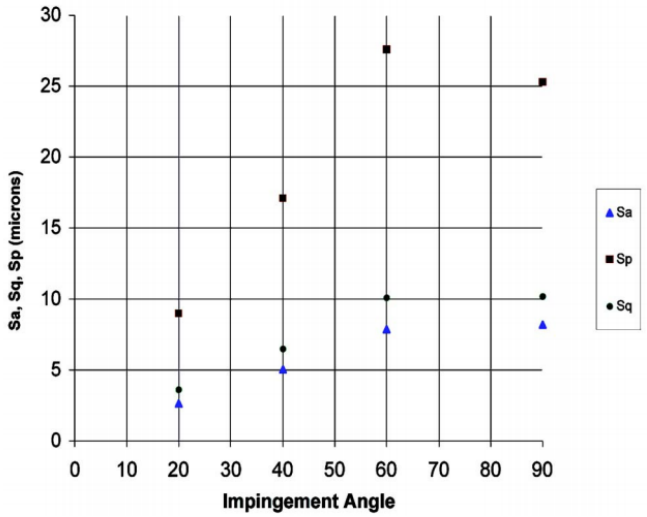

Figure 5-13 Relationship between surface roughness in Amplitude parameters (Sa Sq and Sp) and impact angle for turbine blade eroded by dry sand [98]

However, as described in section 5.1 Sa does not provide a complete description of the texture of a three-dimensional surface, therefore the hybrid parameter, S_{dr}, was also plotted. These results are graphically presented in Figure 5-14, Figure 5-15 and Figure 5-16. From these datasets, it can be seen that the surface texture responds in the same general manner at each interval irrespective of particle size or impact angle. At an impact angle of 15° the surface exhibits the lowest reduction in ΔS_{dr}, with ΔS_{dr} increasing as the angle is increased. The maximum change in S_{dr} was recorded at an angle of 90°. This suggests that the roughest texture will exist at an erosion impact angle of 15°, while the smoothest surface will be generated at 90°.

As outlined in Chapter 2, erosion is mechanistic, and has been found to have a different set of dominant mechanisms at play when eroded at shallow angles compared to angles that tend toward normal. When erosion occurs at angles below 30° it is dominated by abrasive erosion conversely when its orientation between 60° and 90° it is dominated by direct impact events [98]. The details presented in Table 5-5, provide a quantification of the changes in surface texture as the angles is increased, it further groups the values at 15° and 30° degrees (abrasive) and compares them to the ΔS_{dr} at 60° and 90° (impact).

Table 5-5 Tabulated data of the average percentage change in ΔS_{dr} with increase of the impact angle

Percentage difference of ΔS_{dr}					
Impact angle		15° to 30°	30° to 60°	60° to 90°	Abrasive to Impact
Time (hours)	1	28.96%	41.58%	15.88%	71.01%
	2	33.71%	45.14%	21.91%	82.61%
	3	32.98%	32.00%	33.27%	73.48%
	Avg	31.88%	39.57%	23.69%	75.70%

When the angle of impact changes from one of abrasive erosion to impact erosion, there is a significant increase in the ΔS_{dr} value. Which signifies the generation of a smoother surface compared to that generated at lower angles. The mechanisms of erosion occurring at low impact angles manifest itself in the form of scratches, and ploughing while, pitting, micro-cracks and lip formation, tend to characterise erosion at high impact angles.

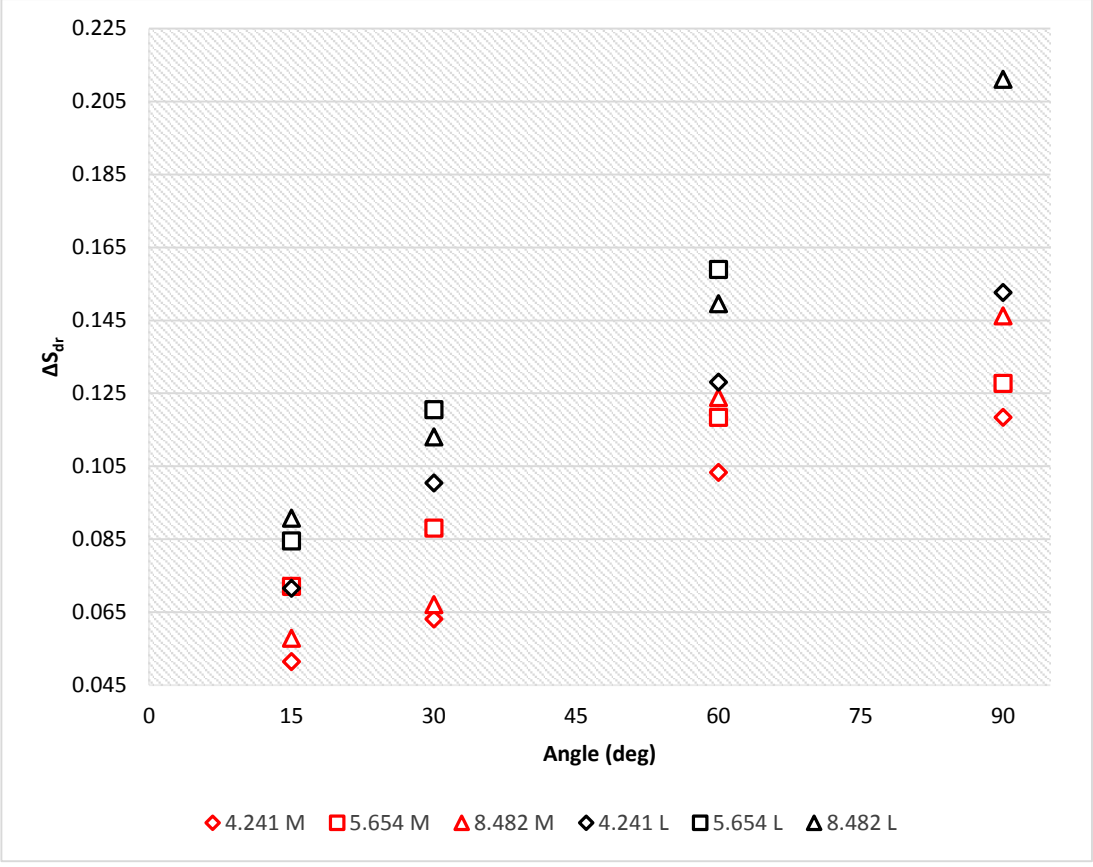

Figure 5-14 Variations in developed interfacial area ratio as a function of target wall orientation angle at one hour erosion interval

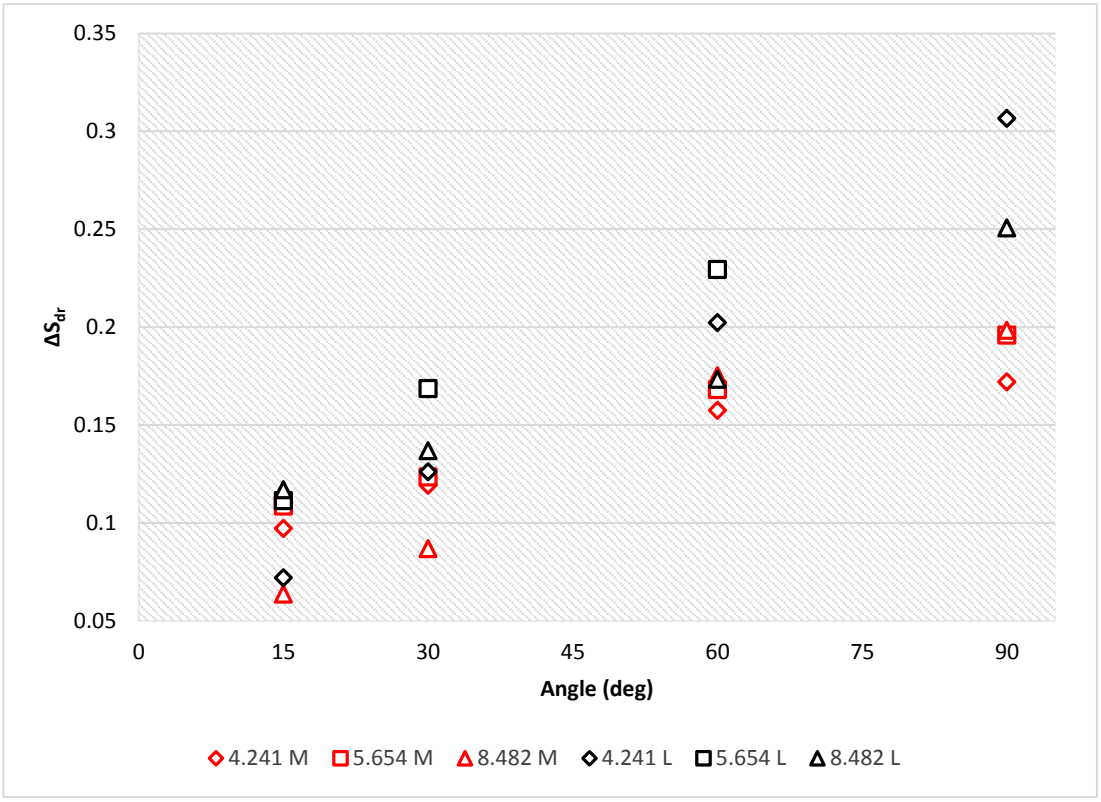

Figure 5-15 Variations in S_{dr} as a function of target wall orientation angle at a two hour interval

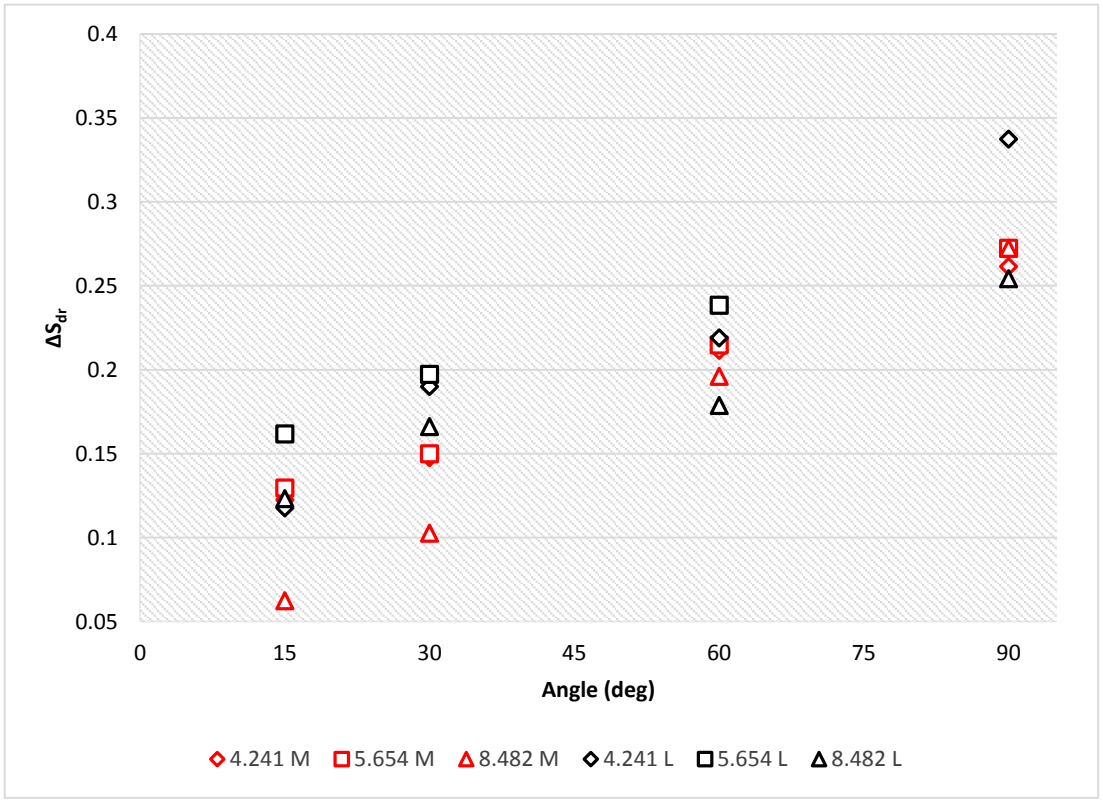

Figure 5-16 Variations in S_{dr} as a function of target wall orientation angle at a three 3 hour interval

5.2.3 Evaluation of Surface Roughness as a Function Time

In assessing the time based, morphology of a surface subjected to slurry erosion, experimentation was conducted over a three hour period. The results of this study have been outlined graphically in Figure 5-17, Figure 5-18 and Figure 5-19, representing flow velocities of 4.241 m s^{-1}, 5.654 m s^{-1} and 8.482 m s^{-1} respectively. A study by Wang et al [99] assessed the time evolution of surface roughness using the dissolving wall method. This study found that, the change in the RMS and peak to valley roughness height, changes linearly with time when evaluated over an eight hour period at flow rates of 0.85 m s^{-1} to 3.4 m s^{-1}.

The results of the current work show a general linear relationship between the change in surface roughness and the exposure time under the erosive flow conditions specified. When the flow is set to the lower velocities of 4.241m s^{-1} and 5.654m s^{-1}, the change in ΔS_{dr} increases linearly over time. However, when target surface is subject to the higher erosive flow of 8.482m s^{-1} (Figure 5-19), the gradient is significantly reduced. Figure 5-20 is a plot of the average ΔSdr at each time interval, for the chosen velocities, this provides a good comparison of the gradient of each dataset.

A study by Hamed et al [97], evaluated the change in surface roughness based on exposure time. It was determined, that the change in surface roughness reaches a plateau after which there is negligible change in the overall topography of the surface. For that study, this plateau was attained between five and ten minutes at an erosion velocity of 182.88 m s^{-1}, as seen in Figure 5-21. Due to the significantly lower flows, it may require a considerably longer experimentation period to determine the time required to achieve maximum ΔS_{dr}.

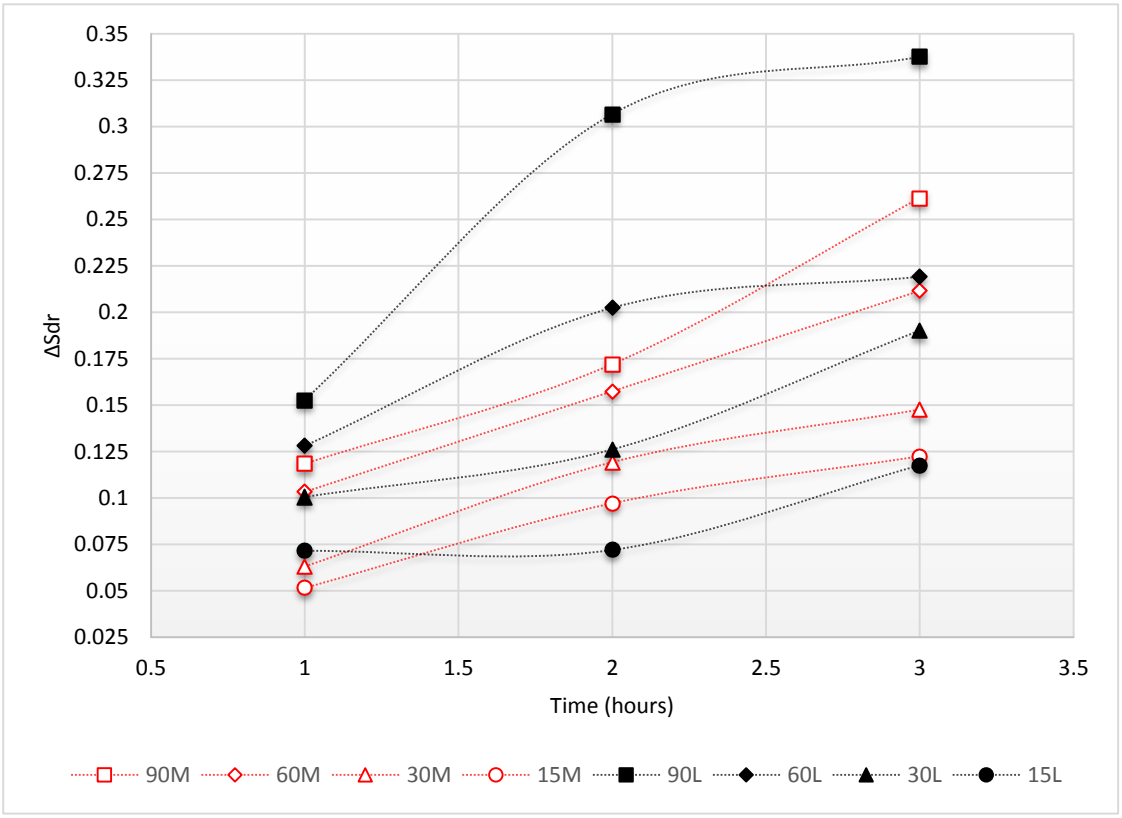

Figure 5-17 Change in the developed interfacial area ratio as a function of time for a flow velocity of 4.241m s^{-1}

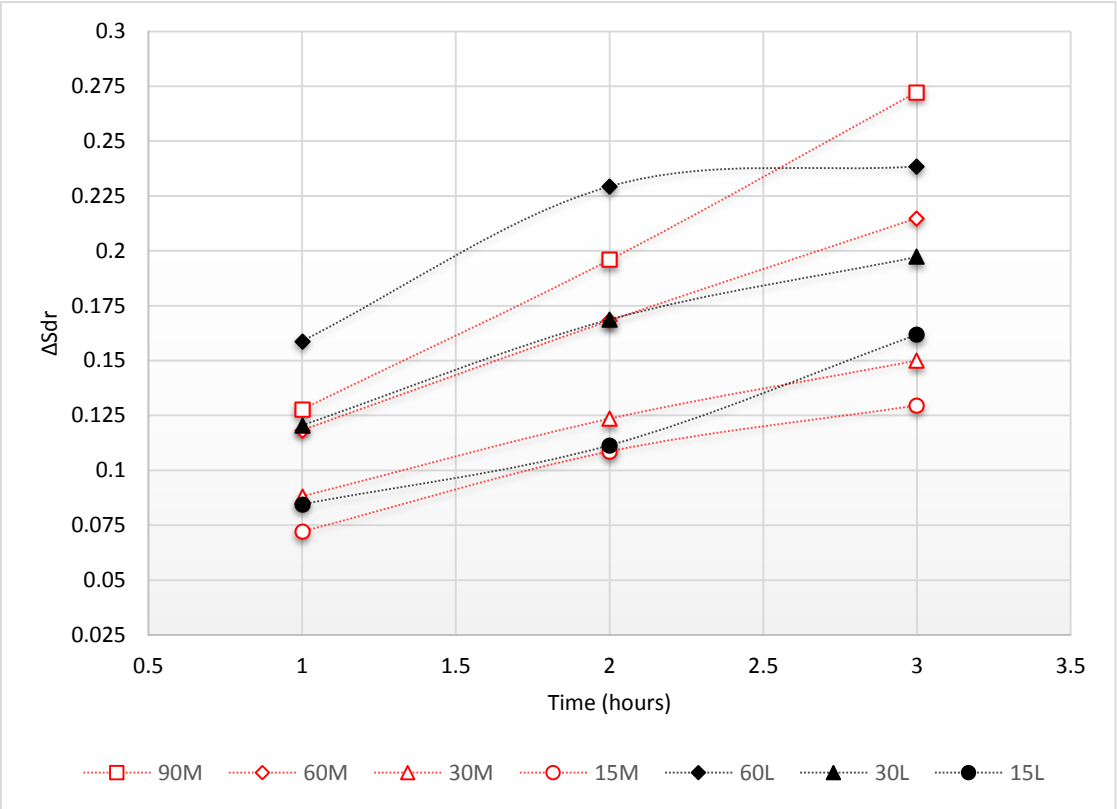

Figure 5-18 Change in the developed interfacial area ratio as a function of time for a flow velocity of 5.645m s^{-1}

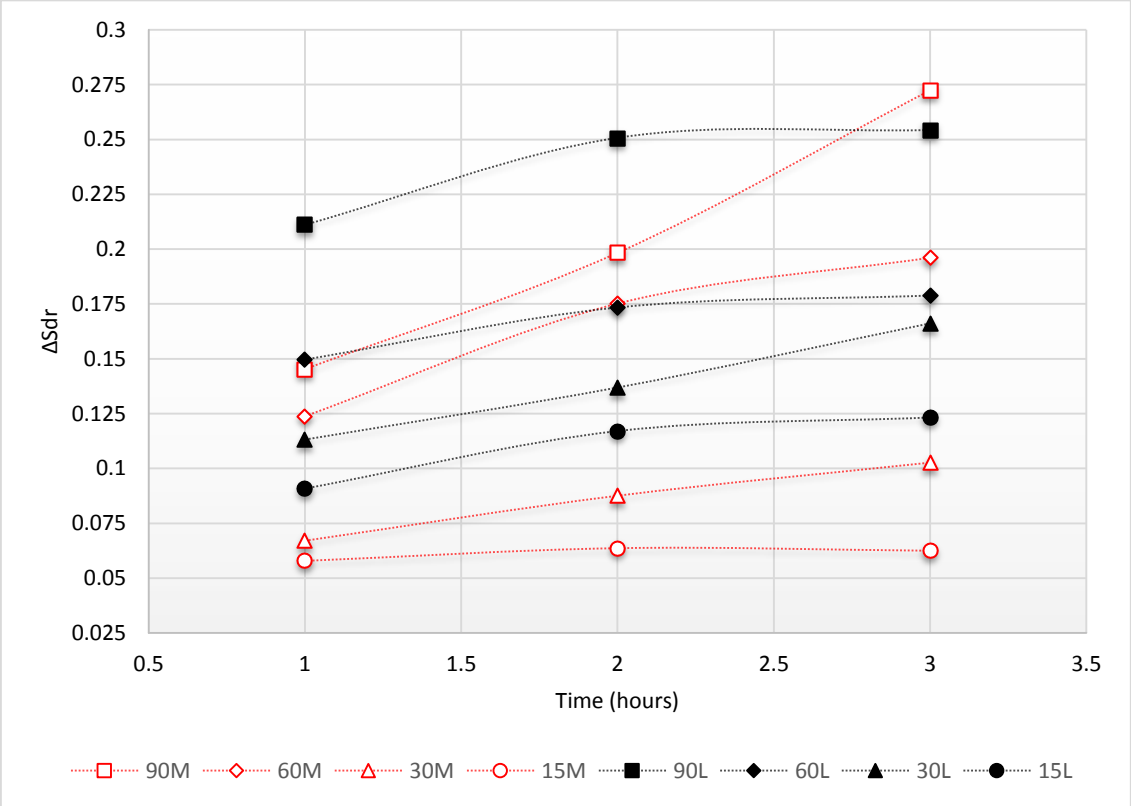

Figure 5-19 Change in the developed interfacial area ratio as a function of time for a flow velocity of 5.645m s^{-1}

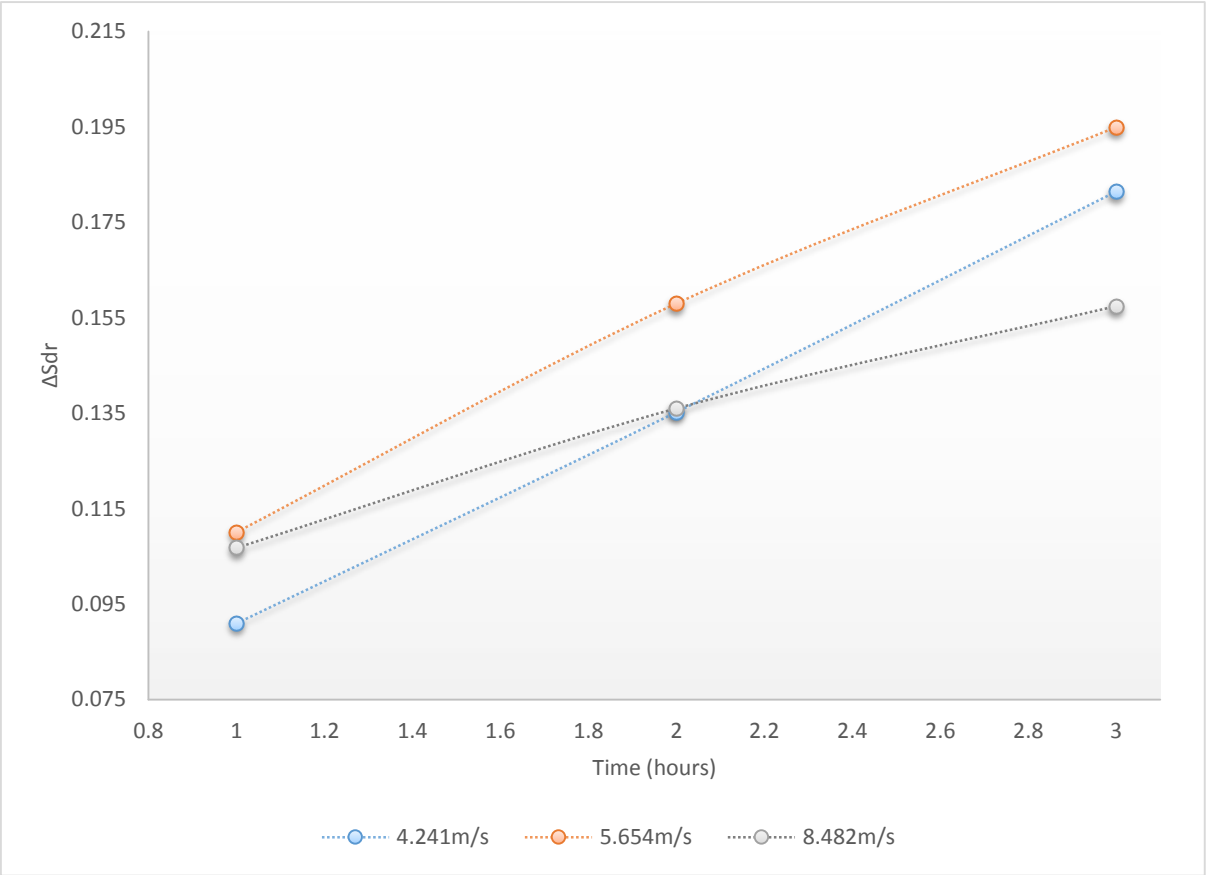

Figure 5-20 Average ΔS_{dr} by velocity at each time interval

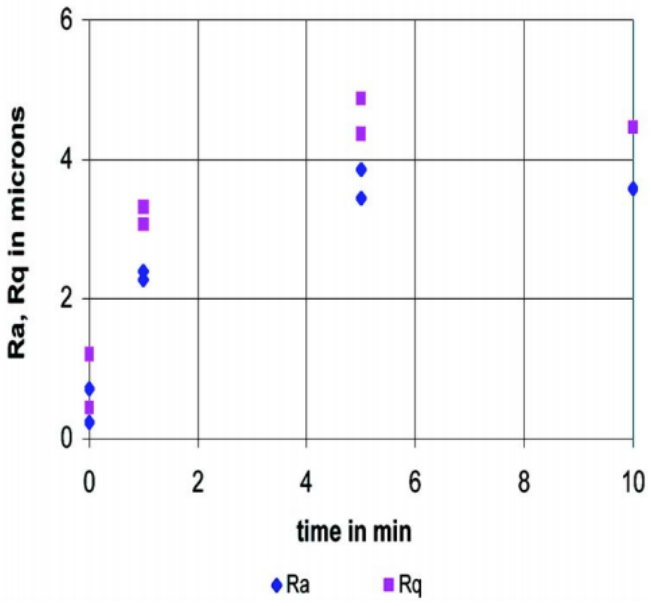

Figure 5-21 Time based surface roughness morphology when eroded by 1500 µm particles at 182.88 m s^{-1} [98]

5.3 Summary of Work

Slurry erosion has been conducted in an erosion test pot in order to establish the surface morphology of a mild carbon steel. Experimentation using water as the bulk medium and olivine at 5 wt.% as the erodent, has been executed. A 3D optical microscope has been used to assess the change in the surface under the given conditions, and an analysis was done to determine the influence of particle size, flow velocity, impact angle and time, on the surface texture of a surface. From this study the following conclusions have been made:

1. A novel contribution has been made to this field of study, as there has been no account of eroded surface texture in earlier literature. Although studies have been conducted to evaluate the material surface using metrological technique, none have assessed the three dimensional surface texture.

2. Most studies that assess the erosion of surface and subsequent assessment of the surface morphology, prepare the surface using very fine grit emery paper. This results in the surface having a fine finish prior to particle impingement. In this study the samples were used as received, in order to replicate as close as possible real world conditions, consequently the surface began with a relatively rough surface. As a result, the surface becomes smoother as opposed to the roughness increasing.

3. The change in surface roughness as a function of the impact angle has been evaluated using both the Sa and S_{dr} parameters. Both are in agreement that the change in roughness increases as the angle increases however the results of Sa show a downturn when approaching 90^{o}, whereas the S_{dr} shows that the maximum change in surface roughness occurs at 90^{o}.

4. The velocity has been found to cause a rise in the change of surface roughness up to a flow velocity of 5.654m s^{-1} however as the velocity increases beyond this point there is an increase in the surface roughness (i.e. a reduction in ΔS_{dr}) from that at 5.654m s^{-1}.

5. Full assessment of the surface scans failed to reveal a cause for this response to the change in velocity. However, the study conducted by Ćurković et al [95] highlights the fact that rounded particles result in a different surface roughness compared to angular particles. In section 4.1.1 it was noted that the higher flow velocity of 8.482m s^{-1}, results in substantial rounding of the olivine particles, which could have been a factor in the decrease seen in ΔS_{dr} at that velocity.

6. When evaluated over time, there is a direct proportional response in the value of S_{dr}. However, time is seen to have a reduced influence at the higher velocity, as evident by the reduction in the gradient.

In the next chapter, the conclusion of the present research study has been presented and the major achievements of the study as well as a series of future recommendations have been outline.

Chapter 6 CONCLUSIONS

Following from the experimental and analysis which has been carried out, several conclusions have been established and outlined in this chapter. Furthermore, this chapter provides a summary of the major achievements and contributions which have been realised in satisfying the research aims and the specific research objectives. Lastly, a summary of the limitations of this work and the recommendations for future work is outlined.

6.1 Research Problem Synopsis

The study of solid particle erosion is increasingly necessary, as oil drilling reaches newer depths, at higher temperatures and pressures, striking different layers of rock formations and minerals. Although efforts are made, to prevent the ingress of particles through sand control, robust investigation, predicting the development of erosion and the erosion rate under different environmental conditions is vital. Two key items have come out of the review of available literature; firstly, the study of solid particle erosion, is notably empirical, as a result, the application of the findings, models and data has still not been fully charted. Secondly, there is a need to collate much more robust data, in order to develop a general model for predicting erosion.

The aims of this study have been structured and outlined in Chapter 1. The specific objectives have been based on some of the gaps identified from the literature review conducted. These have been addressed through experimentation with the full details of these being outlined in Chapter 3, Chapter 4 and Chapter 5. A summary of the realisation of the research aims, the contributions which have been presented through this research work, as well as a detailed conclusion based on the specific objectives has been outlined below.

6.2 Realisation of Research Aims

This section shows the manner in which the work conducted has satisfied the aims which have been outlined in section 1.6 of Chapter 1.

Research Aim #1: Analysis of solid particle erosion, through a parametric investigation of the principle variables influencing material degradation.

This research work provides a detailed analysis of the principle parameters influencing the generation of material degradation, via solid particle erosion occurring in an aqueous environment. This was achieved through a series of experimental studies, using an erosion test pot with water as the bulk fluid and angular olivine particles as the eroding material. The research provides a detailed qualitative and quantitative analysis of the influence of velocity and multi-sized particles on the erosion rate of a mild carbon steel. Moreover the study provides a discussion and comparison, of the effect of exposure time found in this study to other studies with differing and corroborating results. The use of olivine as the erodent allows for direct comparison with other common natural minerals such as silica. Furthermore, the assessment of multi-sized particles allows for a more profound understanding of the effect of erosion in practical applications, while also allowing for direct comparison to equi-sized particle slurries.

Research Aim #2: Surface metrology based investigation, of the surface texture morphology as a result of solid particle erosion.

One of the consequences of solid particle erosion, is the change in the surface roughness of the target material. Many studies have been conducted, assessing the manner in which erosion occurs through use of surface imagery, however this research work extends this knowledge by assessing the manner in which the material changes in reference to its surface texture. Experimentation was carried out to erode a collection of target materials using an erosion test pot. A non-contact method was then utilized in order to provide a detailed three-dimensional surface scan of the target wall texture. A detailed analysis was conducted of the surfaces to determine the influence of velocity, time, impact angle and multi-sized particles on the change in roughness. No literature has been found which assesses the surface morphology due to erosion in an aqueous environment, as such this provides a significant contribution to knowledge in this field.

6.3 Overall Conclusions

The section provides a summary of the major conclusions which have been made based on the specific research objectives outlined in Chapter 2

Objective 1. In an aqueous environment, establish the influence of flow velocity and multi-sizes particles on the erosion rate of EN3B subjected to erosion by olivine particles

An assessment of the influence of velocity and multi-sized particles on the erosion of the mild carbon steel material, was conducted at three velocities and three distinct ranges of multi-sized olivine particles. The erosion of the material was assessed when subjected to a combination of velocities and particle sizes. Despite the use of a different erodent (i.e Olivine) and the use of multi-sized particles, the velocity exponent n has been found to be 2.35, which is comparable to that found in literature for steels. In studies using equi-sized particles researchers have found a limiting particle size at which the erosion rate slows down and regresses. For the multi-sized particles, an increase in the nominal particle size has the effect of increasing the erosion. The particle size was found to have an exponential relationship with the erosion rate and the exponential constant x was evaluated to be 0.56. It can be surmised that within the range evaluated both velocity and particle size have an exponential relationship with the erosion rate.

Objective 2. Determine the temporal nature of eroding EN3B in an environment containing angular olivine particles

Detailed analysis was carried out on the erosion rate of EN3B as a function the exposure time. This was conducted under various test conditions, including multiple particles sizes, and multiple velocities, however the erosion rate was constant throughout the entire assessment. As such it can be concluded that mild carbon steel has no noticeable incubation period or change in erosion rate when eroded by olivine in an aqueous environment at relatively low velocities.

Objective 3. Propose a new erosion model based on the Zhang/Tulsa: E/CRC model of erosion

From the results obtained in this study and after analysing the effects of various erosion factors on the erosion rate of the target material. Empirical relationships have been developed between the velocity and the weighted mass particle size of multi-sized particles. Log-log multiple regression analysis has been employed to determine the exponential effect of the velocity and the particle size, while also determining the effect of the other particle factors by the K constant. As the model is based on modifying the Zhang/Tulsa model the erosion rate is represented by the ratio of mass loss divided the mass of impacting particles kg/kg. The new model is presented below:

$$Er\left(\frac{kg}{kg}\right) = 1.036 * 10^{-7}(B^{-0.59})F_s(f\theta)V^{2.35}\left(\frac{d_{wn}}{D}\right)^{0.56}$$

Objective 4. Topographically investigate the morphology of the target surface when eroded at different at incident angles and particle sizes

Solid particle erosion was conducted on mild carbon steel (EN3B) using angular olivine particles at four impact angles, three flow velocities, and two distinct multi-sized particle ranges. The surface was analysed using a non-contact method of surface roughness measurement, with an infinite focus microscope. A comprehensive assessment was carried out in order to assess the surface texture morphology under a combination of these stated parameters. The study determined that the target surfaces became smoother when eroded. The change in surface roughness has been assessed as a function of the impact angle using both the Arithmetical mean height (Sa) and the Developed interfacial area ratio (S_{dr}). Both are in agreement that the change in roughness increases as the angle increases however Sa suggest that the maximum change in surface roughness is experienced between 60^o and 75^o, whereas S_{dr}, shows the maximum occurring at 90^o. When the particle size range is increased from the medium particles to the large particles a 24% increase in seen in the change of surface roughness. From this work, it has been found that the change in surface roughness is considerably angle dependent however the particle size is an influential parameter.

Objective 5. Provide a quantitative analysis of the change in surface texture as a function of exposure time and flow velocity.

Following on from the work conducted in objective 4, a comprehensive assessment was carried out in order to assess the surface texture morphology under a combination of the above stated parameters. The temporal component of the surface morphology was analysed from which it was determined that at any given velocity the relationship between the change in surface roughness and the exposure time is linear. However, the gradient reduces significantly at the highest flow velocity. Consequently, a detailed assessment of the influence of velocity was also conducted, from which it was determined that ΔS_{dr} increases with flow velocity up to 5.654m s^{-1} but reduces as the velocity approaches the maximum experimental velocity of 8.482m s^{-1}.

6.3.1 Limitation of Research

The section summarised some of the limitations in the work which has been conducted.

- In conducting erosion studies in a test pot, it has been found that having a counter rotating impeller (connected to an independent motor to the sample) provides the best particle dispersion, cost implications limited the possibility of doing this for this study.
- The model has not been hooked onto a CDF package in order to compare against the existing models.
- It has not been possible to bench mark the results against existing results as no published experimentation assesses the erosion of EN3B using Olivine in an aqueous environment. However, the results were comparable to results obtained by [22] which was conducted using silica sand on stainless steel.
- The results obtained for erosion rate and by extension surface measurements at the high velocity could have been compromised slightly by the rounding of the particles.

6.4 Recommendations for Future Work

The study of solid particle erosion is an area of work that requires a great deal of further work by virtue of the complexity of some of the interdependency of many of the variables. Based on the breadth of this are of study, the work conducted in this research endeavour and the limitations which have been regarded, there is still ample prospects for further research to be conducted in this area. Some of the main areas identified are summarised below:

Recommendations:

i. One of the area identified in prior works is the fact that particle size produced a limiting effect on the erosion rate as the particle size increases, as this has not been identified with the multi-sized olivine work can be carried out using equi-sized olivine under the same experimental conditions to determine if this is only a phenomenon experienced with equi-sized particle. Additionally, CFD can be employed to compare the proposed model to compare against results obtained from accepted models using the model describes in Appendix IV.

ii. Further work can be done to quantify the influence of surface roughness on the erosion rate. Furthermore, there is a need to determine the surface roughness value at which no further quantifiable surface roughness changes occurs, through eroding very fine surface until morphology ceases and likewise eroding severely roughened surface until no further change occurs.

REFERENCES

[1] D. P. Bommer, A Primer Of Oilwell Drilling, 7th Edition ed., Austin, Texas: The University of Texas at Austin, 2008.

[2] Royal Dutch/Shell Group of Companies, The Petroleum Handbook, 6th Edition ed., Amsterdam: Elsevier, 1983.

[3] B. Black, The Landscape Of America's First Oil Boom, Baltamore, Maryland: The John Hopkins University Press, 2000.

[4] A. B. Klass and D. Meinhardt, "Transporting Oil and Gas: U.S. Infrastructure Challenges," *Iowa Law Review,* vol. 100, no. 3, pp. 947-1053, 2015.

[5] T. O. Miesner and W. L. Leffler, Oil and Gas Pipelines in Non Technical Language, Tulsa: PennWell, 2006.

[6] R. Fletcher, "New Energy East memo reveals conflicting government views on pipeline's value," CBC/Radio Canada, 14 July 2016. [Online]. Available: http://www.cbc.ca/news/canada/calgary/energy-east-value-jim-carr-memo-pipeline-capacity-1.3677473. [Accessed 6 August 2016].

[7] US Department of State, "New Keystone XL Pipeline Application," US Department of State, 6 November 2015. [Online]. Available: https://keystonepipeline-xl.state.gov/archive/c51958.htm. [Accessed 2 February 2016].

[8] Norwegian Ministry of Petroleum and Energy, FACTS 2013: The Norwegian Petroleum Sector, A. Lars-Jakob and V. M. Eldbjørg, Eds., Akersgata: Norwegian Ministry of Petroleum and Energy, 2013.

[9] R. J. Armentor, M. R. Wise, M. Bowman, G. Collin, V. Rodet, B. Holicek, G. King, C. Lockyear and M. Parlas, "Regaining Sand Control," *Oilfield Review,* pp. 4-13, (Summer) 2007.

[10] B. Ikporo and O. Sylvester, "Effect of Sand invasion on Oil Well Production: A Case study of Garon Field in the Niger Delta," *The International Journal of Engineering and Science,* vol. 4, no. 5, pp. 64-72, 2015.

[11] L. Kleis and P. Kulu, Solid Particle Erosion: Occurrence, Prediction and Control, London: Springer, 2008.

[12] M. Parsi, K. Najmi, F. Najafifard, S. Hassani, B. S. McLaury and S. A. Shirazi, "A comprehensive review of solid particle erosion modeling for oil and gas wells and pipelines applications," *Journal of Natural Gas Science and Engineering,* vol. 21, pp. 850-873, 2014.

[13] I. Finnie, "The mechanism of erosion of ductile metals," in *3rd US National Cong. Applied Mechanics*, 1958.

[14] I. Finnie, "Erosion of Surfaces By Solid Particles," *Wear,* vol. 3, pp. 87-103, 1960.

[15] J. G. Bitter, “A study of erosion phenomena part I,” *Wear,* vol. 6, no. 1, pp. 5 - 21, 1963.

[16] J. G. Bitter, “A study of erosion phenomena: Part II,” *Wear,* vol. 6, no. 3, pp. 169-190, May-June 1963.

[17] S. Hassani, “Solid Particle Erosion, Sand Monitoring and Transport in Oil and Gas,” 6 March 2015. [Online]. Available: https://www.linkedin.com/pulse/solid-particle-erosion-sand-monitoring-transport-oil-gas-hassani. [Accessed 7 March 2016].

[18] H. M. Clark and R. B. Hartwich, “A re-examination of the particle size effect in slurry erosion,” *Wear,* vol. 248, no. 1-2, pp. 147-161, 2001.

[19] H. M. Clark, “Particle velocity and size effects in laboratory slurry erosion measurements OR… do you know what your particles are doing?,” *Tribology International,* vol. 35, no. 10, pp. 617-624, 2002.

[20] H. M. Clark, “On the impact rate and impact energy of particles in a slurry pot erosion tester,” *Wear,* vol. 147, no. 1, pp. 165-183, 1991.

[21] R. S. Lynn, H. M. Clark and K. K. Wong, “On the particle size effect in slurry erosion,” *Wear,* vol. 149, no. 1-2, pp. 55-71, 1991.

[22] S. S. Rajahram, “Erosion - Corrosion Mechanisms of Stainless Steels UNS S31603,” University of Southampton, School of Engineering Science, PhD Thesis, Southampton, 2010.

[23] I. M. Hutchings, Tribology: Friction and Wear of Engineering Materials, London: Edward Arnold, 1992.

[24] H. M. Clark, “The influence of the flow field in slurry erosion,” *Wear,* vol. 152, no. 2, pp. 223-240, 1992.

[25] I. M. Hutchings, R. E. Winter and J. E. Field, “Solid particle erosion of metals: the removal of surface material by spherical projectiles,” in *Proceedings of the Royal Society of London. Series A, Mathematical and Physical*, London, 1976.

[26] H. M. Clark and K. W. Wong, “Impact angle, particle energy and mass loss in erosion by dilute slurries,” *Wear,* Vols. 186-187, no. 2, pp. 454-464, 1995.

[27] H. M. Clark, “The influence of the squeeze film in slurry erosion,” *Wear,* vol. 256, no. 9-10, pp. 918-926, 2004.

[28] A. T. Fry, M. G. Gee, S. Clausen, U. Neuschaefer-Rube, M. Bartscher, D. Spaltmann, M. Woydt, S. Radek, F. Cernuschi, J. R. Nicholls and T. W. Rose, “METROLOGY TO ENABLE HIGH TEMPERATURE EROSION TESTING – A NEW EUROPEAN INITIATIVE,” in *Advances in Materials Technology for Fossil Power Plants: Proceedings from the Seventh International Conference, October 2013*, Waikoloa, Hawaii, 2014.

[29] V. Rao and D. H. Buckley, “Time Dependence of Solid-Particle Impingement Erosion of an Aluminum Alloy,” National Aeronautics and Space Administration: Scientific and Technical Information Branch, Washington, DC, 1983.

[30] G. P. Tilly, "Erosion Caused by Impact of Solid Particles," *Treatise on Materials Science and Technology*, vol. 13, pp. 287-319, 1979.

[31] J. P. Young and A. W. Ruff, "Particle Erosion Measurements on Metals," *Journal of Engineering Materials and Technology*, vol. 99, no. 2, pp. 121-125, 1977.

[32] S. Turenne, M. Fiset and J. Masounave, "The Effect of Sand Concentration on the Erosion of Materials by a Slurry Jet," *Wear*, vol. 133, no. 1, pp. 95-106, 1989.

[33] T. Deng, A. R. Chaudhry, M. Patel, I. Hutchings and M. S. Bradley, "Effect of particle concentration on erosion rate of mild steel bends in a pneumatic conveyor," *Wear*, vol. 258, no. 1-4, pp. 480-487, 2005.

[34] J. A. Humphrey, "Fundamental of fluid motion in erosion by solid particle impact," *Internaltional Journal: Heat and Fluid Flow*, vol. 11, no. 3, pp. 170-195, 1990.

[35] The Engineering Toolbox, "Absolute, Dynamic and Kinematic Viscosity," The Engineering Toolbox, 2016. [Online]. Available: http://www.engineeringtoolbox.com/dynamic-absolute-kinematic-viscosity-d_412.html. [Accessed 10 January 2016].

[36] K. K. Wong and H. M. Clark, "A model of particle velocities and trajectories in a slurry pot erosion tester," *Wear*, vol. 160, no. 1, pp. 95-104, 1993.

[37] A. Mansouri, S. A. Shirazi and B. S. McLaury, "Experimental and numerical investigation of the effect of viscosity and particle size on the erosion damage caused by solid particles," in *Proceedings of the ASME 2014 4th Joint US-European Fluids Engineering Division Summer Meeting FEDSM2014*, Chicago, 2014.

[38] C. E. Smeltzer, M. E. Gulden and W. A. Compton, "Mechanisms of Metal Removal by Impacting Dust Particles," *Journal of Basic Engineering*, pp. 639-652, 1970.

[39] G. Sundararajan and M. Roy, "Solid particle erosion behavious of metallic materials at room and elevated temperatures," *Tribilogy International*, vol. 30, no. 5, pp. 339-359, 1997.

[40] R. Mishra, S. N. Singh and V. Seshadri, "Study of wear characteristics and solid distribution in constant area and erosion-resistant long-radius pipe bends for the flow of multisized particulate slurries," *Wear*, vol. 217, no. 2, pp. 297-306, 1998.

[41] J. Been and F. Ju, "Prediction of Wear of Tailings Pipelines in Oil Sands Slurries," December 2015. [Online]. Available: https://www.atimetals.com/news/corrosion-conference/Documents/CSC11-pdfs/presentation_5d_been.pdf. [Accessed 5 March 2016].

[42] H. Arabnejab, A. Mansouri, S. A. Shirazi and B. S. McLaury, "Evaluation of Solid Particle Erosion Equations and Models for Oil and Gas Industry Applications," in *Society of Petroleum Engineers Annual Technical Conference and Exhibition*, Houston, 2015.

[43] M. Parsi, M. Kara, P. Sharma, B. S. McLaury and S. A. Shirazi, “Comparative Study of Different Erosion Model Predictions for Single-Phase and Multiphase Flow Conditions,” in *Offchore Technology Conference*, Houston, 2016.

[44] Y. I. Oka, K. Okamura and T. Yoshida, “Practical estimation of erosion damage caused by solid particle impact Part 1: Effects of impact parameters on a predictive equation,” *Wear,* vol. 259, no. 1-6, pp. 95-101, 2005.

[45] Y. I. Oka and T. Yoshida, “Practical estimation of erosion damage caused by solid particle impact Part 2: Mechanical properties of materials directly associated with erosion damage,” *Wear,* vol. 259, no. 1-6, pp. 102-109, 2005.

[46] A. Lopez, M. T. Stickland and W. M. Dempster, “Comparative study different erosion models in an Eulerian-Lagrangian frame using Open Source software,” in *12th European Fluid Machinery Congress*, Edinburgh, 2014.

[47] Det Norske Veritas, “RECOMMENDED PRACTICE RP O501 EROSIVE WEAR IN PIPING SYSTEMS: REVISION 4.2 - 2007,” 12 November 2007. [Online]. Available: https://rules.dnvgl.com/docs/pdf/DNV/codes/docs/2011-01/RP-O501.pdf. [Accessed 16 February 2016].

[48] M. M. Salama, “An Alternative to API 14E Erosional Velocity Limits for Sand Laden Fluids,” in *Offshore Technology Conference*, Houston, 1998.

[49] R. Gupta, S. N. Singh and V. Sehadri, “Prediction of uneven wear in a slurry pipeline on the basis of measurements in a pot tester,” *Wear,* vol. 184, no. 2, pp. 169-178, 1995.

[50] M. S. Patil, E. R. Deore, R. S. Jahagirdar and S. V. Patil, “Study of the Parameters Affecting Erosion Wear of Ductile Material in Solid-Liquid Mixture,” in *Proceedings of the World Congress on Engineering*, London, 2011.

[51] Det Norske Veritas DNV GL, “Recommended Practice: Managing Sand Production and Erosion,” August 2015. [Online]. Available: https://rules.dnvgl.com/docs/pdf/DNVGL/RP/2015-08/DNVGL-RP-O501.pdf. [Accessed 27 May 2016].

[52] R. Walter and M. B. Kannan, “Influence of surface roughness on the corrosion behaviour of magnesium alloy,” *Materials & Design*, vol. 32, no. 4, p. 2350–2354, 2011.

[53] L. Blunt and X. Jiang, Advance Techniques for Assessment Surface Topography: Development of a basis for 3D Surface Texture Standards "SURFSTAND", London: Kogan Page Science, 2003.

[54] T. V. Vorburger and J. Raja, Surface Finish Metrology Tutorial, Galthersburg, MD: US Department of Commerce: National Institute of Standards and Technology, 1990.

[55] Digital Metrology, “3 Steps to Understanding Surface Texture,” Digital Metrology, May 2014. [Online]. Available: http://digitalmetrology.com/2014/05/. [Accessed 28 October 2016].

[56] Erosion/Corrosion Research Center, "E/CRC Membership Information," Erosion/Corrosion Research Center, 2016. [Online]. Available: http://www.ecrc.utulsa.edu/membership.html. [Accessed 5 May 2016].

[57] J. H. Neilson and A. Gilchrist, "Erosion by a Stream of Solid Partcles," *Waer,* vol. 11, no. 2, pp. 111-122, 1968.

[58] I. M. Hutchings and R. E. Winter, "The erosion of ductile metals by spherical particles," *Journal of Physics D: Applied Physics,* vol. 8, no. 1, pp. 8-14, 1975.

[59] D. R. Andrews, "An Analysis of Solid Particle Erosion Mechanisms," *Journal of Physics D: Applied Physics,* vol. 14, no. 11, pp. 1979-1991, 1981.

[60] R. J. Bellman and A. Levy, "Erosion Mechanism in Ductile Metals," U.S Department of Energy, Berkeley, CA, 1981.

[61] J. Salik and D. H. Buckley, "The effect of mechanical surface and heat treatments on the erosion resistance," in *International Conference on Wear Of Materials*, San Francisco, 1981.

[62] D. R. Andrews and N. Horsfield, "Particle Collisions in the Vicinity of an Eroding Surface," *Journal of Physics D: Applied Physics,* vol. 16, no. 4, pp. 525-538, 1983.

[63] D. D. Rickerby and P. J. Burnett, "The erosion behaviour of TiN coatings on steels," *Journal of Material Science,* vol. 23, no. 7, pp. 2429-2443, 1988.

[64] H. M. Clark, "A comparison of particle impact in gas-solid and liquid-solid erosion," *Wear,* Vols. 186-187, no. 2, pp. 465-472, 1995.

[65] J. K. Edwards, B. S. McLaury and S. A. Shirazi, "Modeling Solid Particle Erosion in Elbows and Plugged Tees," *Journal of Energy Resources Technology,* vol. 123, no. 4, pp. 277-284, 2001.

[66] G. R. Desale, B. K. Gandhi and S. C. Jain, "Improvement in the design of a pot tester to simulate erosion wear due to solid–liquid mixture," *Wear,* vol. 259, no. 1-6, pp. 196-202, 2005.

[67] B. K. Gandhi, S. N. Singh and V. Seshadri, "Study of the parametric dependence of erosion wear for the parallel flow of solid–liquid mixtures," *Tribology International*, vol. 32, no. 5, pp. 275-282, 1999.

[68] B. K. Gandhi, S. N. Singh and V. Seshadri, "A study on the effect of surface orientation on erosion wear of flat specimens moving in a solid–liquid suspension," *Wear,* vol. 254, no. 12, pp. 1233-1238, 2003.

[69] R. J. Wood, T. F. Jones, J. Ganeshalingam and N. J. Miles, "Comparison of predicted and experimental erosion estimates in slurry ducts," *Wear,* vol. 256, no. 9-10, pp. 937-947, 2004.

[70] Y. Zhang, E. P. Reuterfors, B. S. McLaury, S. A. Shirazi and E. F. Rybicki, "Comparison of computed and measured particle velocities and erosion in water and air flows," *Wear,* vol. 263, no. 1-6, pp. 330-338, 2007.

[71] G. R. Desale, B. K. Gandhi and S. C. Jain, "Particle size effects on the slurry erosion of aluminium alloy (AA 6063)," *Wear,* vol. 266, no. 11-12, pp. 1066-1071, 2009.

[72] R. Mohammadikhah and V. Abdolkarimi, "CFD Modeling of Particulates Erosive Effect on a Commercial Scale Pipeline Bend," *ISRN Chemical Engineering,* vol. 2013, pp. 1-10, 2013.

[73] Y. G. Zheng, Z. M. Yao and W. Ke, "Erosion–corrosion resistant alloy development for aggressive slurry flows," *Matrials Letter,* vol. 46, no. 6, pp. 362-368, 2000.

[74] S. S. Rajahram, T. J. Harvey and R. J. Wood, "Erosion–corrosion resistance of engineering materials in various test conditions," *Wear,* vol. 267, no. 1-4, pp. 244-254, 2009.

[75] M. A. Islam and Z. N. Farhat, "Effect of impact angle and velocity on erosion of APIX42 pipeline steel under high abrasive feed rate," *Wear,* vol. 311, no. 1-2, pp. 180-190, 2014.

[76] J. R. Laguna Camacho, A. Marquina-Chávez, J. E. Escalante-Martínez, C. A. Márquez-Vera, I. Hernández-Romero, A. Galicia-Badillo and M. d. C. Santes-Bastián, "An analysis of the solid particle erosion damage caused on AISI 304," in *Microscopy: advances in scientific research and education (A. Méndez-Vilas, Ed.),* A. Méndez-Vilas, Ed., Badajoz, Spain, Formatex Research Center, 2014, pp. 1053-1063.

[77] M. Patel, D. Patel, S. Sekar, P. B. Tailor and P. V. Ramana, "Study of Solid Particle Erosion Behaviour of SS 304 at Room Temperature," *Procedia Technology,* vol. 23, pp. 288-295, 2016.

[78] J. F. Kiefner and C. J. Trench, "Oil Pipeline Characteristics and Risk Factors: Illustrations from the Decade of Construction," December 2001. [Online]. Available: http://www.api.org/~/media/files/oil-and-natural-gas/ppts/other-files/decadefinal.pdf?la=en. [Accessed 27 March 2016].

[79] N. J. Hyne, Dictionary of Petroleum Exploration, Drilling & Production, Tulsa, OK: PennWell Publishing Company, 1991.

[80] Texas Department of Transportation, "Sieve analysis of fine and coarse aggregates," January 2016. [Online]. Available: https://ftp.dot.state.tx.us/pub/txdot-info/cst/TMS/200-F_series/pdfs/bit200.pdf. [Accessed 25 May 2016].

[81] B. James, "Mixing 101: Baffled by Baffles?: HOW BAFFLE CONFIGURATION CAN OPTIMIZE INDUSTRIAL MIXING," 19 October 2012. [Online]. Available: http://www.dynamixinc.com/baffled-by-baffles. [Accessed 28 January 2016].

[82] ALICONA, "Roughness Measurements with InfiniteFocus," 18 October 2012. [Online]. Available: http://integrita.zcu.cz/download/skola1/alicona_prez.pdf.

[83] Yorhshire Water, "Services: In Your Area," 31 December 2015. [Online]. Available: https://www.yorkshirewater.com/extra-services/in-your-area.aspx. [Accessed 10 July 2016].

[84] B. K. Gandhi and S. V. Borse, "Effects of particle size and size distribution on estimating erosion wear of cast iron in sand-water slurries," *Indian Journal of Engineering and Materials Sciences,* vol. 9, no. 6, pp. 480-486, 2002.

[85] B. K. Gandhi and S. V. Borse, "Nominal particle size of multi-sized particulate slurries for evaluation of erosion wear and effect of fine particles," *Wear,* vol. 257, no. 1-2, pp. 73-79, 2004.

[86] A. A. Gadhikar, A. Sharma, D. B. Goel and C. P. Sharma, "Fabrication and Testing of Slurry Pot Erosion Tester," *Transactions of the Indian Institute of Metals,* vol. 64, no. 4-5, pp. 493-500, 2011.

[87] B. F. Levin, K. S. Vecchio, J. N. DuPont and A. R. Marder, "Modeling Solid-Particle Erosion of Ductile Alloys," *Metallurgical and Materials Transactions A,* vol. 30, no. 7, pp. 1763-1774, 1999.

[88] British Standards Institute, "Geometric Produc Specification (GPS) - Surface texture - Profile method: Rules and procedures for the assessment of surface texture," BSI Standard BS EN ISO 4288, 1998.

[89] British Standards Institute, "Geometrical product specifications (GPS) - Surface texture: Areal Part 3: Specification operators," BSI Standard ISO 25178-3, 2012.

[90] KEYENCE, "Surface Roughness Terminology," KEYENCE Corp, 2016. [Online]. Available: http://www.keyence.com/ss/products/microscope/roughness/line/sampling_length.jsp. [Accessed 22 September 2016].

[91] L. Richard, L. Brown and R. Blunt, "A NATIONAL MEASUREMENT GOOD PRACTICE GUIDE No 108: Guide to the Measurement of Smooth Surface Topography using Coherence Scanning Interferometry," National Physical Laboratory, Teddington, 2008.

[92] A. B. Forbes, "Areal Form Removal," in *Characterisation of Areal Surface Texture*, R. Leach, Ed., London, Springer Heidelberg, 2013, pp. 107-128.

[93] F. Blateyron, "The Areal Field Parameters," in *Characterisation of Areal Surface Texture,* R. Leach, Ed., London, Springer Heidelberg, 2013, pp. 15-43.

[94] Michigan Metrology, LLC, "Michigan Metrology Surface Texture Parameters Glossary," 2014. [Online]. Available: http://www.michmet.com/emailrequestglossary.htm. [Accessed 2 November 2016].

[95] L. Ćurković, I. Kumić and K. Grilec, "Solid particle erosion behaviour of high purity alumina ceramics," *Ceramics International,* vol. 37, no. 1, pp. 29-35, 2011.

[96] E. Avcu, Y. Yildiran, A. E. Sahin, S. Fidan and T. Sinmazcelik, "Influences of particle impingement angle and velocity on surface roughness, erosion rate and 3D surface morphology of solid particle eroded Ti6Al4V Alloy," *ACTA PHYSICA POLONICA A,* vol. 125, no. 2, pp. 541-543, 2014.

[97] A. A. Hamed, W. Tabakoff, R. B. Rivir, K. Das and P. Arora, "Turbine Blade Surface Deterioration by Erosion," *Journal of Turbomachinery*, vol. 127, no. 3, pp. 445-452, 2005.

[98] G. W. Stachowiak and A. W. Batchelor, Engineering Tribology, 4th ed., Waltham, MA: Elsevier, 2014.

[99] D. Wang, D. Ewing and C. Y. Ching, "Time evolution of surface roughness in pipes due to mass transfer under different Reynolds numbers," *International Journal of Heat and Mass Transfer*, vol. 103, pp. 661-671, 2016.

[100] ANSYS, ANSYS Fluent Customization Manual: ANSYS 17.0, Southpointe: ANSYS, Inc., 2016.

[101] G. Grant and W. Tabakoff, "Erosion Prediction in Turbomachinery Resulting from Environmental Solid Particles," *Journal of Aircraft*, vol. 12, no. 5, pp. 471-478, 1975.

[102] A. Mansouri, H. Arabnejab, S. Karimi, S. A. Shirazi and B. S. McLaury, "Improved CFD modeling and validation of erosion damage due to fine sand particles," *Wear*, pp. 339-350, 2015.

APPENDICES

Appendix I Matrix of Parameters in Erosion Equations

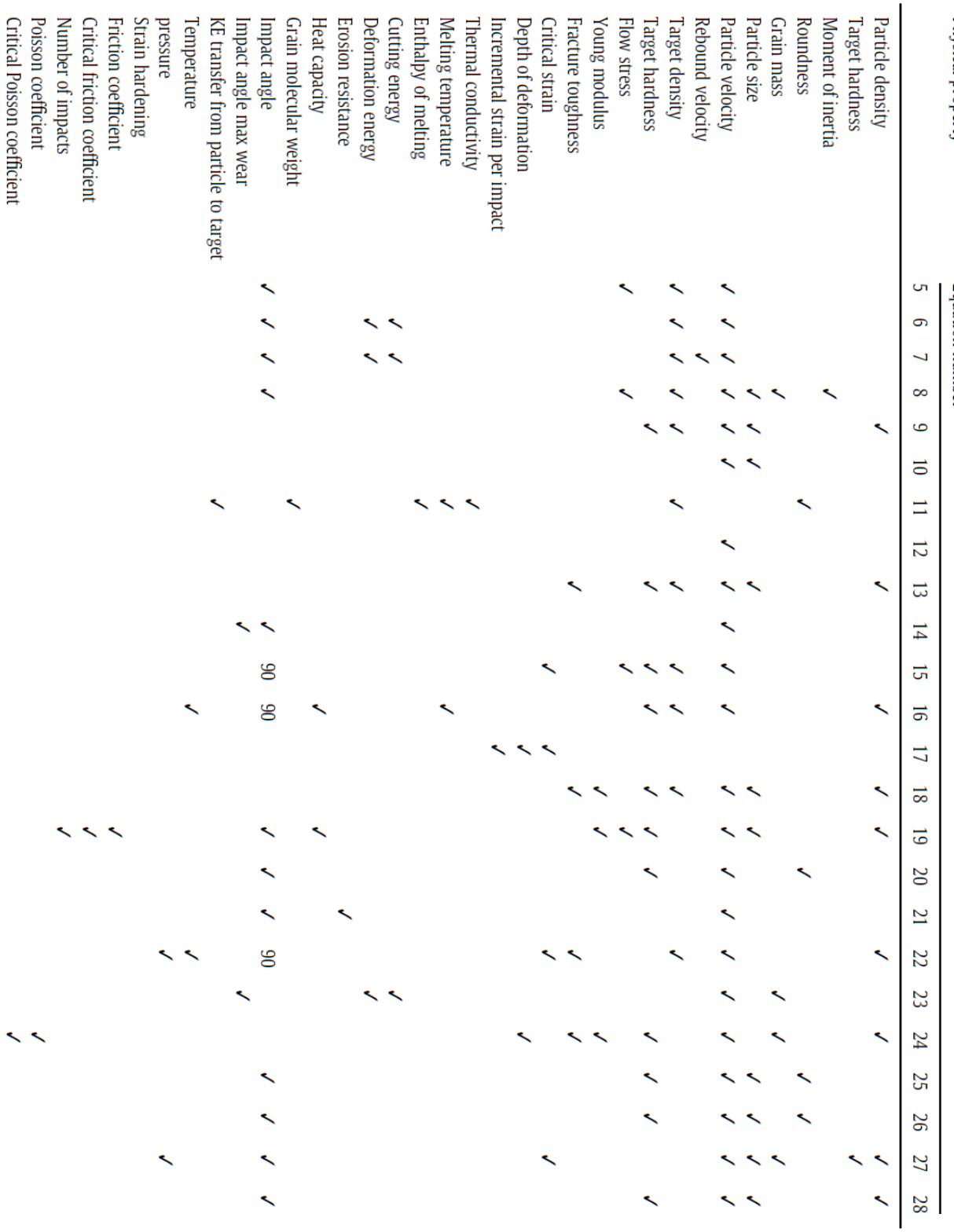

Figure I-1 Physical variables considered in 28 erosion prediction models

Appendix II Olivine Data Sheet

SUBSTANCE INFORMATION SHEET

SCANGRIT

OLIVINE

The substance is not classified as hazardous under the CLP Regulation (1272/2008/EC) or as dangerous under the Dangerous Substances Directive (67/548/EEC), is not persistent bioaccumulative and toxic (PBT) or very persistent and very bioaccumulative (vPvB) as defined in Annex XIII of the REACH Regulation, and is not included in the ECHA candidate list of substances of very high concern. Therefore provision of a Safety Data Sheet (SDS) is not mandatory. This Substance Information Sheet (SIS) is a voluntary presentation of certain information that may assist the user in the handling of the substance.

SECTION 1: Identification of the substance/mixture and of the company/undertaking

1.1 Product Identifier

Product Name:	Olivine
Product Description:	Magnesium Iron Silicate
EINECS:	215-281-7
CAS:	1317-71-1
Registration Number:	Exempted in accordance with Annex V.7

1.2 Relevant identified uses of the substance or mixture and uses advised against

Product use: Blasting abrasive, jet cutting abrasive, non slip aggregate

1.3 Details of supplier of the safety data sheet

Scangrit, Eastfield Road, South Killingholme, Immingham, DN40 3NF, United Kingdom

Email address of person: info@scangrit.co.uk (Dr Gerry Bourke is responsible for this SIS)

1.4 Emergency telephone number of the supplier

Telephone number: Phone +44 (0) 1469 574715 or Fax +44 (0) 1469 571644

Hours of Operation: Office hours

SECTION 2: Hazards identification

2.1 Classification of substance or mixture

Classification according to Regulation (EC) No. 1272/2008 (CLP/GHS)

Classification: Not classified

Classification according to Directive 67/548/EC (DSD)

Classification: Not classified

2.2 Label Elements

2.2.1 Labeling according to Regulation (EC) No. 1272/2008

None

2.2.2 Labeling according to Directive 67/548/EEC

None

2.3 Other hazards

The substance does not meet the criteria for a PBT or a vPvB substance.

Use of this material may generate dust.

SCANGRIT

SECTION 3: Composition/information on ingredients

3.1

Product/Ingredient Name	Identifiers	%	Classification 67/548/EEC	Classification 1272/2008 [CLP]	Type
Olivine	EC:215-281-7 CAS:1317-71-1	100%	Not Classified	Not Classified	[*]
Forsterite	EC: 239-169-2 CAS: 15118-03-3	93%	Not Classified	Not Classified	[A]
Fayalite	EC: 237-687-3 CAS: 237-687-3	7%	Not Classified	Not Classified	[A]

Type
[*] Substance
[A] Constituent
[B] Impurity
[C] Stabilizing additive

SECTION 4: First aid measures

4.1 Description of first aid measures

Eye contact:	Do not rub eyes. Immediately flush eyes with plenty of water, occasionally lifting the upper and lower eyelids. Check for and remove any contact lenses. Get medical attention if irritation occurs.
Inhalation:	Move to fresh air and keep at rest in a position comfortable for breathing. Get medical attention if symptoms occur.
Skin contact:	Use general hygiene measure for contact with the material.
Ingestion:	Wash out mouth with water. Move to fresh air and keep at rest in a position comfortable for breathing. If material has been swallowed and the exposed person is conscious, give small quantities if water to drink. Do not induce vomiting unless directed to do so by medical personnel. Get medical attention if symptoms occur.

4.2 Most important symptoms and effects, both acute and delayed

The product may cause temporary mechanical irritation to the eyes, nose throat and lungs. The effects may be delayed.

4.3 Indication of any immediate medical attention and special treatment needed

Treat symptomatically.

SECTION 5: Fire-fighting measures

5.1 Extinguishing media

Suitable extinguishing media:	Use an extinguishing agent appropriate to the surrounding materials.
Unsuitable extinguishing media:	None known

5.2 Special Hazards arising from the substance or mixture

Hazards from the substance/mixture: No specific hazard

5.3 Advice for fire-fighters

Fire fighters should wear appropriate protective clothing and self contained breathing apparatus.

SCANGRIT

SECTION 6: Accidental release measures

6.1 Personal precautions

Avoid breathing dust. Put on appropriate personal protective equipment.

6.2 Environmental precautions

Avoid dispersal of spilt material and runoff and contact with soil, waterways, drains and sewers.

6.3 Methods and material for containment and clean up.

Ventilate the area thoroughly. Vacuum or sweep up material and place in suitable container for recycling or disposal.

6.4 References to other sections

Section 1 for emergency contact information
Section 8 for information on appropriate personal protective equipment.
Section 13 for Waste disposal.

SECTION 7: Handling and storage

7.1 Precautions for safe handling

Avoid airborne dust generation. Provide appropriate exhaust ventilation at places where airborne dust is generated. In case of insufficient ventilation, wear suitable respiratory protective equipment. Handle packaged products carefully to prevent accidental bursting.

7.2 Conditions for safe storage including incompatibilities

Paper packaging should be kept dry.

7.3 Specific end uses

Check identified uses in section 1.2

SECTION 8: Exposure controls/personal protection

8.1 Control parameters

Product/component name	Exposure Limit Values
Olivine	EH40/2005 WELs (United Kingdom (UK)). TWA: 4mg/m³ 8 hours. Form: Respirable dust TWA: 10mg/m³ 8 hours. Form: Total dust

8.2 Exposure controls

Risk management measures aimed at the protection of human health are to be considered in cases of inhalation of powder or dusts during use. Process enclosures, local exhaust ventilation or other engineering controls should be employed to keep worker exposure to airborne contaminants below any recommended or statutory limits.

Personal protective equipment:	Wear suitable protective clothing.
Hand protection:	Wear suitable gloves. Where necessary, gauntlets should be worn to protect against abrasive ricochet.
Respiratory protection:	Use properly fitted respiratory protection, complying with an approved standard, appropriate for the known or anticipated exposure levels and the hazards of the product. Blasters should wear an air-fed blasting helmet complying with approved standards, to afford the correct level of respiratory and eye/face protection.

SCANGRIT

Eye/face protection:	Safety eyewear complying with an approved standard should be used when a risk assessment indicates this is necessary to avoid exposure to dusts. If operating conditions cause high dust concentrations wear dust goggles.
Hygiene measures:	Handle in accordance with good industrial hygiene and safety practices. Wash hands, forearms and face thoroughly before eating or smoking and at the end of the working period. Routinely wash work clothing and protective equipment to remove contaminants.
Environmental exposure controls:	Emissions from ventilation or work process equipment should be checked to ensure they comply with the requirements of the environmental protection legislation.

SECTION 9: Physical and chemical properties

9.1 Information on the basic physical and chemical properties

Appearance	Solid, sub-angular particles. Colour: Pale Green
Odour	Odourless
Odour threshold	Not applicable
pH	Not applicable
Melting point	1400-1700°C
Initial boiling point and range	Not applicable
Flash Point	Not applicable
Evaporation rate	Not applicable
Flammability (solid, gas)	Non-flammable
Upper/lower flammability or explosive limits	Not applicable
Vapour pressure	Not applicable
Vapour density	Not applicable
Relative Density (ref water at 20°C)	3.3
Solubility	Negligible
Partition coefficient: n-octanol/water	Not applicable
Auto-ignition temperature	Not applicable
Decomposition temperature	Not applicable
Viscosity	Not applicable
Explosive properties	Not applicable
Oxidising properties	Non-oxidising

9.2 Other information

SECTION 10: Stability and reactivity

10.1	Reactivity:	Non reactive
10.2	Chemical stability:	Stable under normal conditions of use, storage and transport
10.3	Possibility of hazardous reactions:	No dangerous reactions known
10.4	Conditions to avoid:	Avoid creating dusty conditions and prevent wind dispersal
10.5	Incompatible materials:	Not applicable
10.6	Hazardous decomposition products:	No hazardous decomposition products should be produced.

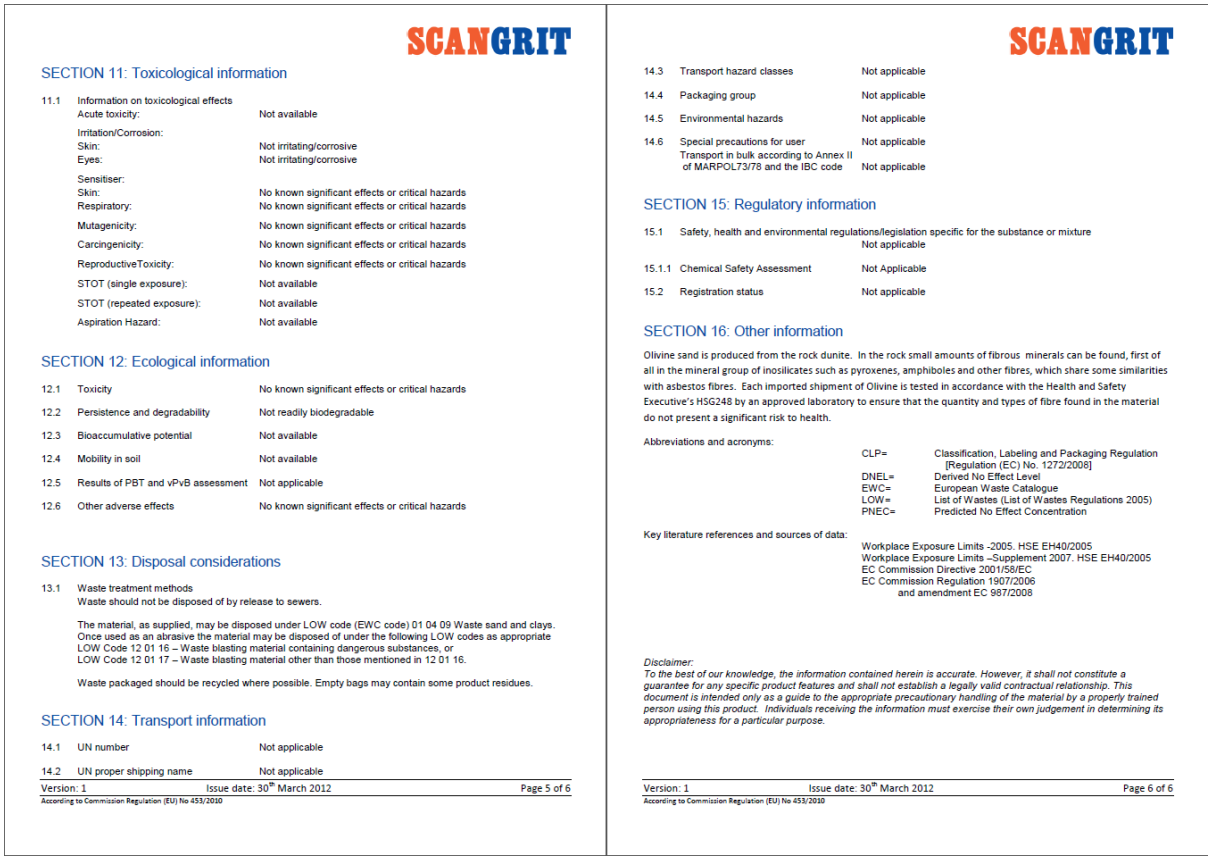

SCANGRIT

SECTION 11: Toxicological information

11.1	Information on toxicological effects	
	Acute toxicity:	Not available
	Irritation/Corrosion:	
	Skin:	Not irritating/corrosive
	Eyes:	Not irritating/corrosive
	Sensitiser:	
	Skin:	No known significant effects or critical hazards
	Respiratory:	No known significant effects or critical hazards
	Mutagenicity:	No known significant effects or critical hazards
	Carcingenicity:	No known significant effects or critical hazards
	ReproductiveToxicity:	No known significant effects or critical hazards
	STOT (single exposure):	Not available
	STOT (repeated exposure):	Not available
	Aspiration Hazard:	Not available

SECTION 12: Ecological information

12.1	Toxicity	No known significant effects or critical hazards
12.2	Persistence and degradability	Not readily biodegradable
12.3	Bioaccumulative potential	Not available
12.4	Mobility in soil	Not available
12.5	Results of PBT and vPvB assessment	Not applicable
12.6	Other adverse effects	No known significant effects or critical hazards

SECTION 13: Disposal considerations

13.1 Waste treatment methods

Waste should not be disposed of by release to sewers.

The material, as supplied, may be disposed under LOW code (EWC code) 01 04 09 Waste sand and clays. Once used as an abrasive the material may be disposed of under the following LOW codes as appropriate
LOW Code 12 01 16 – Waste blasting material containing dangerous substances, or
LOW Code 12 01 17 – Waste blasting material other than those mentioned in 12 01 16.

Waste packaged should be recycled where possible. Empty bags may contain some product residues.

SECTION 14: Transport information

14.1	UN number	Not applicable
14.2	UN proper shipping name	Not applicable

SCANGRIT

14.3	Transport hazard classes	Not applicable
14.4	Packaging group	Not applicable
14.5	Environmental hazards	Not applicable
14.6	Special precautions for user	Not applicable
	Transport in bulk according to Annex II of MARPOL73/78 and the IBC code	Not applicable

SECTION 15: Regulatory information

15.1	Safety, health and environmental regulations/legislation specific for the substance or mixture	Not applicable
15.1.1	Chemical Safety Assessment	Not Applicable
15.2	Registration status	Not applicable

SECTION 16: Other information

Olivine sand is produced from the rock dunite. In the rock small amounts of fibrous minerals can be found, first of all in the mineral group of inosilicates such as pyroxenes, amphiboles and other fibres, which share some similarities with asbestos fibres. Each imported shipment of Olivine is tested in accordance with the Health and Safety Executive's HSG248 by an approved laboratory to ensure that the quantity and types of fibre found in the material do not present a significant risk to health.

Abbreviations and acronyms:

CLP=	Classification, Labeling and Packaging Regulation [Regulation (EC) No. 1272/2008]
DNEL=	Derived No Effect Level
EWC=	European Waste Catalogue
LOW=	List of Wastes (List of Wastes Regulations 2005)
PNEC=	Predicted No Effect Concentration

Key literature references and sources of data:

Workplace Exposure Limits -2005. HSE EH40/2005
Workplace Exposure Limits –Supplement 2007. HSE EH40/2005
EC Commission Directive 2001/58/EC
EC Commission Regulation 1907/2006
and amendment EC 987/2008

Disclaimer:
To the best of our knowledge, the information contained herein is accurate. However, it shall not constitute a guarantee for any specific product features and shall not establish a legally valid contractual relationship. This document is intended only as a guide to the appropriate precautionary handling of the material by a properly trained person using this product. Individuals receiving the information must exercise their own judgement in determining its appropriateness for a particular purpose.

Figure II-2 Olivine Data Sheet

Appendix III Risk Assessment

UNIVERSITY OF HUDDERSFIELD

GENERAL HEALTH AND SAFETY RISK ASSESSMENT FORM

Table III-1 General risk assesstment

Description of activity:			
Location: T4/07	**Assessment by: Eduardo Samuel Matthew**	**Assessment date: 01.04.16**	**Review date:**

GENERIC RISK MANAGEMENT MEASURES
Health and safety risk management measures appropriate to all aspects of the activity being assessed

SPECIFIC ASPECT OF ACTIVITY: Stirring of Solid particles in mixing Pot			
Hazards identified	**Risks to health and safety**	**People at risk**	**Health and safety risk management measures**
Rotating Shaft Spillage Projectile from rotating specimen	Injury due to part of body or clothing becoming entangled in the rotating shaft. Slip and fall hazard Injury due to sample striking individual	Operator, other researching working in the area	Follow Best practice, i.e. no loose clothing in the vicinity of the test pot (appropriate signage must be erected). Appropriate guarding must be in place before the motor is operated. Ensure area is immediately dried up (spillage rags available in workshop) Ensure tank is tough enough to prevent specimen from penetrating tank, and have exterior guard as a secondary barrier

SPECIFIC ASPECT OF ACTIVITY: Using a reservoir tank filled with water			
Hazards identified	**Risks to health and safety**	**People at risk**	**Health and safety risk management measures**
Contamination of water in tank by bacteria/fungus	Due to existence of bacteria/fungus in the contaminated water tank, the people who work in this environment could be affected	Operator, other researching working in the area	Water is changed often during operation, ensure that the water is fully drained when finished experimentation
SPECIFIC ASPECT OF ACTIVITY:			

SPECIFIC ASPECT OF ACTIVITY: Walking around the rig			
Hazards identified	**Risks to health and safety**	**People at risk**	**Health and safety risk management measures**
Trip hazard	Trip Injury	Operator, other researching working in the area	Ensure general working area is kept clear of trip hazards, labels or cable mats to be used where unavoidable

SPECIFIC ASPECT OF ACTIVITY: Sieving and Disposal of Erodent			
Hazards identified	**Risks to health and safety**	**People at risk**	**Health and safety risk management measures**
Breathing in of Olivine dust Incorrect disposal	Respiratory issues from inhaling dust Olivine is inert however once used for blasting purposes must be discarded appropriately	Operator	All the silica in olivine is present in a combined form and therefore Olivine does not present a risk of silicosis. However sieving has to be carried out in a well-ventilated area. All the silica is present in a combined form and therefore Olivine does not present a silicosis Discard in accordance to LOW Code 12 01 17

SPECIFIC ASPECT OF ACTIVITY: Use of Electrical Equipment			
Hazards identified	**Risks to health and safety**	**People at risk**	**Health and safety risk management measures**
Electrocution: VFD Spraying of water onto electrical equipment	Electrical shock Short circuit or electrical shock	Operator	Correct labelling to ensure that drive is not disconnected within ten minutes of being powered down Ensure all liquid connections are fully tested, sure that equipment that are positioned under flow loop are covered.

Appendix IV ANSYS Fluent - User Defined Function: Model Comparison

A User Defined Function, for ANSYS Fluent is implemented where a nonstandard operation is needed. This could be for a processing operation or for a post processing action which can include diffusion functions, customised boundary conditions and enhancing DPM Discrete Phase Modeming. The UDF is written in C language and is a function which can be then loaded or hooked to ANSYS to carry out the desired operation [100]. The model developed in section 4.2.4 can be implemented in a CFD package such as ANSYS Fluent, through the use of a UDF which has been written and is outlined below.

DEFINE_DPM_BC is the boundary condition detailing the manner in which the particle behaves upon impact and after impact. Grant and Tabakoff [101] developed two equations which represent coefficient of restitution (COR) which accounts the change in velocity on impact and rebound. This Grant/Tabaoff - COR model was successfully implemented by Mansouri et al [102] in a study which computationally solved erosion damage due to sand particles, using ANSYS Fluent 14.5.

$$V_{N2}/V_{N1} = 0.993 - 1.76\beta_1 - 1.56\beta_1^2 - 0.49\beta_1^3 \quad (6\text{-}1)$$

$$V_{T2}/V_{T1} = 0.988 - 1.66\beta_1 - 2.11\beta_1^2 - 0.67\beta_1^3 \quad (6\text{-}2)$$

DEFINE_DPM_EROSION is compiled the TULSA (E/CRC), Oka and the modified models, to produce an output file with the erosion rate information.

The ANSYS manual does not specify the output unit of P_diam for the particle pointer (p), in the UDF this is assumed to be in meters an additional line of code can be inserted to convert this to meters if the Fluent output is different. Thread ID would be set as the target wall(s) under investigation this ID number can be captured from Fluent.

```
/*User defined function for comparison of three erosion models*/
#include "udf.h"
/*This defines boundary conditions, inclduing angle of restitution*/

DEFINE_DPM_BC(reflec_coeff, p, t, f, f_normal, dim)
{
 real alpha;
 real vn=0.;
 double nor_coeff;
 double tan_coeff;
 double theta;
 real normal[3];
 int i, idim = dim;
 real NV_VEC(x);

 alpha = M_PI / 2. - acos(MAX(-1., MIN(1., NV_DOT(normal, p->state.V) /
```

```
            MAX(NV_MAG(p->state.V), DPM_SMALL))));

 theta=alpha*180/M_PI;
 nor_coeff=0.988-0.78*theta+0.19*pow(theta,2)-0.024*pow(theta,3)+0.027*pow(theta,4);
 tan_coeff=1-0.78*theta+0.84*pow(theta,2)-0.21*pow(theta,3)+0.028*pow(theta,4)-
0.022*pow(theta,5);

  for (i=0; i<idim; i++)
   normal[i] = f_normal[i];

 if(p->type==DPM_TYPE_INERT)
  {
   alpha = M_PI/2. - acos(MAX(-1.,MIN(1.,NV_DOT(normal,p->state.V)/
               MAX(NV_MAG(p->state.V),DPM_SMALL))));
   if ((NNULLP(t)) && (THREAD_TYPE(t) == THREAD_F_WALL))
    F_CENTROID(x,f,t);

   for(i=0; i<idim; i++)
    vn += p->state.V[i]*normal[i];

   for(i=0; i<idim; i++)
    p->state.V[i] -= vn*normal[i];

   for(i=0; i<idim; i++)
    p->state.V[i] *= tan_coeff;

   for(i=0; i<idim; i++)
    p->state.V[i] -= nor_coeff*vn*normal[i];

   for(i=0; i<idim; i++)
    p->state0.V[i] = p->state.V[i];

   return PATH_ACTIVE;
  }
 return PATH_ABORT;
}
/*Calculating Erosion Based on Tulsa, Oka and Modified Model*/
/* Thread ID 14 and 15: target wall ID from FLUENT */
/*alpha in radians*/
DEFINE_DPM_EROSION(DPMErosion, p, t, f, normal, alpha, Vmag, Mdot)
```

```
{
        if ((THREAD_ID(t) == 14 || THREAD_ID(t) == 15)) {

                        real A[ND_ND];
                        double Hv, oka, G, ER90, ERoka;
                        double ERTulsa;
                        double Theta, Falpha;
                        double B, BH, C, Fs, Vp, n, dia, x;
                        double A1, A2, A3, A4, A5;
                        float nmod = 2.35;
                        double K, Koka, k1, k2, k3, s1, s2, q1, q2, n1, n2, rho;
                        real ModER;

                        FILE *fp;
                        fp = fopen("DPM_erosion.out", "a");

                        dia = P_DIAM(p);
                        Theta = alpha*180. / M_PI;
                        K = 3.284e-04;
                        Koka = 65;
                        BH = 111;
                        C = 2.17*pow(10, -7);
                        Fs = 1;
                        Vp = Vmag;
                        n = 2.41;
                        A1 = 5.40;
                        A2 = -10.11;
                        A3 = 10.93;
                        A4 = -6.33;
                        A5 = 1.43;
                        x = 0.56;

                        Falpha = ((A1*alpha) + (A2*pow(alpha, 2)) + (A3*pow(alpha, 3)) +
(A4*pow(alpha, 4)) + (A5*pow(alpha, 5)));
/*Tulsa Model*/
                        ERTulsa = C*pow(BH, -0.59)*Fs*pow(Vp, n)*Falpha;
/*modified Model*/
                        ModER = (K*Falpha*pow(BH, -0.59)*Fs*pow(Vmag,
nmod)*pow(dia, x));
```

```
/*F Storage F saves the results into the FLUENT file allowing this to be displayed on screen, all others will be produced in the output File DPM_erosion.out */

                        F_STORAGE_R(f, t, SV_DPMS_EROSION) = ModER;

                        s1 = 0.71;
                        s2 = 2.4;
                        q1 = 0.14;
                        q2 = -0.94;
                        k1 = -0.12;
                        k3 = 0.19;
                        Hv = 1.128;
                        rho = 7870;

                        n1 = ((s1)*(pow(Hv, q1)));
                        n2 = ((s2)*(pow(Hv, q2)));
                        k2 = (2.3*(pow(Hv, 0.038)));
                        G = (pow(sin(alpha), n1)*(pow(1 + (Hv*(1 - sin(alpha))), n2)));
                        ER90 = (Koka*pow(Hv, k1)*pow(Vmag, k2)*pow(dia, k3));
                        oka = G*ER90;
/*Oka Model*/
                        ERoka = oka*rho*pow(10, -9);

                        fprintf(fp, "%e,%e,%e,%e,%e,%e\n", dia, Vmag, alpha, Theta, ERTulsa, ModER, ERoka);

                        fclose(fp);
                }
/*for particles that don't hit the target wall, erosion is not recorded*/
        else {

                real A[ND_ND];

                real ModER;

                ModER = 0;

                F_STORAGE_R(f, t, SV_DPMS_EROSION) = ModER;
        }
}
```